Stony Brook University

Design and biological evaluation of new NSAIDs based anticancer agents and their controlled release from an addressable hydrogel based delivery system

A Dissertation Presented

by

Stancy Jana Joseph

to

The Graduate School

in Partial Fulfillment of the

Requirements

for the degree of

Doctor of Philosophy

in

Chemistry

Stony Brook University

August 2010

Stony Brook University

The Graduate School

Stancy Jana Joseph

We, the dissertation committee for the above candidate for the

Doctor of Philosophy degree, hereby recommend

acceptance of this dissertation.

Dr. Basil Rigas MD, DSC -Dissertation Advisor

Department of Medicine

Dr. Elizabeth Boon, PhD- Chairperson of Defense

Department of Chemistry

Dr. Iwao Ojima, PhD - Dissertation Co-Advisor

Department of Chemistry

Dr. Miriam Rafailovich, PhD - Outside Member/Advisor

Department of Material Science and Engineering, Stony Brook University

Dr. Yizhi Meng, PhD - Outside Member

Department of Material Science and Engineering, Stony Brook University

This dissertation is accepted by the Graduate School

Lawrence Martin

Dean of the Graduate School

Abstract of the Dissertation

Design and biological evaluation of new NSAIDs based anticancer agents and their controlled release from an addressable hydrogel based delivery *system*

by

Stancy Jana Joseph

Doctor of Philosophy

in

Chemistry

Stony Brook University

2010

In recent years scientific and technological advancements have been made in the research and development of controlled drug delivery systems and new chemopreventive agents. For many potential drug candidates a modified *in vivo* drug release is desired to improve efficacy, sustain drug effect or minimize drug toxicity. To tackle the problems associated with the delivery of drug, delivery systems (DDS) with multiple functionalities such as environment-sensitive drug release mechanisms have motivated the biomedical community as well as materials chemists for more than a decade. Polymeric drug delivery systems have been extensively studied in an attempt to achieve modified drug release. Here we report on a novel thermo-responsive based system to fabricate biocompatible polymeric hydrogels as drug delivery as well as the development of a new class of non-steroidal anti-inflammatory drugs as chemopreventive agents. Biocompatible Pluronic F127 (PF127), a triblock copolymer, was employed as matrix materials for polymeric-based DDS. This thermo-sensitive

polymeric system have been modified by acrylation and cross-linked to form a hydrogel based drug delivery system. The modified polymeric system contains a hydrophobic polypropylene oxide (PPO) and a hydrophilic polyethylene oxide (PEO) blocks which undergoes a “hydrophilic-hydrophobic” phase transition in aqueous media and around the human body temperature. In addition, poly lactic-co-glycolic acid (PLGA) nanoparticles were assembled by solvent extraction method and incorporated in the modified Pluronic F127 hydrogels as drug carrier units. These modifications of PF127 were monitored by ^{1}H-NMR and rheological studies. The rheological study determined that the degree of cross-linking affect the release rate of the drug from the PF127/PLGA system. The control release rate of the chemopreventive compounds seems to be further enhanced due to the addition of the PLGA nanoparticles. The *in vitro* cellular uptake and the cytotoxicity studies of the PLGA nanoparticles have been considered to determine their enhancement of drug uptake and the lack of acute cytotoxicity. The sensitivity of the polymer to the temperature was shown to facilitate drug release upon administered temperature changes.

This work also focuses on the development and analysis of non-steroidal anti-inflammatory drugs (NSAIDs) as chemopreventive agents. NSAIDs are a class of drugs that are commonly used as medications because of their pain- and fever reducing properties. Several chemopreventive studies have reported that NSAIDs and their derivatives have potential promise as anticancer agents. Based on pharmaco-kinetics, pharmaco-dynamic and structure activity relationship studies performed in this work, a new series of NSAID derivatives have been designed and synthesized. *In vitro* evaluation showed that these new generations of NSAIDs exhibit higher potency than that of traditional NSAIDs such as aspirin, especially against pancreatic and colon cancer.

One of two NSAIDs hydrophobic model drugs, sulindac sulfide or Drug D was loaded in the modified Pluronic F127/PLGA drug delivery system. The NSAIDs have been shown to be successfully release from the modified PF217/PLGA drug delivery system applied both media and cell culture. This

property can find application in externally stimulated drug release applications at the site of the disease.

The studies performed in this dissertation to analysis, design and synthesize the old and new generations of NSAIDs was a collaborative effort of many persons. I performed the majority of the analysis and manuscript workings after the NSAIDs were synthesized and animals were treated and sacrifice by other collaborators. All studies in regards to the construct and design of the PF127/PLGA drug delivery system were done under the guidance or Prof. Miriam Rafailovich and Dr. Basil Rigas.

I dedicate this thesis to my mother, Veronica Anderson, my best friend, Janaki Surage-Polius and my mentor, Jennie L. Williams

Table of Contents

List of Figures

List of Tables

List of abbreviations

ABEs	Aspirin-based benzyl esters
ASA	Aspirin
CMC	Critical micelle concentration
CMT	Critical micelle temperature
DMFO	α-difluoromethylornithine
LCST	Lower critical solution temperature
NO-NSAIDs	Nitric oxide-donating non-steroidal anti-inflammatory drugs
NPs	Nanoparticles
NSAIDs	Non-steroidal anti-inflammatory drugs
PanIN	Pancreatic Intraepithelial Neoplasias
PEO	Polyethylene oxide
PGE_2	Prostaglandin E_2
PLA	Poly(lactic acid)
PLG	Poly(glycolic acid)
PLGA	Poly(lactic-co-glycolic acid)
PPO	Poly(propylene oxide)
SAR	Structure activity relaationship
TxA_2	Thromboxane A_2
TxB_2	Thromboxane B_2

Acknowledgement

This thesis could not have been completed without the generosity and support of many.

First, I want to thank my thesis advisors, Professors Basil Rigas and Miriam Rafailovich and my mentor, Jennie L. Williams for their support of both me and my work. They encouraged me to strive for lofty goals and challenged me to take on the most important problems, thus making it a learning opportunity. Miriam and Jennie have been models of dedication, humility, and generosity that I will strive to emulate in my own career. Special thanks to Jennie for spending long hours patiently teaching me how to conduct experiments in the lab. I thank her for her investment of time in me, as well as her encouragement.

I would like to thank the remaining members of my thesis committee, Professors Iwao Ojima, Elizabeth Boon and Yizhi Meng, who generously gave their time and advice to help further not only this work, but also my own professional development. Also, I would like to thank our collaborators, who were instrumental in laying the groundwork for our research. The text of this dissertation in part is a reprint of the materials as it appears in the International Journal of Oncology. Permission to publish this text was granted by the editor.

I thank the many members of the Peter Tonge groups (Chemistry Department, Stony Brook University), Miriam Rafailovich group (Materials Science and Engineering, Stony Brook University), Iwao Ojima group (Chemistry Department, Stony Brook University), Stephen Koch group (Chemistry Department, Stony Brook University) and Martin Schoonen group (Geosciences Department, Stony Brook University) who have made helpful contributions. These groups permitted me to use their instruments enabling me to complete my research. I thank the members of the different department whose faculty and staff have aided in so many aspects of my graduate experience. The Chemistry department: Katherine Hughes, James Marecek, Prof. Michael White and Prof.

Nancy Goroff, Cancer Prevention/Medicine department: Diane Riccardo, Beth Jaronczyk and Sue Van Horn, and Material Science and Engineering: Jim Quinn.

Finally, none of this work would have been possible without generous financial support from the National Institutes of Health, the National Cancer Institute and the Department of Defense.

My decision to attend graduate school, and the opportunity to come to Stony Brook University, were made possible by a handful of mentors who, through their patience and dedication, exerted a powerful, positive influence on me as an undergraduate student. Professor Nalley offered me research opportunities with her collaborators as a junior and senior. She continually challenged me to become the best scientist I could be. Professor Snider, my undergraduate mentor, showed great concern for my personal development and for that I owe him a great debt.

Finally, as a graduate student, undoubtedly the best memories I will take from my graduate experience stem from the wonderful friendships I made at Stony Brook. Whether things were going well or poorly, my friends were always there to encourage, amuse, and lend valuable perspective. I have been blessed with too many friends to mention individually in this space, but I send my heartfelt thanks to each. In particular, Janine has been a supportive friend; her ability to make me takes breaks was always welcome. Janine as well as Allison, Firat and Kanishk have been loyal friends who were always ready to get together for something fun at a moment's notice. Tatsiana and Jennie were two friends I turned to for understanding when things became unbearable. They have and continue to be constant, loving friends who have wholeheartedly supported me in every step of this journey and I thank them

Finally, this work is possible because of the love and support of my family. Janaki, my best friend, she remained supportive of me through all my decisions. She continues to be an inspiration and friend whose role in my life is irreplaceable. Most of all, I thank my mother, Veronica for all the sacrifices she

made for me and the standard for hard work and dedication that has served as a powerful motivator for me. She taught me to value education, hard work and set standards for me, to love and respect myself and others, and to always do my very best.

They have all my love.

Publication

1. Pharmacokinetic and pharmacodynamic study of NO-donating aspirin in F344 rats. Int J Oncol. 2008 October; 33(4): 799–805

2. Structure-Activity Relationship Study of Novel Anticancer Aspirin-based Compounds. (Submitted for publication)

3. Control Drug Delivery Unit Part1: Structure and Rheological Studies of Pluronic F127 Cross-linked Hydrogels. (Manuscript in progress)

4. Controlled Release Drug Delivery Unit Part 2: Externally regulated controlled release of anticancer agents from photo-cross-linked Pluronic hydrogels. (Manuscript in Progress)

Patent

1. Patent disclosure pending for drug delivery unit

1. Introduction

1.1 Cancer

Cancer, one of the major medical challenges of our time, is a disease characterized by uncontrolled growth and spread of abnormal cells. Cancer represents a principal cause of death, accounting for nearly a quarter of deaths in the US. In 2009 there was an estimated 1,479,350 new cases of cancer. Of these, the expected number of Americans to die from cancer was 562,340, making cancer the second most common cause of death in the US, exceeded only by heart disease [1] . Two of the most common types of cancer in the US are pancreatic and colorectal cancer.

1.1.1 Pancreatic cancer

Pancreatic cancer is a malignant mass of tissue in the pancreas, an organ located in the upper middle section of the abdomen[2]. The pancreas is surrounded by the stomach, small intestine, liver and spleen, and aids in the process of digestion. It contains both exocrine glands (which produce enzymes that help the body digest food) and endocrine glands (which produce hormones i.e. insulin that help control blood sugar levels in the body) [3] . Of the total number of people diagnose with cancer of these approximately 42,470 had pancreatic cancer. This makes pancreatic cancer is the fourth most commonly diagnosed cancer in the United States. Most cases occur in people over the age of 55. However, pancreatic cancer can occur at earlier ages, particularly to individuals with a family history of the disease. Aside from age and a family history, there are other risk factors that are associated with pancreatic cancer.

Other diseases such as diabetes and chronic pancreatitis have been found to be associated with the increase risk of pancreatic cancer. To facilitate the understanding of pancreatic cancer, the disease has been divided into several classifications. One such classification is based on the development of pancreatic cancer through a series of duct lesions termed Pancreatic Intraepithelial Neoplasias (PanIN) (Fig 1)[4]. In the disease, normal cuboidal duct epithelium develops into PanIN-1A, then PanIN-1B, then PanIN-2 and finally to PanIN-3 prior to becoming invasive carcinoma (Fig 1). PanIN-1A lesions are flat epithelial lesions composed of tall columnar cells with basally located nuclei and abundant supranuclear mucin. The nuclei are small and round to oval in shape. When oval the nuclei are oriented perpendicular to the basement membrane. PanIN-1B lesions are identical to PanIN-1A except these epithelial lesions have a papillary, micropapillary or basally pseudostratified architecture. Architecturally, PanIN-2 mucinous epithelial lesions may be flat or papillary. By definition, these lesions must have some nuclear abnormalities. These nuclear abnormalities fall short of those seen in PanIN-3. PanIN-3 lesions are usually papillary or micropapillary, however, they may rarely be flat. True cribriforming, budding off of small clusters of epithelial cells into the lumen and luminal necroses should all suggest the diagnosis of PanIN-3. Cytologically, these lesions are characterized by a loss of nuclear polarity, dystrophic goblet cells (goblet cells with nuclei oriented towards the lumen and mucinous cytoplasm oriented toward the basement membrane), mitoses which may occasionally be abnormal, nuclear irregularities and prominent (macro) nucleoli[4-7].

Of the total number of people diagnosed with pancreatic cancer 35,240 were expected to die from it (83% mortality rate) [1] . This is due primarily to difficulty in the diagnosis of the disease. Because the pancreas sits deep within the digestive system, traditional methods for diagnosis of cancer are limited when applied to pancreatic cancer. Thus, the location of the pancreas makes it particularly difficult to detect pancreatic cancer in early and hopefully curable stages. Consequently, symptoms often do not appear until the disease has progressed to an advanced sometimes incurable stage [2,3].

1.1.2 Colorectal cancer

Colorectal cancer is cancer that develops in the colon or the rectum. The colon and rectum are parts of the digestive system, which is also called the gastrointestinal, or GI, system. The GI system processes food for energy and rids the body of solid waste (fecal matter or stool). Colorectal cancer usually develops slowly over a period of many years. Before cancer develops, it usually begins as a noncancerous polyp, a growth of tissue that develops on the lining of the colon or rectum, which may eventually change into cancer[8]. More than half of all individuals will eventually develop one or more adenomas, a certain kinds of polyps. Most adenomas do not become cancerous. About 96% of colorectal cancers are adenocarcinomas, which evolve from glandular tissue[8]. Colorectal cancer is the third leading cause of cancer death in the US in men and women. Colorectal cancer is one of the few cancers that can also be prevented through screening because precancerous polyps, from which colon cancers often develop, can be identified and removed. The relative five-year survival is 90% for colorectal cancer patients diagnosed at an early, localized stage; however, only 40% of cases are diagnosed at this stage. Of the 49,920 people expected to die of colorectal cancers in 2009, early detection could save more than half[1,8].

Unlikely pancreatic cancer there is currently methods for the detection of colorectal cancer. Some current detection methods of colorectal cancer consist of stool home-test kits such as the guaiac-based fecal occult blood test (gFOBT), the fecal immunochemical test (FIT) and the stool DNA test. Other methods entail structural examinations such as flexible sigmoidoscopy, colonoscopy, CT colonography, and double-contrast barium enemar[8]. Once detected the disease is usually classified or staged. Staging colorectal cancer is a process of finding out how far the cancer has spread. This method of classification also enables the physician to determine what type of treatment is needed. There are four stages of colorectal cancer (Fig.2). In stage I, the cancer has not spread beyond the inside of the colon or rectum. Stage II the disease has spread into the muscle wall layers of the colon or rectum, whereas in stage III the disease has spread to

one or more lymph nodes in the areas. In the final stage, stage IV, the disease has spread to other parts of the body such as the liver[8]. Cancer detected and staged in the early stages, before it spreads to other organs, allows for the removal of the adenomatous polyps/lesions, which are associated with an increased risk of colorectal cancer.

A person's genetic background is an important factor in colorectal cancer risk. Hereditary colon cancer syndromes where the affected family members will develop countless numbers of colon polyps increase the risk of developing colon cancer. Two of these syndromes are familial adenomatous polyposis (FAP) which starts during the teen years and MYH polyposis syndrome which typically develop 10-100 polyps occurring at around 40 years of age. Unless the condition is detected and treated (treatment involves removal of the colon) early, a person affected is almost sure to develop colon cancer from these polyps. Studies have also demonstrated that inflammatory bowel disease such as chronic ulcerative colitis, which causes inflammation of the inner lining of the colon, is a recognized complication of colorectal cancer. In addition, diets high in fat are also believed to predispose humans to colorectal cancer. It is believed that the breakdown products of fat metabolism lead to the formation of cancer-causing chemicals (carcinogens)[8].

1.2 Chronic Inflammation and Cancer

It has become increasingly apparent that inflammation, especially chronic inflammation has a role in carcinogenesis. For many years it has been recognized that states of chronic immune activation in some instances can lead to cancer. These chronic inflammatory states can be brought about by either infectious or noninfectious disease processes. Among the chronic infections that can lead to cancer are those caused by viruses, bacteria and parasites [9]. The first conclusive report of viruses causing cancerous lesions was in the early

1900s when Peyton Rous noted the cause of sarcomas in chicken Rous-Sarcoma Virus (RSV), a filterable agent [10]. Since then a number of other viral induced cancers have been found. Among these are Human papilloma virus (HPV) which induces cervical cancer, Hepatitis B and C virus (HBV and HCV) which induces hepatocellular carcinoma and Epstein Barr virus (EBV) which induces lymphoproliferative carcinoma. Cancer caused by chronic bacterial and parasitic infections has also been discovered. Among these are Helicobacter pylori (bacteria) which induce gastric cancer [11] and Schistosomiasis (parasite) which can cause infection in the bladder has also been shown to increase the risk of bladder cancers in those chronically infected with it [12].A number of other non-infectious conditions have been noted in which chronic inflammation results in increased occurrence of cancer. For example, inflammatory bowel disease, a long-standing inflammatory disease of the large intestine, is associated with increased risk of colon cancer. Additionally chronic pancreatitis is associated with an increased risk of pancreatic cancer.

1.3 Problems associated with cancer prevention

With the increase in the number of people being diagnosed with cancer every year it is worrisome that there is a lack of any recent significant preventive progress in solving “the cancer problem.” For example in the US the rate of cancer has shown a modest but steady decline of 1.6% per year in the U.S. over six years for both deaths from the disease and new diagnoses[13]. The improvement is driven largely by declines in the big four cancer killers; lung, colon, prostate, and breast. This decline is attributed to a reduction in the smoking rate, better and earlier detection, and improved treatments[13]. While for example the death rate from heart disease has shown a remarkable reduction. They found that, while in 2002 there were 1131 admissions for heart attacks per

100 000 individuals, by 2007 that number had dropped to 866 per 100,000 individuals [13]. This is a 23.4% decline.

The reason for this decline in heart attacks is not completely clear. Since the majority of the drop was attributed to a reduction in initial heart attacks rather than in recurrent heart attack. Most likely the decline was due to improvements in primary heart attack prevention, rather than to more aggressive treatment after a heart attack. That is, one or more of the improved risk reduction measures such as a broader use of preventive drugs such as aspirin, is likely responsible for this striking drop in heart attacks[13]. The use of preventive methods to reduce the number of occurrence of heart disease has provided a conceptual stimulus to explore alternative means to decrease cancer incidence. One prevention strategy that has gained acceptance is cancer chemoprevention.

1.4 Chemoprevention

Chemoprevention which is a pharmacological approach describes the use of chemical compounds, natural or synthetic, to intervene in the early stages of carcinogenesis to reverse, suppress or prevent its progression to invasive cancer [14-17]. In recent years, there have been many studies that involved the discovery and testing of potential chemopreventive compounds, but there are few that have been adopted for routine clinical use. The most widely studied drugs for chemoprevention are finasteride (Fig 3B: prostate cancer prevention), tamoxifen (Fig 3A: breast cancer prevention) and non-steroidal anti-inflammatory drugs. (NSAIDs) Finasteride and tamoxifen have been adopted for routine clinical use as cancer prevention agents but NSAIDs have not. Numerous studies have demonstrated NSAIDs having therapeutic potential. However, it has also been found to have side effects that prevent them from being used widely in cancer prevention[13-16].

1.5 NSAIDs

Non-steroidal anti-inflammatory drugs (NSAIDs) have a long and distinguish history in internal medicine. Aspirin, a well known NSAID, has served as an anti-inflammatory drug, analgesic, and antipyretic for more than a century. More recently aspirin has emerged as an effective agent for the secondary prevention of cardiovascular disease. Recent finding regarding aspirin and other NSAIDs have suggested a new role for these compounds as chemopreventive agents.

Extensive studies have established that conventional NSAIDs, such as aspirin, prevent cancer but with significant side effects. These considerations have fueled research to develop derivatives of NSAIDs, as alternative agents. One set of derivatives that have been developed was NO-donating NSAIDs (Fig 3). NO-NSAIDs will be discussed in greater details below.

1.6 NO-NSAIDs

One of the most studies NSAIDS, NO-NSAIDs consist of a conventional NSAIDs and a NO-donating group linked to it via a spacer. The rationale for their development was to add to the pharmacological activities of the NSAID those of NO, hoping to achieve higher efficacy and safety. Here, we summarize the development, pharmacological properties and preclinical efficacy data concerning the novel anticancer NO-NSAIDs, which may represent a more desirable alternative to their conventional counterparts.

Structure and metabolism of NO-donating NSAIDs

NO-releasing compounds are prodrugs that elevate NO levels, inhibit NO synthesis and act as NO scavengers [18]. Examples of NO-releasing compounds are the NO-chimeras, a pharmacophore plus a NO mimetic group, [19], diphenyloxidazoles synthesized as cyclooxygenase (COX)-2 inhibitors/NO donors [20], and the NO- NSAIDs such as NO-ASA, NO-ibuprofen, NO-salicylic acid and NO-indomethacin (Fig 4).

NO-NSAIDs represent a group of anticancer agents that exploit the biological properties of NO, one of the simplest yet most powerful biological molecules in nature. Initially identified as a signaling molecule in the cardiovascular system [21], NO, a free radical, is the product of the conversion of L-arginine to L-citrulline by three nitric oxide synthases (NOS). This small molecule is an important mediator in physiological as well as pathological functions, including the regulation of blood flow, thrombosis and inflammation.

NO-NSAIDs have three structural components; the conventional NSAID, the NO-donating moiety ($–ONO_2$), and a chemical spacer that links the two. The spacer as well as the conventional NSAIDs can vary providing a rather large number of possible NO-NSAIDs. Indeed, given the ease of formation of these nitrate-ester compounds, for a given spacer, the number of derivatives is almost equal to the number of available conventional NSAIDs. In the case of NO-ASA, the best studied NO-NSAID; the benzene ring of the spacer provides three positional isomers (*ortho*, *meta* and *para* with respect to the ester bond linking ASA and spacer).

The defining character of NO-NSAIDs is their ability to release NO. By using electron paramagnetic resonance, Govoni *et al* have provided direct evidence that NO-flurbiprofen, in the presence of hemoglobin, generated NO in erythrocytes [22]. Their work and that of others indicates that $–ONO_2$ undergoes 1 e^- reduction to NO_2^-, which is then either converted to NO or oxidized to NO_3^-.

Their data also revealed that NO-flurbiprofen released NO at a slower rate than nitroglycerin, which may account at least in part for the NO-NSAIDs' lack of a hypertensive effect (in contrast to organic nitrates). The proposed metabolism of NO-NSAIDs involves two steps [22-24]. First, the parent NSAID and the spacer moiety attached to the NO-donating group are released through the rapid hydrolysis of the carboxyl ester, likely catalyzed by esterases, which, as of now, have not been identified. The second step involves the release of NO, a slow process, which may proceed as described above. This biotransformation utilizes cytosolic glutathione-S-transferases found in the liver. Following the oral administration, NO-ASA (the only one studied) survives essentially intact in the stomach, with its O-deacetylated derivative being the only metabolite identified there at very low concentrations. Neither intact NO-NSAIDs nor their denitrated derivatives have been detected in the circulation [23]. Whether this explains the safety of NO-ASA remains unclear.

The safety of NO-NSAIDs

Numerous animal data as well as human studies indicate that NO-NSAIDs have very limited side effects, having, in particular, superior gastrointestinal safety[25,26]. Further clinical trials are needed to determine the full range of their side effects, as existing studies are limited in scope.

A relevant issue is whether the NO released from NO-NSAIDs can promote cancer. The background to this question is the well-known property of NO to not only inhibit carcinogenesis but also promote it, including the possibility of genotoxicity. Data from the Farmingham Heart and Offspring Study indicated that long-term use of nitrates, pharmacological agents not too dissimilar from NO-NSAIDs, did not increase the incidence of colorectal cancer [27]. The apparent safety of NO-ASA, if this is indeed proven, remains puzzling, especially since the

parent compounds, which as far as can be assessed are released during their biotransformation, can have by themselves significant toxicity.

Two critical requirements of any anticancer drug are safety and efficacy, both of which are not met by conventional NSAIDs [28]. That NO-NSAIDs may represent a promising alternative to conventional NSAIDs is mainly based on *in vitro* and *in vivo* preclinical studies. The mechanistic studies performed to date indicate that NO-NSAIDs have a fairly wide range of effects on the cancer cell, all consistent with anticancer activity. Although delineating their mechanism of action is important, what is needed the most at this stage are further clinical studies assessing their anticancer effect.

Mechanisms of action of NO-donating NSAIDs

Reported data on the mechanism of action of NO-NSAIDs against cancer can be grouped into four major categories: the structure-activity relationships (SAR), the cell kinetic effect, the effect on cell signaling pathways and effects on the redox status of the target cell.

Structure-activity studies of NO-ASA have established the roles of the acetyl group of ASA moiety, the NO-releasing moiety and its positional isomerism, and the spacer moiety for their biological effects. The best-known pharmacological activity of ASA is its ability to inhibit of cyclooxygenase (COX) through the acetylation of COX. The deacetylated analogs of NO-ASA have similar effects on cancer cell growth compared to the full molecule, suggesting that COX inactivation via acetylation is not required, at least for its *in vitro* effect [29]. One interesting aspect of NO-ASA pharmacology that is yet not fully explained is the effect of positional isomerism on cancer cell growth. The NO-donating moiety seems to play an essential role in the inhibition of cancer cell growth, but this effect depends on the position of the NO-donating group. The *ortho* and *para*

isomers have similar IC_{50}s (1-5 μM) for colon cancer cell growth inhibition, whereas the IC_{50} of the *meta* isomer is 200-500 μM. Animal studies have shown a similar but less pronounced difference in efficacy [29]. Previous studies have shown that the rate of release of NO by the three positional isomers of NO-ASA, the presence of the NO-donating group and the type of spacer are directly correlated with the ability of NO-NSAIDs to inhibit cell growth[29-31].

Interestingly, our most recent studies seem to suggest an entirely different explanation of these observations. The NO-releasing moiety of NO-ASA may not even be needed, while the spacer moiety is the moiety vital to its biological function [32]. The mechanism of action of NO-ASA seems to involve the formation of quinine methide from its *para* and *ortho* isomers and of a carbocation from the *meta*. If this is the case, the NO-releasing moiety will function only as a leaving group. However, the relevance of these findings to the overall biology of NO-NSAIDs remains to be established. Our current data and previous findings can, however, be easily reconciled by considering that the $–ONO_2$ functions as a leaving group.

The induction of apoptosis by NO-ASA appears to be a major cytokinetic effect. Gao et al. performed a detailed study of the proapoptotic effect of NO-ASA in the SW480 colon cancer cell line [30]. Enhanced levels of reactive oxygen species were found in the target cells, signifying the induction of oxidative stress. This first and crucial event is partially due to the reduction by NO-ASA of the levels of glutathione, the major antioxidant in mammalian cells. Subsequent steps included the activation of the intrinsic apoptotic pathway that culminated in cell death.

We and others have attempted to understand the enhanced potency of NO-NSAIDs by assessing their effects on potentially informative pathways. Most of these studies concern NO-ASA, which has been shown to influence MAPK, NOS, Wnt, NF-κB and COX pathways (Fig 5) [33]. According to the studies of Hundley *et al* on MAPK, the ability of NO-ASA to inhibit the growth of HT-29 colon cancer cells is dependent on both p38 and JNK (Fig 6). NO-ASA blocked

the activation of both these signaling proteins, which decreased the phosphorylation of downstream targets ATF-2 and cJun[34]. NO-ASA has also been demonstrated to inhibit the expression and the catalytic activity of the inducible form of NOS (iNOS or NOS2), an enzyme implicated in colon carcinogenesis [35,36]. Another important event, likely contributing to cell death, was and the inhibition of Wnt signaling (Fig 7). Interestingly, Wnt signaling was inhibited by a dual mechanism: inhibition at low concentrations of the formation of the transcriptionally active β-catenin/TCF complex (dominant mechanism) and cleavage of β-catenin at higher NO-ASA concentrations [30]. NF-κB, a protein dimer, acts as regulator of genes that promote cell proliferation and cell survival and such response depends on the cell type. NF-κB is constitutively expressed in most cancer cells leading to increased in cell proliferation and tumor growth[37]. NF-κB levels are inhibited by increasing levels of NO-NSAIDs. -Results regarding the COX pathway are conflicting. Williams *et al* first reported that the inhibition of COX-2 is not required for the role of NO-ASA on colon cancer cell growth [38]. A recent animal study showed that both NO-ASA and NO-indomethacin inhibited COX-1 and COX-2 activity in the colonic mucosa of azoxymethane-treated rats [36]. However, Tesei *et al* and Corazzi et al failed to observe a similar inhibition phenomenon after treatment with NO-ASA. Using two different cell lines compared to the cell lines used by Williams *et al* the induction of COX-2 by NO-ASA was observed [31]. This study was supported by experiments done by Corazzi who showed both the expression of COX-1 and COX-2.This finding was thought to be mainly due to the acetyl group of the ASA moiety with NO making at best a modest contribution [39]. These finding indicates the COX effect caries base on the type of cells and the NO-NSAID utilized for treatment. The effect of COX and cancer is further expanded below.

The various mechanistic effects of NO-ASA indicate that it modulates a large array of molecular targets. Each of these targets alone can, in theory, inhibit or suppress carcinogenesis but whether only one, all or a combination of

more than one of these effects are required to achieve the anticancer effect of NO-ASA is still unclear.

1.7 COX-2 and Cancer

One of the possible mechanisms previously mentioned underlies the association between chronic inflammation and cancer is the upregulation of the enzyme Cyclooxygenase (COX) (COX pathway: Fig.8). COX is the key enzyme that catalyzes the conversion of arachidonic acid into prostaglandins and other eicosanoids. Two isoforms of COX have been identified to date, COX-1 and COX-2. COX-1 expression is constitutively active in a wide variety of cells where its primary role involves the homeostatic production of prostaglandins, represented by balanced blood flow to the kidney and protection of the gastrointestinal tract. COX-2 expression is inducible by factors such as cytokines, growth factors and tumor promoters [40]. COX-2 expression is believed to be selectively expressed in the inflammatory response and its products are involved in pain and inflammation following injury [41]. Non-selective inhibition of COX enzymes with long-term use of nonsteroidal anti-inflammatory drugs (NSAIDs) has been shown to increase the risk of gastric ulcer and, to a lesser extent kidney failure via their inhibition of COX-1. Selective COX-2 inhibitors do not exhibit these side effects [42]. Previous studies have shown that colon produce greater amounts of prostaglandins than normal tissue derived from the same organ [43,44]. Studies have also shown that in a number of cancerous tissues such as breast, ovarian, prostate, lung, colon and pancreas, the associated tumors and cells exhibit increased COX-2 expression. Furthermore, when these cancers are treated with NSAIDs, their growth is inhibited *in-vitro* [45-52]. Additional reports have implicated COX-2 expression and Prostaglandin E_2 (PGE_2) production with increased mitogenesis, cell differentiation to malignancy, increased metastasis, decreased immune responses and decreased apoptosis as well as linking COX-2 expression with tumor angiogenesis. These findings suggest a role for COX-2 in

the development of cancer [53-58]. COX-2 expression has also been correlated to increased formation of reactive oxygen species (ROS), due primarily to the peroxidase action of COX. ROS molecules have been shown to result in increased oxidative DNA damage, which is thought to lead to tumorigenesis [59]. For cancers where COX-2 expression is specifically upregulated and is important to tumor survival and tumor progression, selective inhibition of COX-2 enzymes may prove to be beneficial in the prevention and treatment. Knockout studies of COX-2 have given credence to this theory showing that Min (multiple intestinal neoplasia) mice with homozygous COX-2 deletion have 75-80% less tumor formation than wild type Min mice. In tumors not showing COX-2 expression this may also be true as it has been shown that colon cancer cell lines lacking COX-2 are induced to undergo apoptosis with COX-2 inhibitors [60]. The use of COX-2 inhibitors in preventing colon and pancreatic cancer in animal models has shown to be quite promising. This hypothesis is strengthened by epidemiologic evidence that shows inverse relationships between intake of NSAIDs and risk of prostate, ovarian, gastric, breast, skin and colon cancer in humans. In fact, celecoxib, a COX-2 inhibitor, has been approved by the Food and Drug Administration for the chemoprevention of colon cancer in familial adenomatous polyposis patients [61].

1.8 Cox-2, NSAIDs and Apoptosis

Increased expression of the COX-2 gene is associated with increase in a number of cancer cells. Evidence suggests that these increases are not only due to enhanced cell proliferation, but also decreased death of cancer cells. The process by which most cells undergo death is apoptosis [62]. The mechanism by which COX-2 overexpression might inhibit apoptosis is still unknown. However, studies point to alterations in the bcl-2 family of proteins as the end product of increased COX-2 expression. Studies showing the overexpression of COX-2 protein, which increase inhibition of apoptosis in colon adenocarcinoma cells *in*

vitro, show statistically significant increases in expression of the antiapoptotic protein, bcl-2 [63]. It is further shown that *in vitro* administration of a COX-2 metabolic byproduct, PGE_2, leads to a 4.5 fold increases in bcl-2 expression after administration. Further, this increase expression of bcl-2 after the administration of PGE_2 is preceded by a 4 to 5 fold induction of MAPK (MAP kinase) activation leading to speculation that the MAPK pathway is involved in COX-2/PGE_2 mediated apoptosis resistance [55]. Similar phenomena are also shown *in vivo* in transgenic Min mice forced to overexpress COX-2. In addition to increased bcl-2 expression, another anti-apoptotic protein bcl-xl is upregulated and the pro-apoptotic protein bax is reduced in expression in the studies [62]. Based upon the observed findings mentioned above, it would seem most likely that NSAIDs, which block the action of the COX enzymes and hence block production of prostaglandins, the effectors of COX, bring about increased apoptosis by reducing the levels of bcl-2 and bcl-xl and raising the levels of bax. One NSAID which upregulates bax levels is indomethacin [62,64,65]. Interestingly, studies have shown that the upregulation of bax by indomethacin in some esophageal adenocarcinoma cell lines is independent of COX-2 protein expression indicating that other pathways other than the COX pathway may be affected by certain types of NSAIDs [64]. In fact, multiple mechanisms have been shown for NSAIDs increasing the level of apoptosis in cancer cells. Kinzler et al has reported on a mechanism for non-prostaglandin repression mediated NSAID induced apoptosis. In their work, two colon cancer cell lines, SW480 and HCT116, were shown to undergo apoptosis in response to the COX inhibiting drug, sulindac sulfide. The mechanism by which these cells underwent apoptosis was shown to be due to an arachidonic acid increase. The increase in arachidonic acid stimulated neutral sphingomyelinase, which converted sphingomyelin into ceramide, a known inducer of apoptosis. Ceramide levels were shown to increase up to 10 fold and this induction of apoptosis occurred in immortalized keratinocytes and primary fibroblasts treated with sulindac sulfide, however not to the degree of the colon cancer cells [66]. In another report arachidonic acid accumulation as a mechanism for apoptosis induction was also found. In this

report, increases in arachidonic acid were brought about in COX-2 expressing colon cancer cells, HT-29, by either a COX inhibiting drug, sulindac sulfide or by a triascin C, a drug which blocks the action of fatty acid CoA ligase, an enzyme that like COX, utilizes arachidonic acid. Apoptosis was induced by using either sulindac or triascin C, however in a non-ceramide increasing manner that resulted in the activation of caspase-3 [63]. Lastly, it has been reported that very high doses of NSAIDs inhibit the activity of other pathways such as NF-kappa B pathway and could bring about non-prostanoid mediated cell death in this manner [67].

1.9 Obstacles of chemoprevention

Chemoprevention is not a short term fix as the risk of cancer is ongoing. Therefore lifelong prevention and usage of any chemopreventive agent will be required to provide adequate protection[68]. There are several challenges which have to be overcome when developing chemopreventive agents. They include the bioavailability of the compound, the half-life of the compound within the body, the route of eliminations and the toxicity of the compounds. Without knowing the metabolic activity of the chemopreventive compounds it becomes difficult to determine whether there is sufficient active compound available for the desire chemopreventive effect. The lack of bioavailability is one of the leading problems in chemopreventive agents, and needs to be carefully considered when developing new chemopreventive agents. At the present there are efforts to modify natural compounds and develop better NSAIDs derivatives so that they are more biologically available within the body and delivered to their favored site of action. Another consideration in using chemopreventive agents is the potential drug-drug interaction. Many patients who have multiple medications for other conditions and drug-drug interaction can be serious leading to hospitalization even death. Therefore the need for new chemopreventive agents with effective mechanisms of action to prevent cancer is still perhaps the most urgent need in

the field of cancer prevention. It is the problem with the side effects of NSAIDs that lead to the proposal to determine the components of the compounds which are necessary for its potency and to develop new derivatives of NSAIDs for chemoprevention. Although there are numerous chemopreventive agents' studies and ongoing studies to discover better, more effective compound, the route of delivery is still a crucial stage of treatment.

Drug delivery is a method of administering the chemical compounds such as chemopreventive agents, to achieve maximum therapeutics effect to treat the disease such as cancer. In this thesis, NSAIDs are used as a tool for the treatment of cancer and incorporated in a biocompatible polymer system for controlled drug delivery.

1.10 Polymers

Polymers consist of structural or repeating units of low molecular weight small molecules covalently connected to each other to give high molecular weight compounds. The small molecules that combine with each other to form these macromolecules are called monomers. Based on their architecture polymers can be classified into linear polymers and branched polymers (Fig 9). Likewise, branched polymers can be sub-classified according to their structure into starlike, ramified, comb-like or dendrimers[69]. Polymers that consist of only one type of repeating unit are referred to as homopolymers, whereas polymers containing two different repeating units are named copolymers (Fig 10). The sequence in which two different repeating units appear gives rise to a further classification within copolymers. A copolymer in which the repeating units alternate is called an alternating copolymer, if the repeating units do not have any specific sequencing the copolymer is known as a random or statistical copolymer[70].If relative long segments of a monomer are present in a block fashion, it is termed a block-copolymer.

Block-copolymers (Fig 11) consist of at least two, covalently bound, segments or blocks of different homopolymers[71]. For instance, a triblock-copolymer can have a general form A_a-B_b-C_c, with A, B, C, being different monomer types constituting the different blocks. The subscripts a, b, and c, represents the average number of each monomer (the degree of polymerization) present in each respective block. Branched structures can also be found among copolymers. Graft copolymers are one type of branched copolymer. Graft copolymers can be considered as a special case of block-copolymers, a comb-like structure in which several blocks of homopolymer B are grafted as branches onto a main chain of homopolymer A, known as the backbone[71]. By covalently linking two intrinsically different homopolymers, i.e. hydrophilic and hydrophobic homopolymers, this gives rise to the wide variety of morphologies of Amphiphilic block copolymer. These morphological structures include micellar structures, depending on the relative volume fractions of the blocks and have the tendency to self-assembly in solution.

1.11 Aggregation of amphiphilic block-copolymers in aqueous media

Amphiphilic block-copolymers, hydrophobic and hydrophilic blocks, covalently linked together[72,73],assembly behavior in selected solvents depends on numerous factors [74-78]. It has been found that the formation of different morphologies is a function of total and relative block lengths, temperature, block (chemical) composition, type of solvent, and concentration among other variables[79-81]. One special feature of block-copolymer chemistry is that it enables the change of the chemical composition, length, and structures of the constituting blocks in order to tune the association characteristics and thus the obtained various morphologies. Although it is broadly accepted that an aqueous medium is a prerequisite for the self aggregation of low molecular weight

amphiphiles into macrostructures, this is not necessarily the case for block-copolymer amphiphiles. Many examples have been presented in which aggregation takes place in other solvents than water[82,83]. Nevertheless, the aggregates formed in aqueous solutions still pose the main interest since they closely resemble biological systems. The most interesting macrostructures obtained from block copolymers in solution are vesicles and micelles.

1.12 Vesicles

Vesicular structures are particularly interesting since they are straightforward encapsulation devices, can be used as transport systems, and protection devices for unstable substances. Vesicles in the case of lipids consist of a closed spherical bilayer[75]. Diblock-copolymer vesicles also form closed hollow spherical aggregates with bilayer walls[75], whereas triblock-copolymers self-assemble into vesicles with a more complex association, such as bilayer and stretched or spanning polymers in the membrane (Fig 14). Polymer vesicles are known for their higher stability and toughness when compared to liposomes[84].

1.13 Micelles

Simple micelles are aggregates with a core-shell structure, occurring in a given concentration range. Micelles form above what is known as the critical micelle concentration (cmc). In aqueous solutions, micellization results from the selective solubilization of the shell forming block, whereas the core is formed by the hydrophobic non-soluble block. This intermicellar chain exchange is mainly a function of the type of blocks, i.e. their relative polarity, the overall chain length, and relative block lengths[73,79]. On advantage of these types of aggregates

compared aggregates formed from low molecular weight surfactants, is that self-assembled structures based on block-copolymers show higher structural stability. Depending on the asymmetry of the constituting block copolymer, a variety of structures can be obtained. Micellar diblock structures can be classified as crew-cut micelles and star micelles[85-87]. In crew-cut micelles the relative long blocks form the core where the short ones constitute the corona, whereas star micelles have their cores filled with the short hydrophobic chains, and coronas formed by the long hydrophilic ones (Fig 12). In the case of triblocks with hydrophobic middle block, normal micelle structures are formed. However, for triblocks with hydrophobic side chains, flower-like micelle structures are observed as shown in Fig 12). These different structural assemblies are useful for encapsulation of labile molecules.

1.14 General concept of encapsulation

Encapsulation of labile molecules is an important technology field found in many areas of chemistry, pharmaceutics, and biotechnology. Different strategies have been developed and established as encapsulations units' i.e microspheres, microcapsules, nanoparticles and liposomes. Nevertheless, it is still a challenge for scientists to design and to fabricate micro- and nano-containers for various substances with the desired storage, release, and stability properties required for each specific application, therefore this research field for the purpose of drug delivery is in constantly active.

1.14 General concept of drug delivery

The concept behind drug delivery is to provide more constant concentrations of a drug to the organism, and to bring the compound with pharmaceutical activity directly to the site of need in order to enhance the effectiveness of action. One way to bring the active substance to the site of action is to modify their bio-distribution by entrapping them in particulate drug carriers such as nanospheres, nanocapsules, or liposomes[88]. The need for encapsulation lies in the instability of many drugs, and in some cases it can improve the bioavailability of the therapeutic compounds. By using drug carriers or delivery systems are the poor solubility of some drugs, which may be enhanced by choosing the right “carrier”. For hydrophobic meolecules/drugs, usually micellar systems are used since the hydrophobic molecules/drugs will solubilize in the micellar cores. By encapsulating drugs in designed carriers, labile drugs are protected from the hostile conditions that they might encounter for instance at the low pH of the stomach. Furthermore, in many cases adsorption can be enhanced and side effects of therapeutic compounds can be minimized. Within the concept of drug delivery two mechanisms must be taken into account to design such carrier systems, site directed drug delivery and sustained or controlled drug delivery. Site directed or targeted drug delivery occurs when the drug, with the aid of a carrier is delivered to a specific site or organ. Whereas, controlled drug delivery takes place when a polymer, whether natural or synthetic, is combined with a drug or therapeutic agent in such a way that the active agent is released from the material in a pre-designed fashion. Additionally, the release can be externally triggered by environmental events or devices.

1.16 Drug delivery based on liposomes

One exhaustively explored research area in the field of drug delivery, controlled drug delivery and targeted drug delivery is the use of liposomes as carriers for hydrophilic drugs [84,89]. The interest in liposomes as carriers of molecules was based on their potential to enclose and protect different materials of biological interest and to deliver them, functionally intact and in significant quantities to the interior of many cell types. Two mechanisms are basically used to deliver the substances when using liposomes, a general mechanism of membrane fusion and the more specific receptor mediated endocytosis. Nevertheless, in many instances, the use of liposomes proved to be inadequate[89-91]. One of the main limitations of liposomes is their storage instability which leads to leaking of the encapsulated material. By combining liposomes with hydrophilic polymers, more stable systems could be obtained, such as “Stealth liposomes[92,93]. In these systems, liposomes are covalently attached to PEG chains and helps prolonging the circulation times.

1.17 Polymer based drug delivery systems

Since the use of liposomes as drug delivery systems are plagued with some technical limitations, the need to find new and more stable systems has increased and new preparation methods for drug delivery units are continoulsy being developed. Several systems have been tested within the last decade or so, mainly consisting of polymeric drug carriers[94-96]. Similar to liposomes, polymeric carriers could provide a protective environment for labile molecules to deliver them intact to desired targets. Parameters of the polymeric carriers such as size, surface charge, membrane fluidity and stability, presence of coupling groups on the surface can be used to design the carrier to be adapted to a wide range of

experimental conditions. The use of polymeric carriers for drug delivery brings several advantages; one of which is the control release of the labile molecule.

1.18 Controlled-release systems

Controlled drug delivery is one of the most rapidly developing areas of medical technology. It is aimed at obtaining enhanced effectiveness of the therapeutic treatment by minimizing both under- and over-dosing. It offers numerous advantages compared to conventional dosage forms including improved efficacy, the enhancement of the activity of labile drugs protect the labile drug against hostile environment, reduced toxicity, and improved patient compliance and convenience[88,97,98]. For example, in the field of chemotherapy treatment of cancer, a conventional method involves the systemic administration of anti-cancer drugs to kill cancer cells. This exposes the entire body to the drug and usually results in severe side effects. Controlled drug delivery provides a method to deliver anti-cancer drugs only to cancer cells. This increases the local drug concentration at the tumor, yet maintains a low concentration in the whole body, thus reducing toxic side effects.

Controlled-release systems can be classified according to the mechanism that controls the release. Three types of processes are involved in the delivery of substances from a carrier system: diffusion, degradation, and swelling followed by diffusion or a combination of processes. The most common release mechanism is diffusion. Controlled-release based on diffusion takes place when a compound diffuses through the delivery system, usually a polymer system. The type of polymer system dictating whether macroscopic diffusion occurs is usually a polymer matrix containing pores. On the other hand, diffusion can also occur between the polymer chains. These types of delivery systems are the simplest ones in the sense that the polymer matrix does not undergo any changes in the

body, when this happens the system is known as stimuli-responsive. Swelling-controlled release systems are initially dry and, when in contact with body fluids will swell. Consequently, in the case of nanospheres, the swelling increases the pore size of the matrix and promotes the diffusion of the active agents into the bulk medium.

One property that is desirable in control release system is their ability to degrade. Biodegradable polymers are of great interest since these materials are processed within the body under biological conditions giving degraded sub-units that are easily eliminated by the normal pathways of excretion. In most cases, hydrolysis is the degrading reaction which produces smaller and biologically acceptable by-products. Mainly two types of degradation exist: uniform hydrolysis throughout the matrix and surface degradation, or erosion[95]. The last process results in a release rate that is proportional to the surface area of the particle. The most commonly used biodegradable polyesters are poly (lactic acid) (PLA) and poly (glycolic acid) (PGA), and especially their copolymers poly (lactic-co-glycolic acid) (PLGA), their degradation is controlled by both drug diffusion and polymer erosion[99].

More sophisticated features can be introduced in the control release drug delivery systems in order to obtain systems that might deliver the active substance by responding to changes in the environment. These systems are then collectively known as environmentally- or stimuli-responsive systems, and can be designed in such a way that they are incapable of releasing the encapsulated material until it is placed in an appropriate biological environment. Other features of a polymer can be used to externally trigger the drug delivery system, such as changes in pH, temperature, or ionic strength[80,84,100-103]. These systems are usually termed intelligent or environmentally stimulated systems. One additional requirement of these triggered systems is that the structural changes are reversible and repeatable upon additional changes in the external environment.

Amphiphilic copolymers, such as Pluronic, are polymers that have a hydrophobic (water repelling) part and a hydrophilic (water attracting) part on the same molecule. They can self–assemble to core-shell structures in aqueous solutions and thus form micelles[79,98,104]. The hydrophobic core of the polymeric micelle can trap hydrophobic drugs, while their hydrophilic shells make the micelle soluble and decrease the rate of clearance from the blood. The release of the drug from theses micelles can be achieved by exposure to stimuli such as ultrasound [84], thus providing a mechanism by which the drug can be deposited at the desired place and desired time. Polymeric micelles dissolve if their concentration drops below the critical micelle concentration (CMC), which is defined as the concentration at which micelles form at a given temperature; thus most non-stabilized micelles would dissolve into individual polymer molecules quickly when injected into the blood and therefore no longer retain hydrophobic drugs. Drug delivery systems that dissolve, degrade, or are readily eliminated are preferred.

This dissertation research focused on developing a stable polymeric micelle system using a triblock copolymer, Pluronic F127, which may be externally thermally regulated.

1.19 Pluronic

Pluronic is a trade name (BASF Corporation) of a family of nonionic polymer surfactants with the structure containing poly (ethylene oxide)-poly (propylene oxide)-poly (ethylene oxide) (PEO-PPO-PEO), as shown in Fig 15. Pluronic is formed by first polymerizing the moderately hydrophobic PPO middle segment to the desired molecular weight. Ethylene oxide is finally polymerized onto both hydroxyl ends to form the flanking hydrophilic blocks. Pluronics are widely used by industry as de-foamers, surfactants and cleansing agents.

Both polymer blocks of Pluronic, PEO and PPO, are lower critical solution temperature (LCST) polymers. The LCST of PPO is around 10℃, and it is insoluble in aqueous solutions at room temperature[105]. The LCST of PEO is around 100℃. Pluronics are amphiphilic at temperatures between the LCST of PPO and PEO, and thus they may form spherical micelles in this temperature range at concentrations higher than their CMC. When the temperature of Pluronic aqueous solution approaches the LCST of PEO, the micelle undergoes a sphere-to-rod transition before finally forming a macroscopic gel and precipitating out from the aqueous solution, and exhibit thermo-reversible properties.

At low concentrations, Pluronics exist in aqueous solutions as individual Pluronic chains. As concentration is increased, Pluronic polymers undergo a transition from individual chains to loose aggregates interpenetrated with water to dense micelles that almost entirely exclude water [106-108]. This transition from individual chains to dense micelles occurs over a concentration range of an order of magnitude or more. At higher concentrations (typically >20 %wt), a “gel” region appears. The viscosity in Pluronic micelles is much higher than that observed in conventional surfactant micelles and depends strongly on the size of the hydrophobic PPO block. The larger the PPO block, the higher the viscosity[109].

In pharmaceutical applications, Pluronic has been found to be a suitable drug carrier because of its amphiphilic nature and low toxicity[97,108]. Anderson et al. report at low temperatures, some types of Pluronic solutions containing drugs are liquid that can be injected into the body [97]. At higher temperatures, but lower than body temperature, the micelles, into which hydrophobic drugs can dissolve, will form. At body temperature, the micelles can subsequently undergo transition to the gel state, and thus the release rate of anti-cancer drugs is reduced. This may allow for a simple method of targeting drug release to a specific location in the body, while keeping the drug within the micelle when a stimulant is not present.

The major problem of using Pluronic micelles as a drug delivery system is that the polymer concentration will decrease when injected into the body because of dilution in the blood circulation. When the concentration of polymer drops below the CMC, the micelle dissolves and the drug inside the micelle will be released immediately.

1.20 Research Objectives

The overall goal of this research was to design and investigate several NSAIDs derivatives to evaluate their structural requirements for potential chemopreventive agents. And finally to design new polymeric hydrogel stystem that allows for the control release of chemopreventive agents. The overall goal was divided into the following three objectives:

1. To determine the pharmaco-dynamics and pharmaco-kinetics of NO-NSAIDs, one of the well known NSAID derivatives

2. Investigation the structural requirements of NSAID derivatives for its anti cancer effect

3. Design, develop and evaluate a new implantable drug delivery system using the photo-cross-linked Pluronic F127 hydrogel

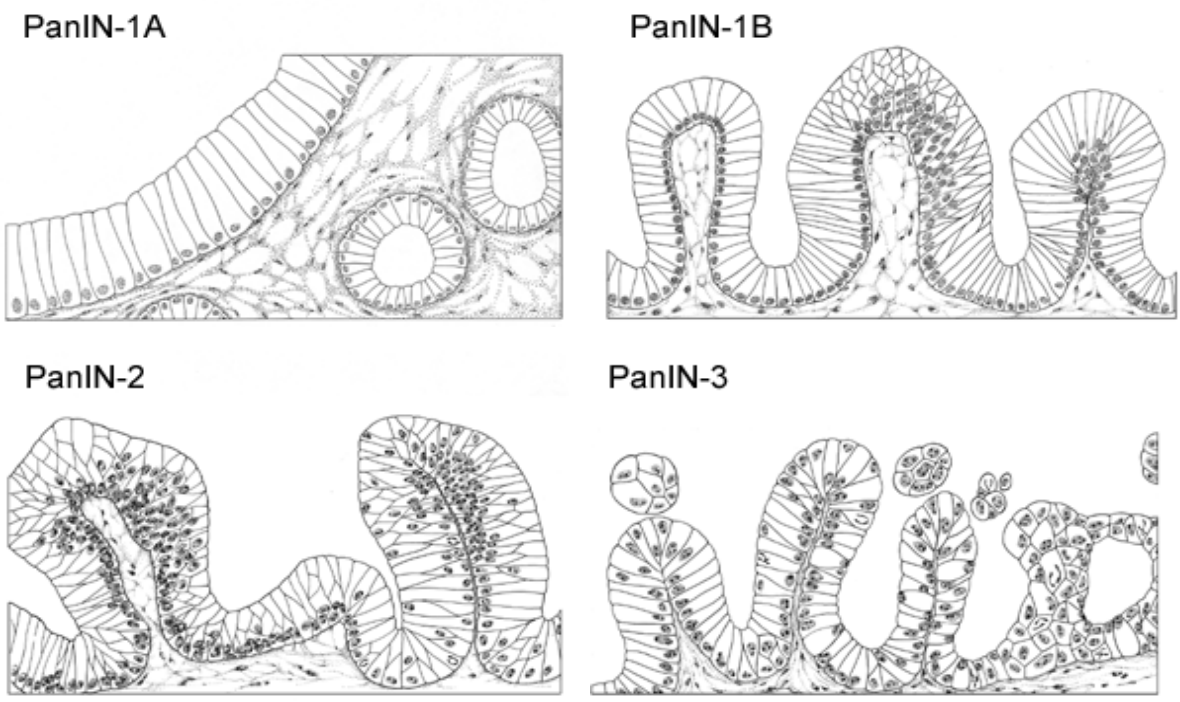

Figure 1. Progression model of pancreatic cancer[4]

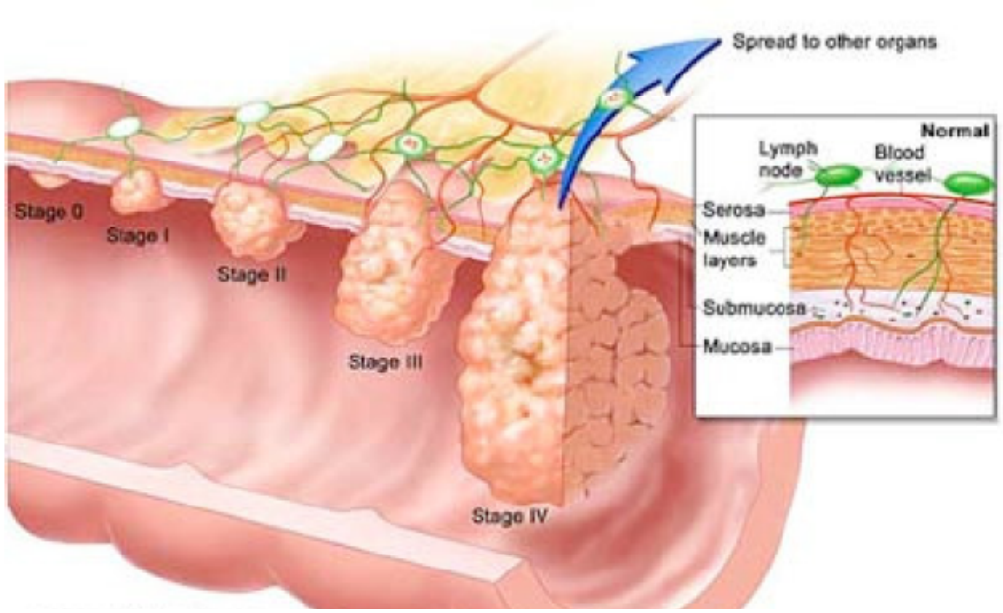

Figure 2. Progression model of colon cancer[8]

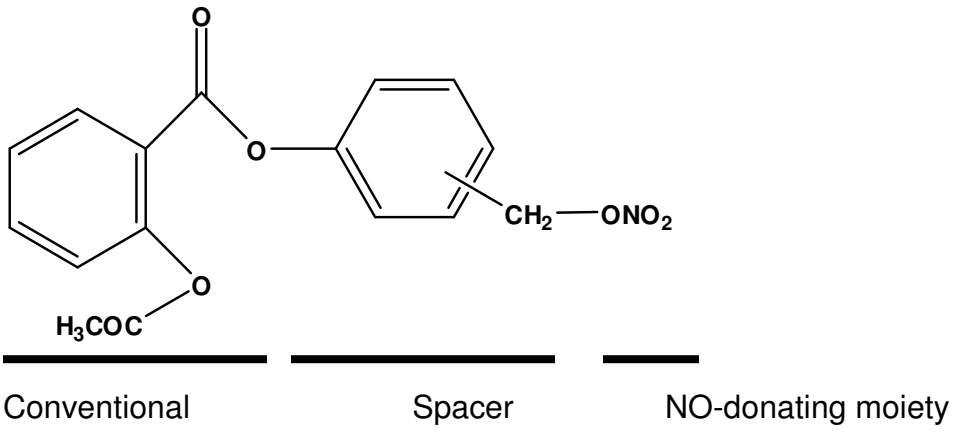

Figure 3. Structure of NO-NSAIDs illustrating the three components of NO-NSAIDs.

Conventional NSAID Spacer NO-releasing group

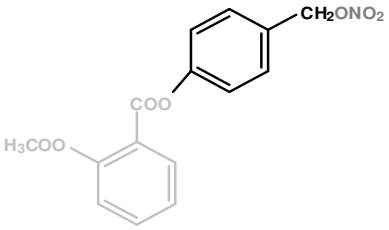

NO-Aspirin

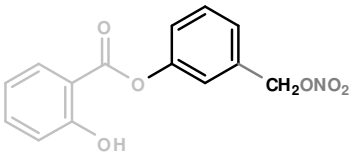

NO-Salicylic acid

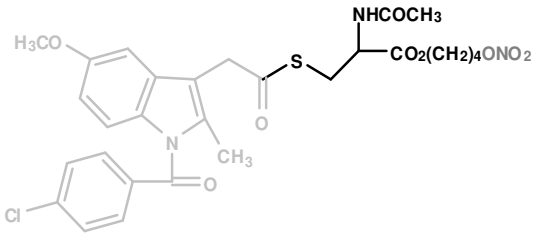

NO-Indomethacin

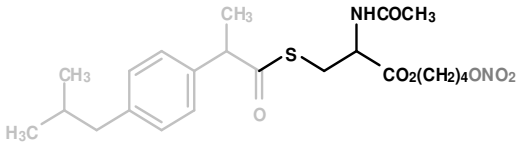

NO-Ibuprofen

Figure 4. Chemical Structures of NO releasing -NSAIDs and conventional NSAIDs[110]

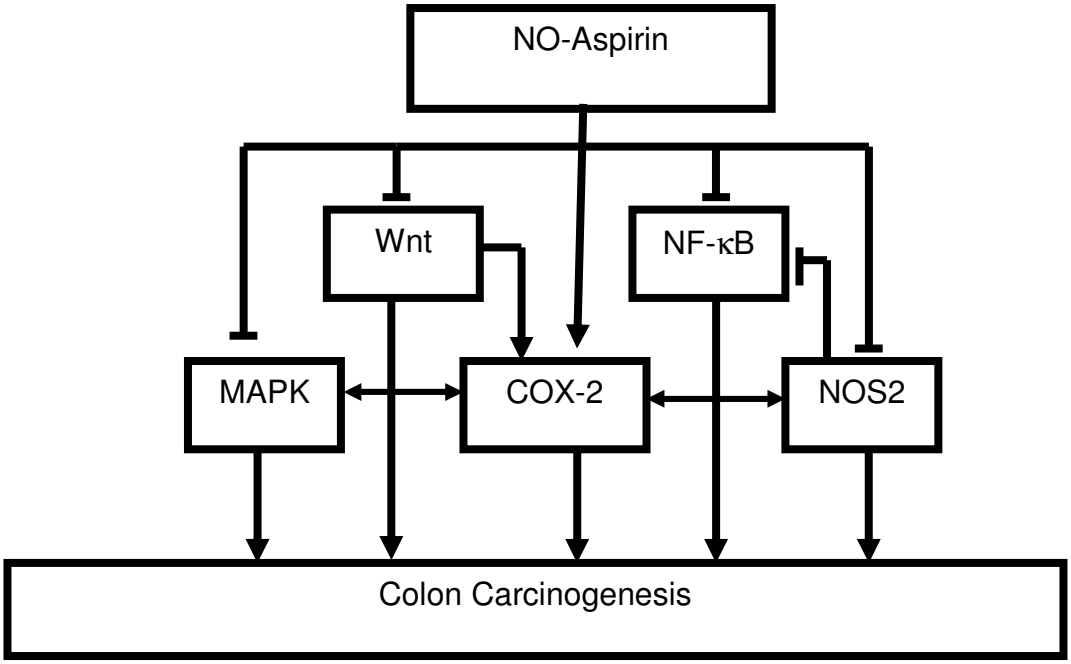

Figure 5. Model of the effect of NO-ASA on Molecular targets of Colon Carcinogenesis

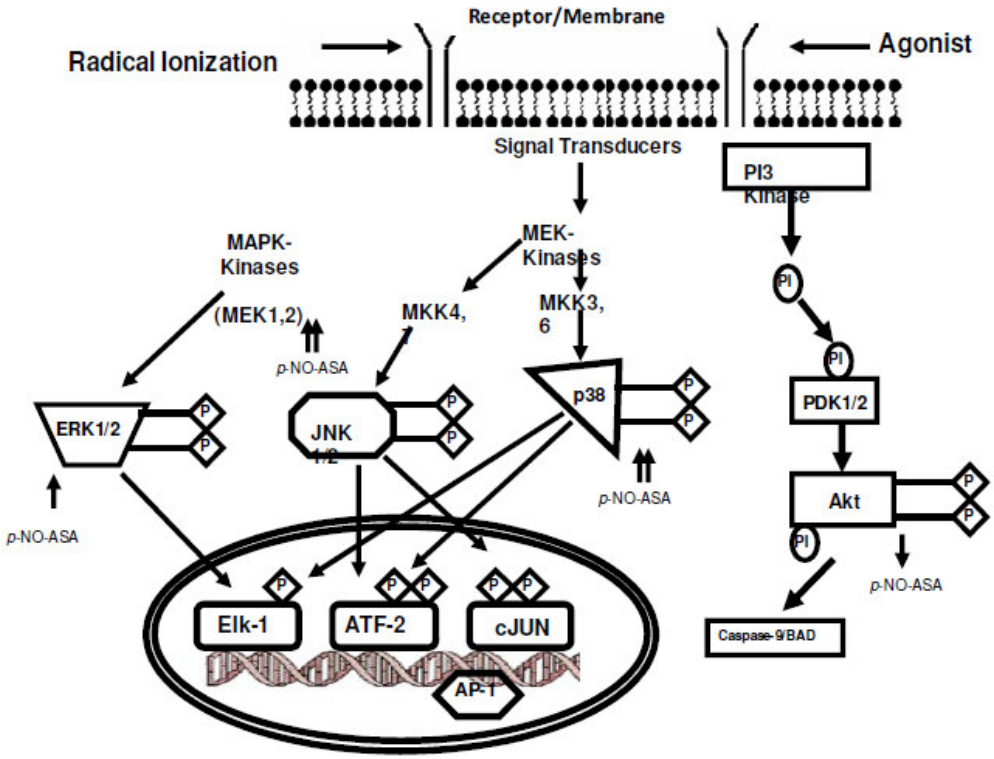

Figure 6. Model of the signaling effect on Molecular targets of Colon Carcinogenesis

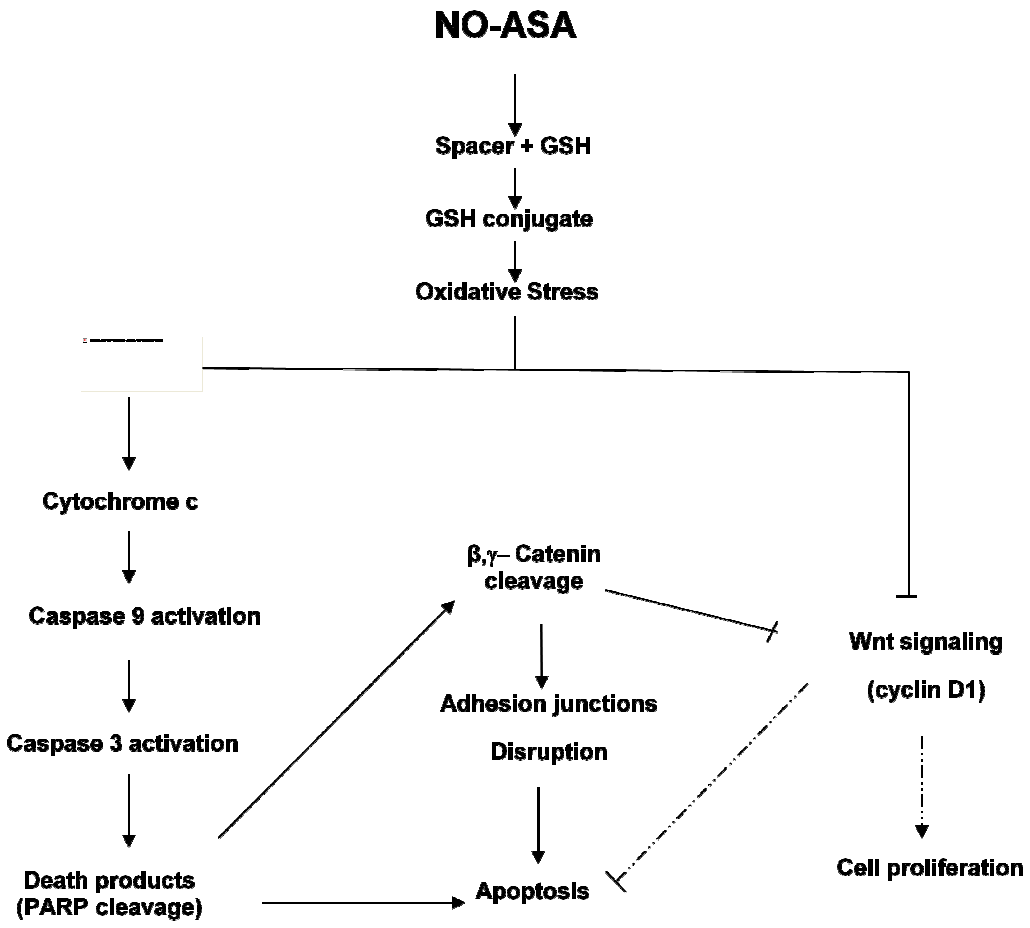

Figure 7. Model of the effect of NO-ASA on Enhanced levels of Reactive Oxygen species due to the induction of Oxidative Stress

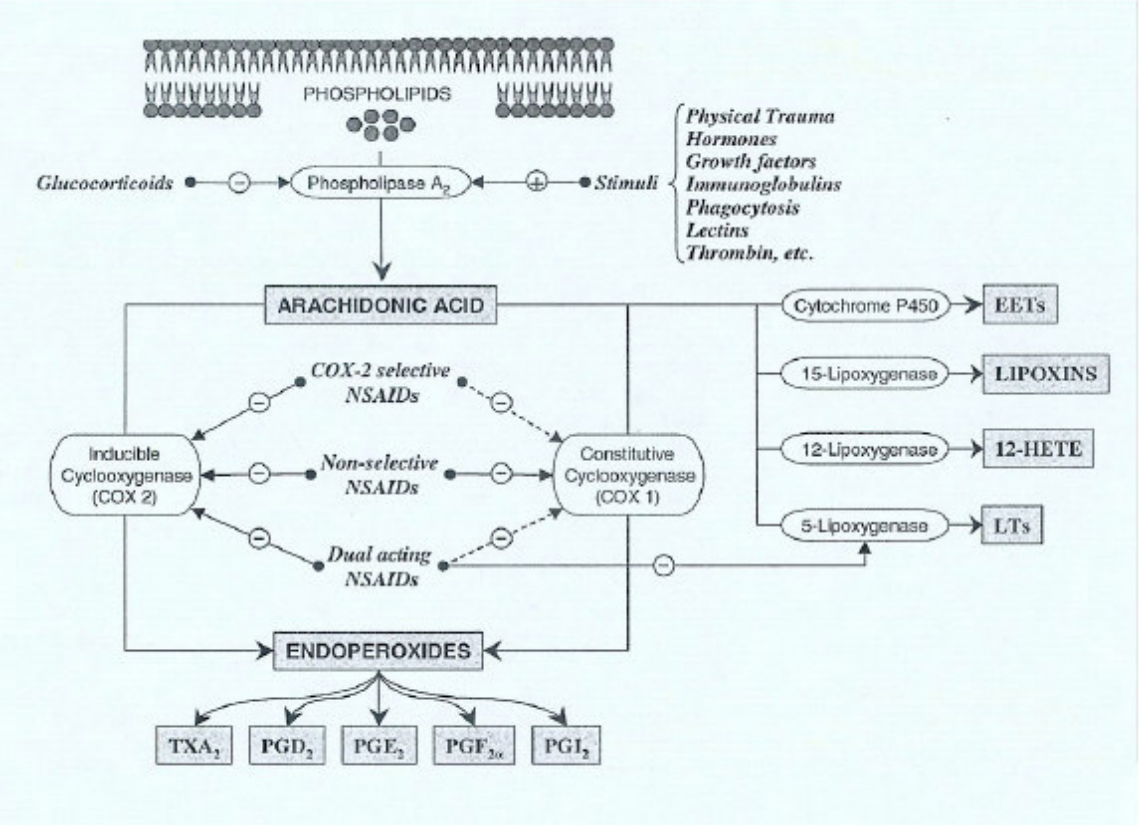

Figure 8. An Overview of the Cyclooxgenase Cascade. Pictured above is the pathway from which arachidonic acid s converted into mediators of inflammation, specifically prostaglandins, thromboxanes and leukotrienes. As seen, the non-steroidal anti-inflammatory drugs are able to block this cascade by inhibiting the conversion of arachidonic acid into downstream products via their inhibition of the cyclooxygenase enzymes. (Table from Bertolini et al. 2001 (188)).

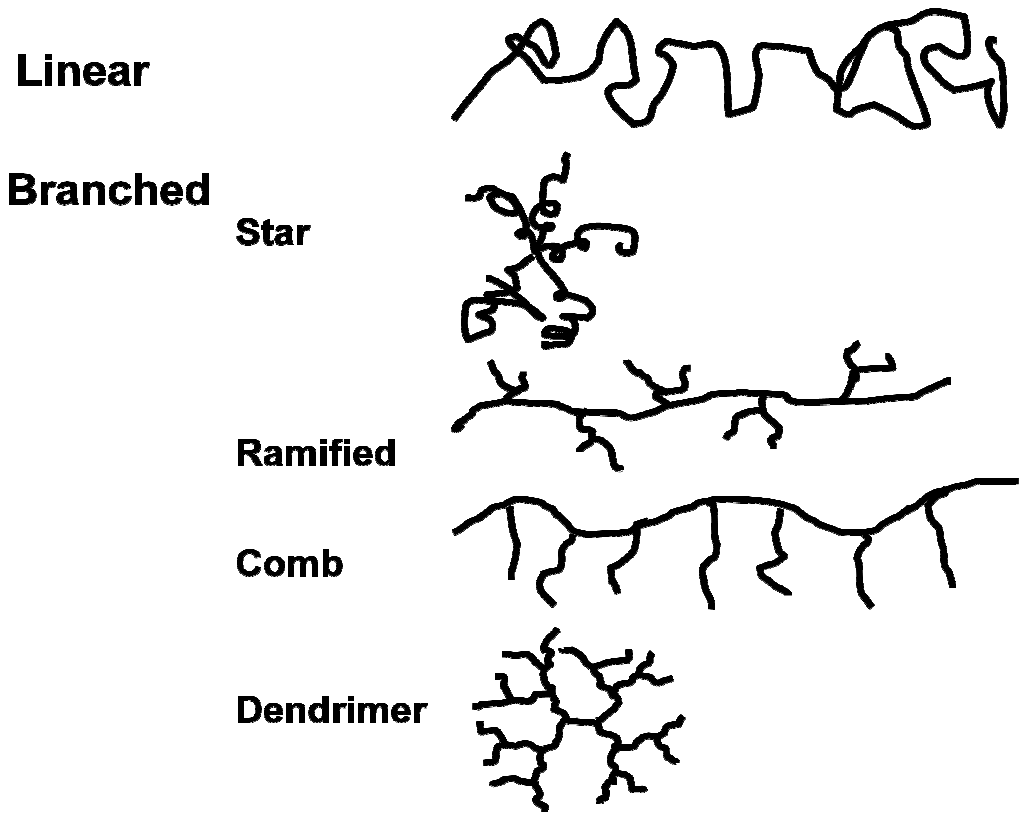

Figure 9. Representation of the different types of homopolymer architecture

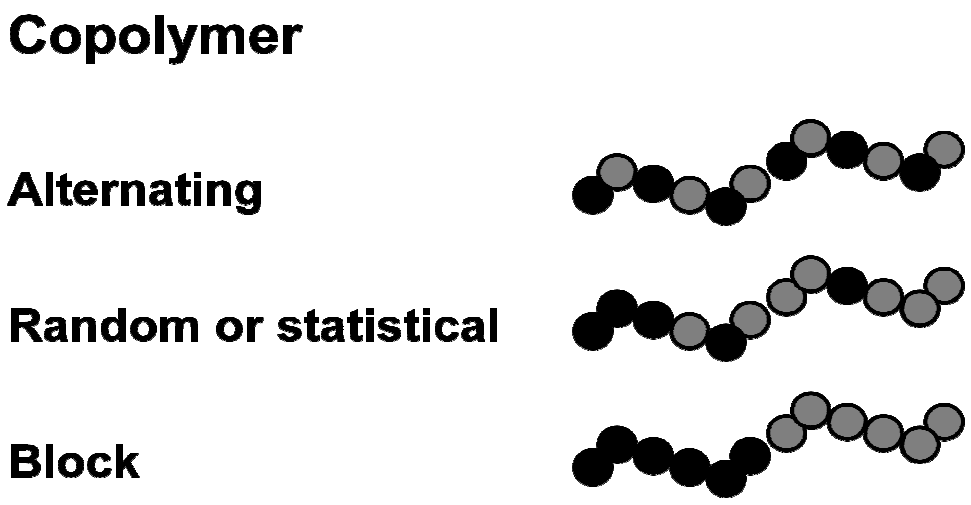

Figure 10. Representation of linear copolymer

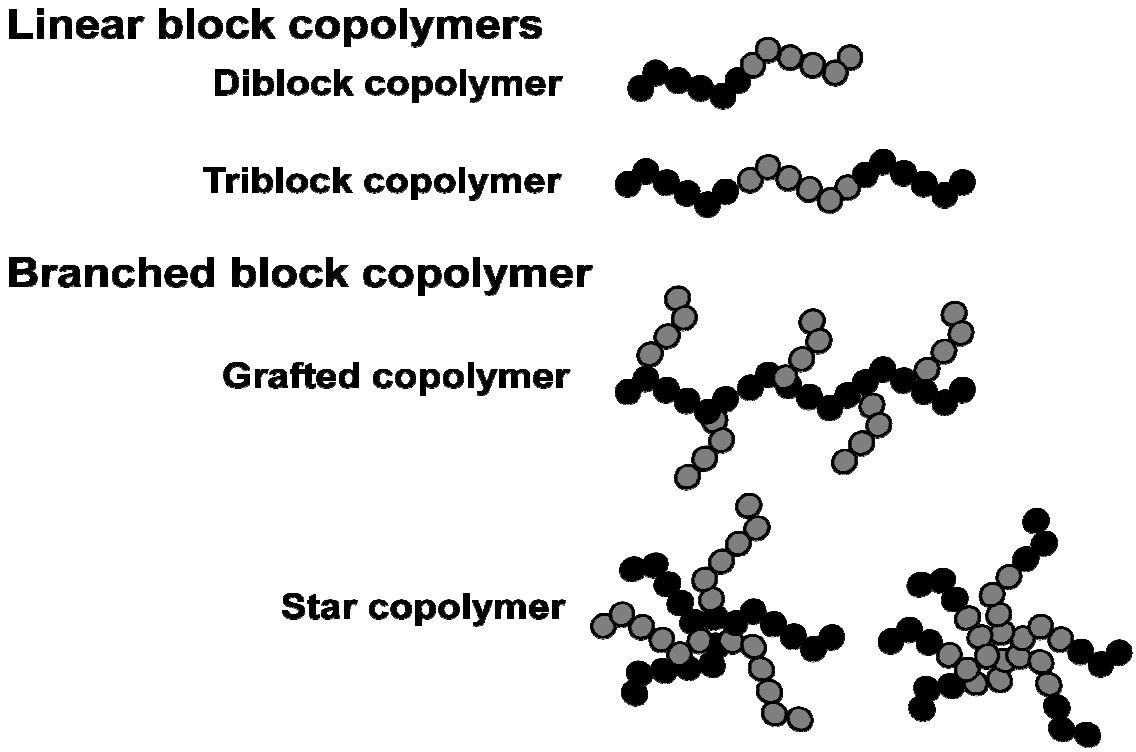

Figure 11. Representation of different architectures of block-copolymers; linear diblock, triblock, star, and graft copolymer

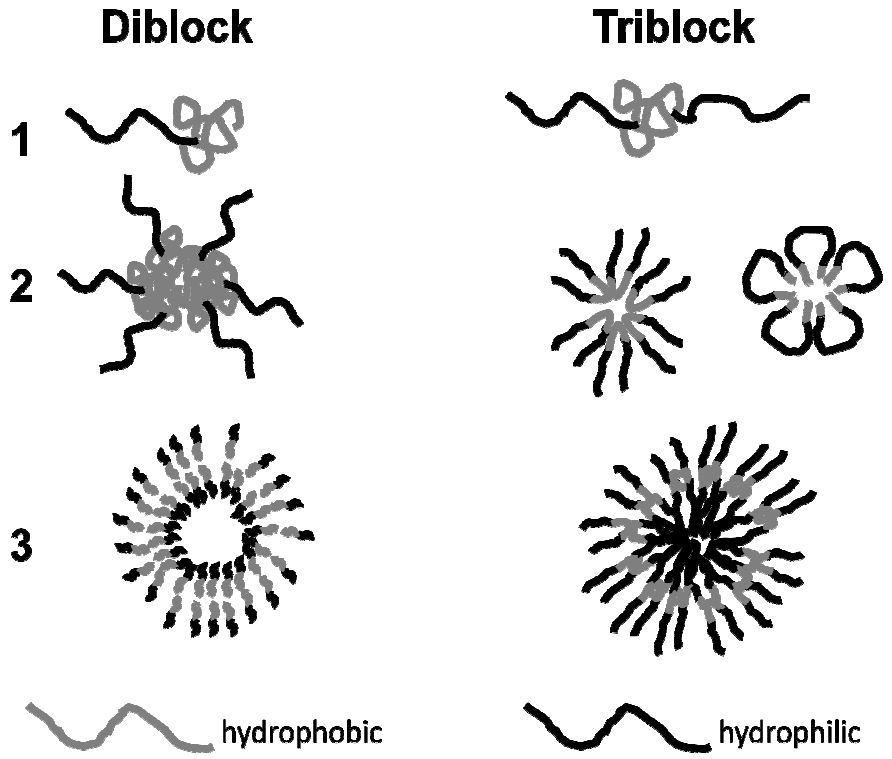

Figure 12. Schematic representation of: 1) di- and triblock copolymer, 2) star micelle (diblock-copolymer) and normal (ABA) and flower-like (BAB) micelles (triblock-copolymer), 3) vesicle formation for a diblock and triblock-copolymer

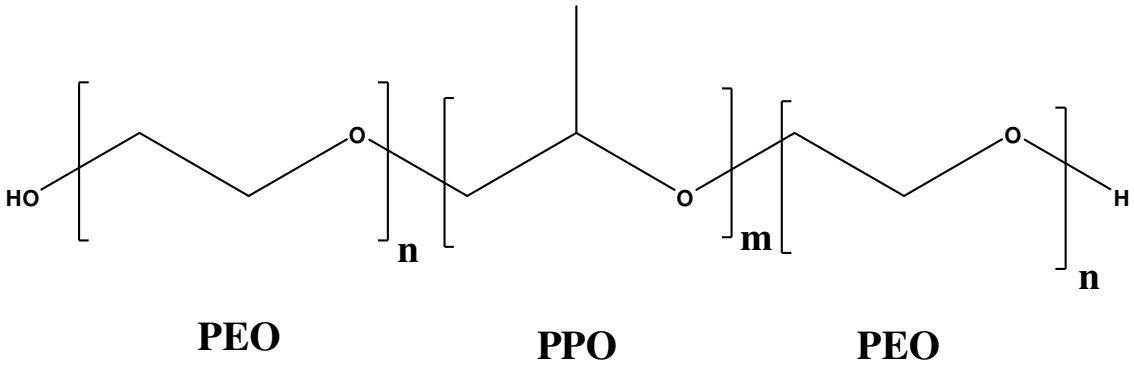

Figure 13. General Structure of Pluronic. Pluronic consists of locks of PPO and PEO. n and m represents the number of blocks of PEO and PPO, respectively

Chapter 2. Pharmacokinetic and pharmacodynamic study of NO-donating aspirin in F344 rats

2.1 Introduction

NO-donating aspirin is the best studied member of an emerging class of compounds, the NONSAIDs, which hold significant promise as chemopreventive agents against colon and other cancers[111]. NO-ASA consists of an aspirin molecule which has been covalently modified to contain a NO-releasing moiety. Extensive preclinical data both *in vitro* and *in vivo* indicate that NO-ASA is a pleiotropic agent that may bring about its chemopreventive effect by modifying multiple signaling pathways in the preneoplastic cell, including inhibition of proliferation, induction of apoptosis and inhibition of cell cycle phase transitions.

Certain aspects of NO-ASA pharmacology and its effects on the eicosanoid cascade remain, however, unclear. It has been previously shown that while NO-ASA induces the expression of COX-2 in colon cell lines, it inhibits the production of eicosanoids by intestinal mucosa in rats[37,112]. NO-ASA's effect on PGE_2 and TxA_2 production is of particular importance since PGE_2 is considered a mediator of carcinogenesis [113,114], whereas TxA_2 is critical to vascular tone and platelet aggregation, both significant parameters of vascular physiology[115]. At present, it would appear that NO-ASA traverses the low pH environment of the stomach intact, followed by progressive deacetylation and hydrolytic cleavages at its salicyloyl ester and/or benzyl nitrate ester bonds[116-119]. The exact stage of NO release remains unclear, but it seems to be tightly linked to these biotransformation; esterases are likely involved in its hydrolytic cleavage[120]. To date no complete pharmacokinetic and pharmacodynamic study of NO-ASA has been reported. Therefore, we undertook the present study to assess both its

pharmacokinetics and its pharmacodynamic effect on the levels of PGE_2 and TxB_2 in tissue and plasma (TxB_2 is the spontaneous degradation product of TxA_2 and reflects the levels of TxA_2 accurately). In our study, NO-ASA was administered either by oral gavage or admixed with their diet, thus assessing two commonly employed methods of drug administration to experimental animals.

Here, we describe the pharmacokinetics of NO-ASA in rats and document its significant suppressive effect on PGE_2 levels in colon tissue and plasma and its suppressive effect on plasma TxB_2 levels.

2.2 Experimental Methods and Materials

Animals, diets, NO-ASA

Weanling male F344 rats were from Charles River Breeding Laboratories (Kingston, NY). NO-ASA (NCX-4016; meta positional isomer) was provided by the NCI's DCP repository. The purity of NO-ASA, ascertained by HPLC analysis, was ≥98%. All ingredients of the semi-purified diet (Bioserv, Frenchtown, NJ) were stored at 4°C prior to its preparation. The composition of the modified AIN-76A semi-purified diet was as follows: casein, 20%; DL-methionine, 0.3%; corn starch, 52%; dextrose, 13.2%; alphacel, 5.0%; corn oil, 5.0%; mineral mix, 3.5%; vitamin mix, 1.0%; and choline bitartrate, 0.20%. NO-ASA was incorporated into the diet with a Hobart mixer; its uniform distribution in the diet was monitored as described [121]. Control and NO-ASA-containing diets were prepared weekly in our laboratory and stored at 4°C. NO-ASA was stable in the diet under our experimental conditions, as determined periodically in multiple samples by HPLC; recoveries from the diet were >96%.

Experimental design

At seven weeks of age, 144 male F344 rats were randomized into 9 groups [16 rats/group (Table 1)] and fed the AIN-76 modified control diet. At eight weeks of age groups 2–5 were administered four different doses of NO-ASA (33, 66, 132 and 264 mg/kg) by gavage for two weeks. NO-ASA was dissolved in corn oil every day prior to its administration to rats by gavage. At eight weeks of age, groups 6–9 were fed for 2 weeks diets containing 350, 700, 1,400 and 2,800

ppm NO-ASA. The control group (Group 1) received no NO-ASA and was fed only AIN-76 modified control diet. Body weights were recorded twice weekly. All animals were examined daily for signs of toxicity. Rats were sacrificed 2 and 10 h after completion of the two weeks of treatment with NO-ASA either by gavage or through their diet. At each of these two time-points rats were bled and plasma was harvested after centrifugation. All rats were necropsied and the colonic mucosa was harvested by scrapping the mucosal epithelial layer with a glass slide at 4℃. Plasma and mucosal samples were stored at –80℃ until analyzed.

Reagents

Phosphoric acid, aspirin (ASA), salicylic acid (SA) and acetonitrile were purchased from Sigma-Aldrich Chemical Co. (St. Louis, MO). All general solvents and reagents were of HPLC-grade or of the highest grade commercially available.

HPLC analysis

A Waters 2690 series HPLC System with a HP (G1314A) UV absorbance detector and a LiChrospher C8 reverse-phase column (250×4.6 mm; particle size 5, Alltech Inc., Beerfied, IL) with a manual sample injector was used to analyze metabolites of NO-ASA. The column was maintained at room temperature. Buffer A consisted of water-acetonitrile-phosphoric acid (9:1:0.01, v/v/v); Buffer B consisted of acetonitrile. The flow rate was 1 ml/min. We applied gradient elution from 100% buffer A to 60% buffer B from 0 to 30 min; it was maintained at 60% buffer B until 43 min, becoming 100% buffer B at 50 min. The linearity and recovery of the method regarding salicylic acid were assessed; salicylic acid was

the major metabolite of NO-ASA detectable in plasma. The response was linear between salicylic acid concentrations of 19.3 and 483.1 μg/ml (R2 = 0.9996); the recovery (defined as: Recovery = Detected Salicylic Acid ÷ Actual Salicylic Acid × 100)% was complete.

Eicosanoid assays

0.7–0.9 g of tissue samples were sonicated in homogenization buffer (0.1 M phosphate, pH 7.4, containing 1 mM EDTA and 10 μM indomethacin) and 500 μl of plasma samples were used for the analysis. Several samples were spiked with tritium-labeled PGE_2 and all samples were purified in accordance with the manufacturer's protocol (Prostaglandin E_2 EIA Kit Monoclonal/Thromboxane B_2 EIA Kit; Cayman Chemicals, Ann Arbor, MI). All purified samples were stored at −80°C until assayed. TxB_2 and PGE_2 concentrations were measured directly by the enzyme-linked immunosorbent assay (ELISA) kits according to the manufacturer's directions. Sample and standard dilutions were made with experimental medium.

Statistical analysis

Experimental values were expressed as mean ± SEM. Differences between mean values were evaluated using Student's t-test and the association between variables was determined using regression analysis; $p<0.05$ was considered statistically significant.

2.3 Results

2.3.1 Pharmacokinetic results

In agreement with previous findings [120], the most prominent and consistently detectable peak in the HPLC chromatograms was that corresponding to salicylic acid. Shown in Table 2 and Fig. 14 are the concentration of salicylic acid in plasma at 2 and 10 h post-dosing. At either time point, no intact NO-ASA was detected in the plasma, which is in line with the findings of Carini *et al* [117,118]. The higher the dose of NO-ASA, whether by gavage or through diet, the higher the salicylic acid levels; this was true for both time-points. The ratio of the salicylic acid level between the highest and the lowest drug intake ranged between 3.74 and 4.93. Thus, at every level of NOASA intake, gavage produced consistently higher plasma salicylic acid levels at both time- points. The ratios of plasma salicylate levels between gavage and diet for each corresponding level of NO-ASA were always >1 (range 1.33–2.76).

In all instances, the highest salicylic acid levels occurred at 2 h. By 10 h salicylic acid levels were substantially lower than those at 2 h. For gavaged animals, the 10 h levels were on average 83% (range 75.22–90.77) of those at 2 h. For animals receiving NO-ASA admixed with their diet the corresponding value was 56.67% (range 44.21–63.12). In all instances the levels of the diet groups were lower than those of the gavage groups. Specifically, the 10 h salicylic acid levels of the diet group were on average 68.27% (range 58.77–74.65) of those of the gavage group.

2.3.2 The effect of NO-ASA on colon tissue and plasma levels of PGE_2 and TxB_2

As summarized in Table 3 and Fig. 15, NO-ASA inhibited strongly the levels of PGE_2 in colonic tissue in a manner that was: a) dose-dependent, b) time-dependent, and c) administration route-dependent. Compared to controls, the colon tissue levels of PGE_2 at 2 h in the gavage groups were decreased progressively from 53.78 at the lowest NO-ASA dose to 77.89% at the highest (average 66.49%). At 10 h the corresponding values were 48.74 and 68.75% (average 63.57%).

The diet groups displayed a similar pattern wherein the PGE_2 colon tissue levels at 2 h decreased between 29.52% for the lowest NO-ASA dose and 58.45% at the highest (average 43.18%) and at 10 h between 26.63% and 60.18% (average 49.18%). In all instances the values for the gavage group were significantly lower than the corresponding values for the diet group. On average, at 2 h the PGE_2 levels of the gavage groups were lower by 35% compared to diet groups and 27% at 10 h. The apparent association between NO-ASA dose and the suppression of colon tissue PGE_2 levels is statistically significant ($p<0.001–0.05$ for all except for gavage at 10 h where it is significant for trend).

As shown in Table 4 and Fig. 16, the inhibitory effect of NO-ASA on tissue levels of PGE_2 was also observed in plasma PGE_2 levels. Gavaged NO-ASA reduced plasma PGE_2 levels dose-dependently. This reduction at 2 h was 17.1% at the lowest dose increasing to 97.61% at the highest (average 48.39%) and correspondingly at 10 h, 9.66 increasing to 77.26% (average 53.87%). PGE_2 plasma levels were also inhibited in those groups receiving NO-ASA through the diet. At 2 h this reduction went from 30.5% for the lowest dose to 83.3% for the highest (average 56.94%) and at 10 h from 70.4% to 79.28% (average 46.38%). In all cases, the degree of association between the dose of the drug and the levels of PGE_2 was statistically significant ($p<0.001–0.05$). The levels of salicylic acid correlated with the levels of PGE_2 in colon tissue, the target tissue for its

chemopreventive effect. As shown in Fig. 17, there is a statistically significant inverse association ($p<0.05$) between salicylic acid levels and PGE_2 levels at both 2 and 10 h, suggesting that it was indeed the NO-ASA treatment that brought about the suppression of the PGE_2 synthesis in the colon.

NO-ASA also had a significant inhibitory effect on plasma levels of TxB2 (Table 5 and Fig. 18). As was the case for PGE_2, suppression of TxB_2 plasma levels was both dose- and time-dependent. NO-ASA decreased TxB_2 levels in the gavage group on average by 68.3% at 2 h and by 33.4% at 10 h. The diet group displayed similar responses: 61.8% average reduction at 2 h and 35.8% at 10 h. It is of interest that the levels of TxB_2 were nearly completely suppressed at the two highest NO-ASA doses at 2 h (below our analytical methodology). In general, NOASA administered through the diet was less effective in suppressing plasma TxB_2 levels than when given by gavage

2.4 Discussion and Conclusion

The findings presented here demonstrate that in rats NO-ASA undergoes metabolic transformations similar to those previously described in rats[117], humans[118], rat liver[116] and in cultured cells[119], regardless of its route of administration. The results also demonstrate that NO-ASA has a significant and unambiguous *in vivo* inhibitory effect on the metabolic transformations of arachidonic acid via the cyclooxygenase pathway.

There are three notable findings from our pharmacokinetic study. First, no intact NO-ASA was detected in plasma examined at 2 and 10 h post last dosing. Second, NO-ASA is rapidly metabolized, producing predominantly salicylic acid. Both findings are in close agreement with studies previously reported by us and others on the metabolic fate of NO-ASA[37,111,112]. Third, the route of administration of NO-ASA has a significant effect on the plasma levels of its main metabolite, salicylic acid. Compared to administering NO-ASA though the diet, gavaging consistently generated much higher salicylic acid levels over a wide range of doses and over a relatively broad time period (10 h). Although the reason for this result is unclear, it is possible that the 'bolus' administration, such as represented by gavage, may allow NO-ASA to overcome a saturable inactivation mechanism, albeit alternative explanations are also plausible. Nevertheless, this finding may have practical implications for the administration of NO-ASA to humans.

The data herein also demonstrate that NO-ASA inhibits the transformation of arachidonic acid. The levels of PGE_2 in colon tissue and in plasma as well as the plasma levels of TxB_2 were all suppressed by NO-ASA in a manner that is clearly dose- and time-dependent. In keeping with the pharmacokinetic findings, the prostanoid levels of gavaged animals were, in general, lower than those of animals receiving NO-ASA in their diet. These findings are consistent with those reported by Ukawa *et al* [122], who studied the effect of NO-ASA on the ulcerogenic and healing responses of the stomach. Gastric prostaglandin levels in murine

stomach were reduced by NO-ASA, including increased prostaglandin generation in the ulcerated mucosa. Consistent with the present finding on the effects of NONSAIDs on rat colonic mucosa are results previously published by us[112], showing that NO-indomethacin and NO-ASA significantly inhibited the total COX of colon tumors, including COX-2 activity and formation of PGE_2, $PGF_{2\alpha}$, 6-keto-$PGF_{1\alpha}$ and TxB_2 from arachidonic acid.

The significant correlation between salicylic acid levels and colon PGE_2 levels indicates that this effect is brought about by NO-ASA. It is uncertain, however, whether salicylic acid per se is responsible for the observed effect. Both salicylic acid and NO-salicylic acid inhibit the growth of cancer cell lines, with the latter being more potent than the former [110]. While no *in vivo* comparisons are available, NO-ASA is much more potent than either one *in vitro*. It is conceivable that salicylic acid may merely reflect the decomposition of NO-ASA that may generate with similar kinetics other bio-active moieties, such as NO or its spacer or both[116-119]. It is noteworthy that here too the suppressive effect of NO-ASA on eicosanoid production extends to two products, PGE_2 and TxB_2, and is not restricted to a single tissue.

In conclusion, our data determined the pharmacokinetics of NO-ASA in rats, established its differential bioavailability depending on its mode of administration and demonstrated a direct effect on arachidonic acid metabolism leading to markedly suppressed levels of PGE_2 and TxA_2. Whether suppression of arachidonic acid metabolism by NO-ASA is responsible for its chemopreventive effect is more difficult to assess, since both COX-dependent and COX-independent effects have been described for conventional ASA and NO-ASA [123]. These findings could prove useful in devising strategies for future human applications of NO-ASA.

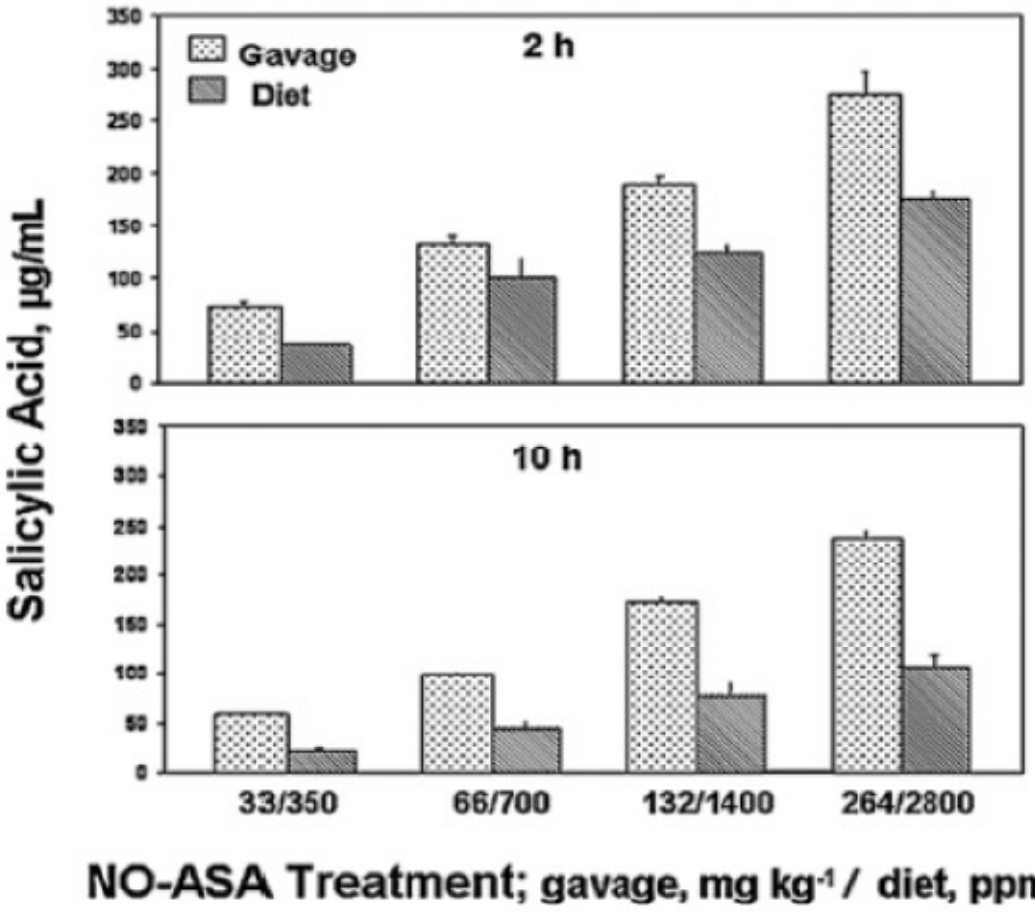

Figure 14. **Salicylic acid plasma levels in rats treated with NO-ASA.** F344 rats were treated with NO-ASA administered by oral gavage and added into their diet. Four increasing NO-ASA doses were used as previously described. Plasma salicylic acids levels, 2 and 10 h post dosing, were determined by HPLC as described in Materials and Methods. Values are mean ± SEM

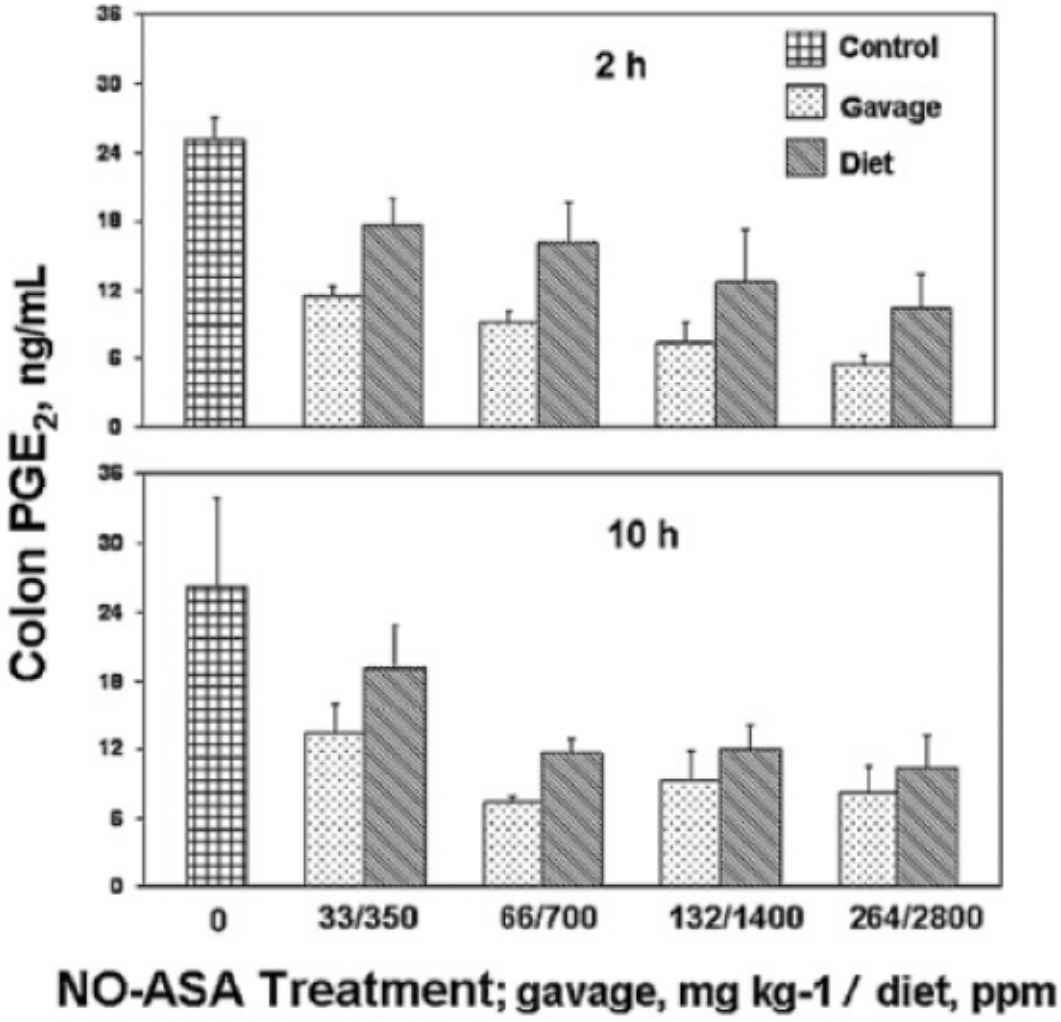

Figure 15. **Prostagladin E_2 colon tissue levels in rats treated with NO-ASA**. F344 rats were treated with NO-ASA administered by oral gavage or added into their diet. Four increasing NO-ASA doses were described. Colon tissue PGE_2 levels, 2 and 10 h post dosing, were determined by ELISA as in Materials and Methods. Values are mean ± SEM

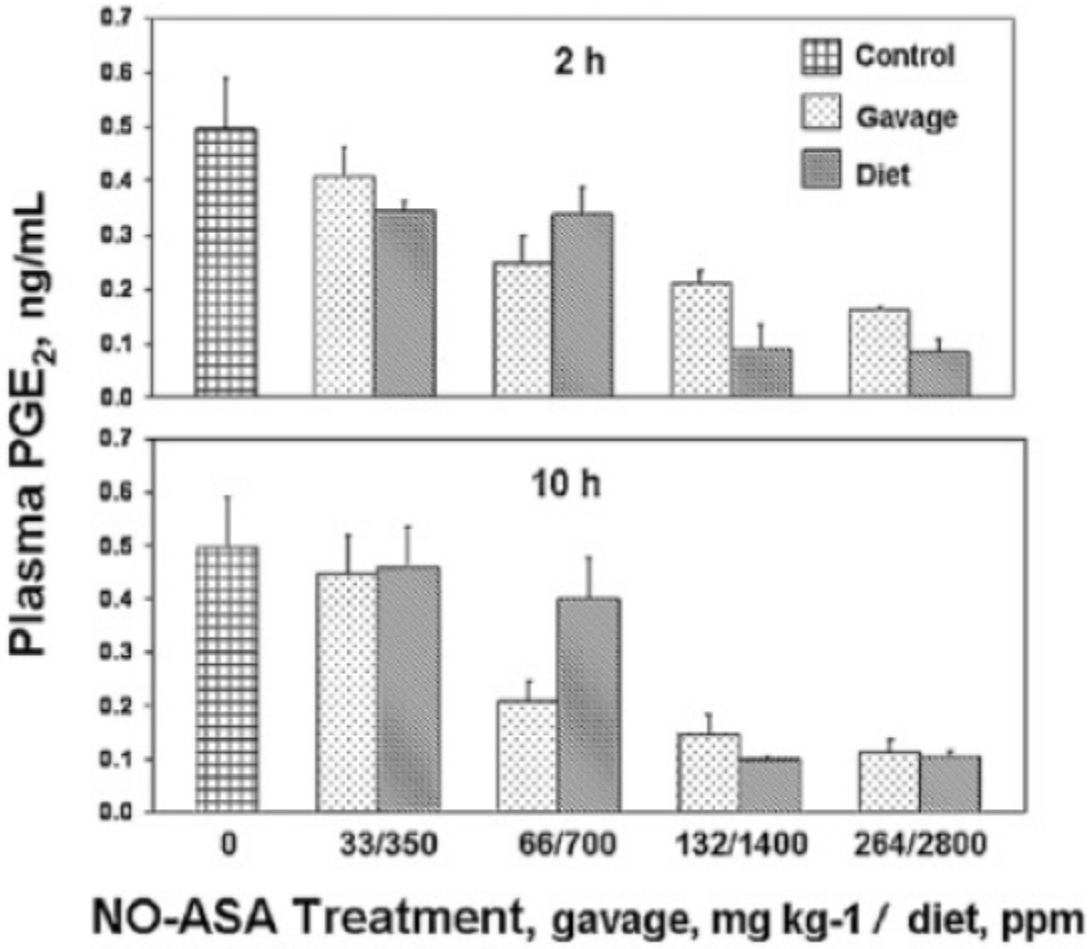

Figure 16. **Prostagladin E_2 plasma levels in rats treated with NO-ASA.** F344 rats were treated with NO-ASA administered by oral gavage or added into their diet. Four increasing NO-ASA doses were described. Plasma PGE_2 levels, 2 and 10 h post dosing, were determined by ELISA as in Materials and Methods. Values are mean ± SEM

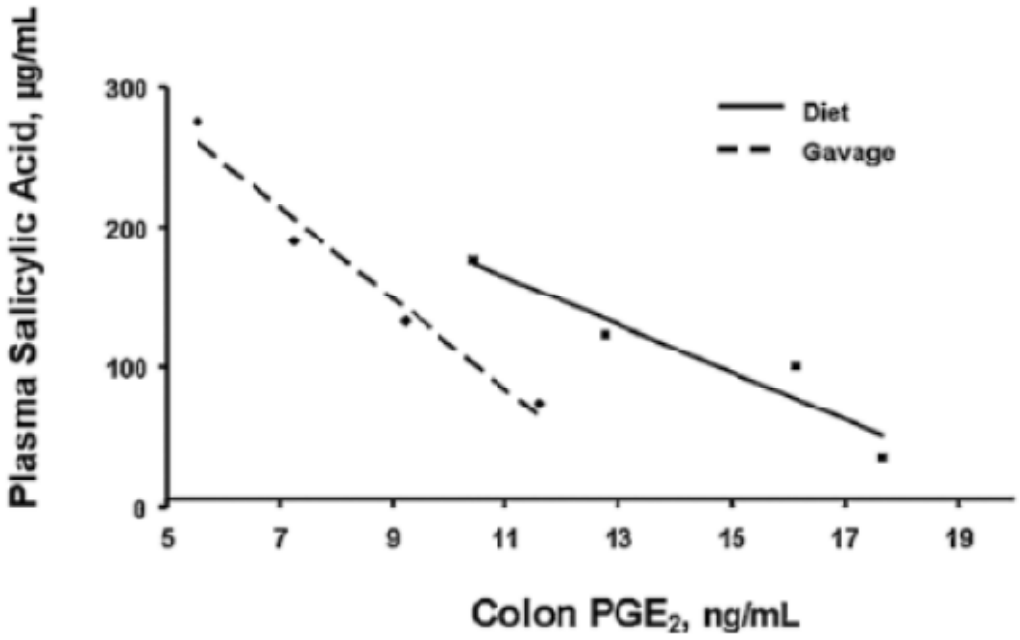

Figure 17. Association between plasma salicylic acid levels and colon PGE_2 levels in NO-ASA treated rats. The 2 h salicylic levels in rats treated with NO-ASA administered to rats either by gavage or added to their diet are significantly correlated ($p<0.05$ for both) with the corresponding PGE_2 levels in colon tissue. Both parameters were determined as in Materials and Methods

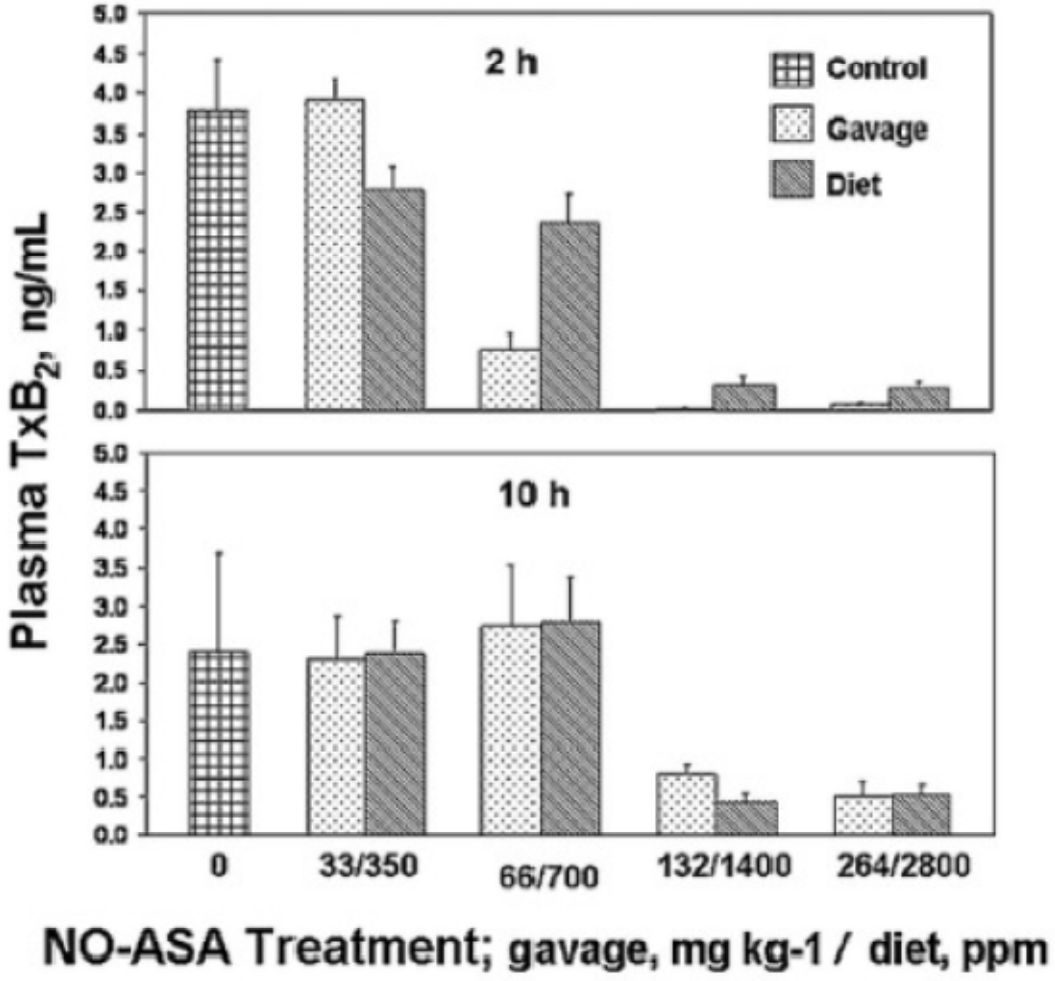

Figure 18 . **Thromboxane B_2 plasma levels in rats treated with NO-ASA**. F344 rats were treated with NO-ASA administered by oral gavage or added into their diet. Four increasing NO-ASA doses were described. Plasma TxB_2 levels, 2 and 10 h post dosing, were determined by ELISA as in Materials and Methods. Values are mean ± SEM

Table 1

Experimental design to determine the optimal and effective dose of NO-ASA

Group No.	NO-ASA	Route of administration
1	0 ppm	Diet
2	33 mg/kg BW	Gavage
3	66 mg/kg BW	Gavage
4	132 mg/kg BW	Gavage
5	264 mg/kg BW	Gavage
6	350 ppm	Diet
7	700 ppm	Diet
8	1,400 ppm	Diet
9	2.800 ppm	Diet

16 F244 rats/group; all treated for 2 weeks; BW body weight

Table 2

The effect of NO-ASA on rat plasma salicylic acid levels

Salicylic acid, µg/ml, mean ± SEM			
Gavage, mg/kg BW			
33	**66**	**132**	**264**
2 h			
73.46±4.00	132.70±7.47[a]	189.55±8.70[b]	275.30±21.64[c]
N=8	N=8	N=8	N=8
10 h			
58.48±1.27	99.82±1.48	172.06±5.52[d]	237.88±7.46[e]
N=8	N=8	N=8	N=8
Diet, ppm			
350	**700**	**1,400**	**2,800**
2 h			
35.64±1.52	100.00±17.57[f]	122.44±10.25	175.54±7.74
N=8	N=8	N=8	N=8
10 h			
21.18±3.39	44.21±7.32	77.28±13.29	105.19±13.79
N=8	N=8	N=8	N=8

Salicylic acid was not detected in vehicle control animals. The differences in salicylic acid levels between the gavage and diet groups were statistically significant for all doses at both time pointes except for: a vs. f, b vs. d and c vs. e.

Table 3

The effect of NO-ASA on rat PGE_2 colon tissue levels.

PGE_2, ng/ml, mean ± SEM				
Gavage, mg/kg BW				
0	**33**	**66**	**132**	**264**
		2 h		
25.01±1.93[a]	11.60±0.83[b]	9.23±1.02[c]	7.26±2.04[d]	5.55±0.70[e]
N=4	N=8	N=8	N=8	N=6
		10 h		
26.14±1.93[f]	13.40±2.59[g]	7.36±0.52[h]	9.16±2.67[i]	8.17±2.34[j]
N=3	N=8	N=6	N=5	N=8
Diet, ppm				
0	**350**	**700**	**1,400**	**2,800**
		2 h		
25.10±1.93[k]	17.69±2.40[l]	16.16±3.56[m]	12.77±4.43[n]	10.43±3.02[o]
N=4	N=7	N=5	N=6	N=7
		10 h		
26.14±7.62[p]	19.18±3.70[q]	11.65±1.17[r]	11.90±2.12[s]	10.41±2.66[t]
N=3	N=4	N=6	N=4	N=7

Statistical comparisons were made between controls and PGE2 levels of individual NO-ASA doses; between 2 and 10 h for each NO-ASA level in the gavage and diet groups; and between gavage and diet groups at each dose and time-point. All differences were statistically significant except for the following: d vs. n; e vs. o; g vs. q; i vs. s; j vs. t; k vs. m; f vs. g; p vs. q; p vs. s; d vs. i; e vs. j; l vs. q; n vs. s; o vs. t.

Table 4

The effect of NO-ASA on rat plasma PGE_2 levels

PGE_2, ng/ml, mean ± SEM				
Gavage, mg/kg BW				
0	**33**	**66**	**132**	**264**
		2 h		
0.50±0.09[a]	0.41±0.05[b]	0.25±0.05[c]	0.21±0.02[d]	0.16±0.00[e]
N=6	N=7	N=4	N=3	N=4
		10 h		
0.50±0.09[f]	0.45±0.07[g]	0.21±0.04[h]	0.15±0.04[i]	0.11±0.02[j]
N=6	N=3	N=6	N=7	N=4
Diet, ppm				
0	**350**	**700**	**1,400**	**2,800**
		2 h		
0.50±0.09[k]	0.35±0.02[l]	0.34±0.05[m]	0.09±0.05[n]	0.08±0.02[o]
N=6	N=3	N=4	N=3	N=3
		10 h		
0.50±0.09[p]	0.46±0.07[q]	0.40±0.08[r]	0.10±0.00[s]	0.10±0.01[t]
N=6	N=5	N=4	N=3	N=4

Statistical comparisons were made between controls and PGE_2 levels of individual NO-ASA doses; between 2 and 10 h for each NO-ASA level in the gavage and diet groups; and between gavage and diet groups at each dose and time-point. The following differences were statistically significant: g vs. q; h vs. r; k vs. n; k vs. o; f vs. h; f vs. i; f vs. j; p vs. s; p vs. t.

Table 5

The effect of NO-ASA on rat plasma TxB_2.

TxB_2, ng/ml, mean ± SEM				
Gavage, mg/kg BW				
0	**33**	**66**	**132**	**264**
		2 h		
3.77±0.65[a]	3.91±0.27[b]	0.77±0.18[c]	0.02±0.01[d]	0.08±0.02[e]
N=5	N=5	N=4	N=4	N=3
		10 h		
2.39±1.31[f]	2.30±0.56[g]	2.74±0.80[h]	0.81±0.13[i]	0.51±0.19[j]
N=2	N=4	N=3	N=5	N=3
Diet, ppm				
0	**350**	**700**	**1,400**	**2,800**
		2 h		
3.77±0.65[k]	2.78±0.30[l]	2.37±0.35[m]	0.32±0.11[n]	0.29±0.07[o]
N=5	N=8	N=6	N=3	N=3
		10 h		
2.39±1.31[p]	2.37±0.45[q]	2.80±0.60[r]	0.44±0.12[s]	0.53±0.13[t]
N=2	N=5	N=6	N=3	N=4

Statistical comparisons were made between controls and TxB2 levels of individual NO-ASA doses; between 2 and 10 h for each NO-ASA level in the gavage and diet groups; and between gavage and diet groups at each dose and time-point. All differences were statistically significant except for the following: g vs. q; h vs. r; i vs. s; j vs. t; a vs. b; k vs. l; k vs. m; f vs. g; f vs. h; f vs. i; f vs. j; p vs. q; p vs. r; p vs. s; p vs. t; e vs. j; l vs. q; m vs. r; n vs. s; o vs. t.

Chapter 3. Structure-Activity Relationship Study of Novel Anticancer Aspirin-based Compounds

3.1 Introduction

Accounting for nearly one quarter of the deaths in the US, cancer remains one of the major medical challenges of our time. In 2009, it is estimated that 292,540 and 269,800 American males and females, respectively, died of cancer.[1] The US death rate from cancer has remained unchanged in recent decades, in contrast to that of heart disease, which has decreased by >60%[1]. Much of the progress in cardiology stems from the development of a wide variety of novel agents aimed at both the treatment and prevention of cardiovascular diseases. The oncology field, although it has witnessed some remarkable advances, is still in considerable need of new and effective agents.

We have recently reported our findings on the anti-cancer activity of a novel benzyl ester-based derivative of acetylsalicylic acid (ASA) or aspirin provisionally named phospho-aspirin (Fig 19, compound **1a**). This compound showed two potentially significant properties: a) anticancer efficacy in a murine model of cancer, achieving over 60% reduction in tumor volume of xenografted HT-29 human colon cancer cells, and b) no apparent toxicity, evidenced, among other parameters, by no reduction in body weight during treatment and no organ damage on necropsy[124] .The mode of action of this compound includes, at the cytokinetic level, brisk induction of apoptosis and to a lesser degree, suppression of proliferation. Of note, similar cytokinetic effects were observed in cultured HT-29 cells, in which the 24-h IC_{50} for compound **1a** was 276 μM[124]. The *para* positional isomer of phosphoaspirin (compound **1b**) inhibited the growth of 10

human cancer cell lines originated from colon, lung, liver, pancreas and breast, with an 18- to 144-fold greater potency than conventional ASA[125].

Prompted by these encouraging results, we developed a new series of ASA-benzyl esters, based on conventional ASA, which consist of benzyl derivatives having an ASA or an acyloxy substituent (Fig 19). We have pursued the study of ASA-based benzyl esters (ABEs), primarily for their anticancer effects. In addition to synthesizing positional isomers of compound **1a**, we undertook an SAR study to ascertain those features of the molecule that contribute to its pharmacological activity. It is worthy of mention that compound **1a** is much more potent than conventional ASA[124] of which it can be considered a derivative.

The potential importance of ASA and other NSAID (nonsteroidal anti-inflammatory drugs) derivatives in cancer control originates from their well-established efficacy in the prevention of human cancer and the accompanying understanding of their mechanisms of action, one of which centers on the role of cyclooxygenase-2 (COX-2) overexpression in carcinogenesis; inhibition of COX enzymes is the best recognized mode of action of NSAIDs. For example, epidemiological studies demonstrated that NSAID use prevents cancer of the colon by up to 50%, whereas interventional studies showed that ASA prevents 21-30% of colon polyp recurrence in humans[126-128]. Combined with a vast amount of preclinical data, such findings underscore the potential of NSAIDs for cancer control[129].

Here, we report the synthesis of several congeners of compound **1a** and a SAR study with respect to their ability to inhibit cancer cell growth, a parameter that defines whether a drug can suppress cancer. Our findings provide a mechanistic understanding of the novel ABEs in terms of their chemistry.

3.2 Experimental Methods Materials

Synthesis of ABEs

Compounds **1c, 1d, 1e, 1f, 1g** and **2d** were prepared according to a published method[130]. For the preparation of the diethyl phosphate esters, a general method is described illustrated by the synthesis of **1b,** which in this and all other cases began with the corresponding alcohol.

Reagents and Relevant Methods

All reagents and solvents were of commercial grade and used as such unless otherwise specified. ^{1}H NMR spectra were recorded on Varian 300 spectrometer. Samples prepared for NMR analysis were dissolved in $CDCl_3$. Chemical shifts are reported in ppm relative to TMS. Electron ionization mass spectra were recorded on a Thermo Scientific DSQ (II) mass spectrometer. Thin-layer chromatography (TLC) was performed on silica gel sheets (Tiedel-deHaën, Sleeze, Germany) containing a fluorescent indicator. Flash column chromatographic separations were carried out on 60 Å (230-400 mesh) silica gel (TSI Chemical Company, Cambridge, MA). All experiments dealing with moisture- or air-sensitive compounds were conducted under dry nitrogen. The starting materials and reagents, unless otherwise specified, were the commercially best grade available (Aldrich, Fluka) and were used without further purification. All new products showed a single spot on TLC analysis in two different solvent systems, after purification.

General Procedure

Synthesis of 2-acetoxy benzoic acid 4-(diethoxy phosphoryl oxymethyl) phenyl ester (1b): Diethylchlorophosphate (2.5 mL, 17.26 mmole) was added drop-wise to a solution of alcohol (**1e**, 1.9 g, 6.64 mmole) in methylene chloride (10 mL) containing diisopropylethylamine (2.2 mL, 13.28 mmole), followed by 4-(dimethylamino)pyridine (25 mg) as a solid. The reaction mixture was heated under reflux overnight. The reaction solution was washed with water (2 x 25 mL), dried over anhydrous sodium sulfate, filtered and concentrated. The crude residue was purified by column chromatography using hexane:ethyl acetate (60:40) as the eluant. The pure fractions were combined and evaporated to give a solid which was triturated with hot hexane several times to give pure title compound **1b** as a solid (690 mg, 25%). ^{1}H NMR ($CDCl_3$): δ 1.3 (m, 6H), 2.3 (s, 3H), 4.05 (m, 4H), 5.05 (d, 2H), 7.2 (m, 3H), 7.4 (t, 1H), 7.45 (d, 2H), 7.62 (t, 1H), 8.20 (d, 1H). MS: 422 (M+).

Using the above general procedure, the following compounds were made, all of which were isolated as viscous oils.

2-Acetoxy benzoic acid 3-(diethoxy phosphoryloxymethyl) phenyl ester (1a): Yield 29%, ^{1}H NMR ($CDCl_3$): δ 1.3 (m, 6H), 2.32 (s, 3H), 4.1 (m, 4H), 5.08 (d, 2H), 7.2 (m, 3H), 7.28 (d, 1H), 7.4 (m, 2H), 7.65 (t, 1H), 8.20 (d, 1H). MS: 422 (M+).

2-Acetoxy benzoic acid 3-(diethoxy phophoryloxymethyl)-4-methoxy phenyl ester (1h): Yield 29%, ^{1}H NMR ($CDCl_3$): δ 1.3 (m, 6H), 2.3 (s, 3H), 3.8 (s, 3H), 4.15 (m, 4H), 5.1 (d, 2H), 6.9 (d, 1H), 7.1 (d, 1H), 7.2 (m, 2H), 7.4 (t, 1H), 7.6 (t, 1H),), 8.20 (d, 1H). MS: 452 (M+).

2-Acetoxy benzoic acid 4-(diethoxy posphoryloxymethyl)-3-methoxy phenyl ester (1i): Yield 26%, ^{1}H NMR ($CDCl_3$): δ 1.4 (m, 6H), 2.4 (s, 3H), 3.9 (s,

3H), 4.2 (m, 4H), 5.2 (d, 2H), 6.8 (s, 1H), 6.83 (d, 1H), 7.22 (d, 1H), 7.5 (m, 2H), 7.75 (t, 1H) 8.3 (d, 1H). MS: 452 (M+).

2-Acetoxy benzoic acid 3-chloro-4-(diethoxy phosphoryloxymethyl) phenyl ester (1j): Yield 24%, ^{1}H NMR ($CDCl_3$): δ 1.39 (m, 6H), 2.3 (s, 3H), 4.15 (m, 4H), 5.18 (d, 2H), 7.18 (m, 2H), 7.2 4(d, 1H), 7.4 (t, 1H), 7.6 (d, 1H), 7.62 (t, 1H) 8.2 (d, 1H). MS: 456 (M+).

Acetic acid, 2-(diethoxy phosphoryloxymethyl) phenyl ester (2a): Yield 28%, ^{1}H NMR ($CDCl_3$): δ 1.38 (m, 6H), 2.05 (s, 3H), 4.22 (m, 4H), 5.2 (s, 2H), 7.17 (t, 1H), 7.32 (t, 1H), 7.4 (m, 2H). MS: 302 (M+).

Acetic acid, 3-(diethoxy phosphoryloxymethyl) phenyl ester (2b): Yield 29%, ^{1}H NMR ($CDCl_3$): δ 1.3 (m, 6H), 2.3 (s, 3H), 4.05 (m, 4H), 5.02 (d, 2H), 7.02 (d, 1H), 7.1 (s, 1H), 7.24 (d, 1H), 7.4 (t, 1H). MS: 302 (M+).

Acetic acid, 4-(diethoxy phophoryloxymethyl) phenyl ester (2c): Yield 30%, ^{1}H NMR ($CDCl_3$): δ 1.38 (m, 6H), 2.4 (s, 3H), 4.1 (m, 4H), 5.05 (d, 2H), 7.18 (d, 2H), 7.5 (d, 2H). MS: 302 (M+).

Acetic acid, 3-chloro-4-(diethoxy phosphoryloxymethyl) phenyl ester (2d): Yield 24%, ^{1}H NMR ($CDCl_3$): δ 1.3 (m, 6H), 2.3 (s, 3H), 4.1 (m, 4H), 5.12 (d, 2H), 7.0 (d, 1H), 7.18 (s, 1H), 7.55 (d, 1H). MS: 336(M+).

Benzoic acid, 3-(diethoxy phosphoryloxymethyl) phenyl ester (3): Yield 24%, ^{1}H NMR ($CDCl_3$): δ 1.33 (m, 6H), 4.11 (m, 4H), 5.09 (d, 2H), 7.20 (d, 1H), 7.26 (m, 2H), 7.5 (m, 3H), 7.62 (m, 1H), 8.20 (d, 2H). MS: 364 (M+).

Phosphoric acid, 4-(diethoxy phosphoryloxymethyl) phenyl diethyl ester (4): Yield 27%, ^{1}H NMR ($CDCl_3$): δ 1.34 (m, 12H), 4.12 (m, 4H), 4,22 (m, 4H), 4.66 (s, 2H), 7.2 (d, 2H), 7.32 (d, 2H). MS: 398 (M+).

Phosphoric acid, diethyl 4-fluoro benzyl ester (5): Yield 26%, ^{1}H NMR ($CDCl_3$): δ 1.3 (m, 6H), 4.05 (m, 4H), 5.0 (d, 2H), 7.02 (m, 2H), 7.4 (m, 2H). MS: 262 (M+).

Phosphoric acid, benzyl diethyl ester (6): Yield 29%, ^{1}H NMR ($CDCl_3$): δ 1.3 (m, 6H), 4.05 (m, 4H), 5.02 (d, 2H), 7.4 (m, 5H). MS: 244 (M+).

Acetic(diethyl phosphoric) Anhydride (7): Yield 28%, ^{1}H NMR ($CDCl_3$): δ 1.4 (m, 6H), 2.2 (s, 3H), 4.3 (m, 4H). MS: 196 (M+)

Cell culture studies

Stock (200 mM or 100 mM) solutions were prepared in DMSO (Fisher Scientific, Fair Lawn, NJ).

Cell lines

HT-29 and SW480 human colon adenocarcinoma cell lines, and BxPC-3 and MIA PaCa-2 human pancreatic adenocarcinoma cell lines (American Type Culture Collection, Manassas, VA) were grown as monolayers in either McCoy 5A medium (HT-29), RPMI 1640 (SW480 and BxPC-3) or DMEM (MIA PaCa-2). Media were supplemented with 10% fetal bovine serum (FBS; Mediatech, Herndon, VA), except for DMEM that was supplemented with 2.5 % horse serum); penicillin (50 units/mL); and streptomycin (50 mg/mL) (Life Technologies, Inc., Grand Island, NY). Cells were seeded at a density of 1.5-3×10^4 cells/cm^2 in a culture dish and incubated at 37°C in 5% CO_2 at 90% relative humidity. Single-cell suspensions were obtained by trypsinization (0.05% trypsin/EDTA), and cells were counted using a hemacytometer. Viability was determined by the trypan blue dye exclusion method.

Determination of IC_{50}

Cells, plated into 96-well plates (424 cells/mm^2), were grown overnight and then treated with various concentrations of each test compound for 24 h. The final DMSO concentrations were adjusted accordingly, but never exceeded 1%. After treatment, viable cells were assayed using the "MTT cell proliferation assay" according to the manufacturer's instructions (Sigma). The plates were read at 595 nm and the data were handled with SoftmaxPro Version 3.1.1 (Molecular Devices, Sunnyvale, CA). For each compound and each cell line, IC_{50}s were determined at least in triplicate.

3.3 Results

We synthesized the compounds listed in Fig 19 and used their ability to inhibit the growth of cancer cells *in vitro* as a measure of their anticancer pharmacological effect. For each compound, we determined its 24-hr IC_{50}, i.e. the concentration of the test compound that inhibits cell growth 50% at 24 hr. Under our experimental conditions, IC_{50} values >500 μM could not be determined accurately. We employed four human cancer cell lines, two derived from colon (HT-29 and SW480) and two from pancreatic cancer (BxPC-3 and MIA PaCa-2). In each pair, one cell line expresses COX-2 (HT-29 and BxPC-3) whereas the other does not. This is of potential mechanistic value, because our compounds are structurally related to ASA, whose best-recognized molecular target is COX, which is thought to play a role in carcinogenesis[131,132].

3.3.1 The effect of the X group

To assess the effect of the salicyloyl group (X group in Fig 19) on the anticancer potency of the drug, we studied a series of compounds containing the benzyl spacer and diethylphosphate as the leaving group and as the X moiety any one of the following groups: a salicyloyl group (**1b**), an acetoxy group (AcO-, **2a, 2b** and **2c**), a benzoyloxy group (C_6H_5COO-, **3**), a diethylphosphate group (-$OP(O)(OEt)_2$, **4**), a fluorine atom (-F, **5**), or hydrogen (-H, **6**) (Table 6). Most of these compounds are *p*- isomers.

It is clear from the results summarized in Table 6 and Fig 19, that the X group plays a role in determining the anticancer potency of ABEs. We studied six different X groups in compounds sharing the same benzyl spacer and leaving groups. Of them, only the salicyloyl, acetoxy and benzoyloxy showed appreciable

(<500 μM, i.e. measurable) potency in inhibiting cancer cell growth. All three have an enzyme cleavable ester bond. A convincing demonstration of the importance of the ester bond for biological activity was obtained when the acyloxy group was replaced by $–OP(O)(OEt)_2$ (**4**), F (**5**) or H (**6**). In all three cases, this change prevented the formation of drug intermediates and led to complete loss of biological activity. Of further interest, the IC_{50} of the *p*-acetoxy containing compound (**2c**) was 5 - 20 fold lower than that of the *p*-ASA containing compound (**1b**). The proposed mechanisms for compounds **1b** and **2c** are shown in Fig 21, where compound **1b** needs one more step to generate quinone methide, thus leading to a lower reaction rate and lower pharmacological potency. It is, however, possible that the differential biological activity of **1b** and **2c** is due to different rates of hydrolysis of the ester bond ($k_1 >> k_1'$).

3.3.2 The requirement of the spacer for biological activity

The importance of the spacer for the biological activity of ABEs was directly accessed by omitting it from the most potent compound **2c.** This shortened version (compound **7**) shows virtually no activity against any of the cell lines (data not shown). If we consider compounds **3, 5, 6** as not containing a spacer molecule (which is reasonable), then the requirement for the spacer is underscored further; none of them have any detectable biological activity as determined in our assays.

3.3.3 The effect of the leaving group

To determine the effect of the leaving group on the pharmacological activity of ABEs, we studied a series of analogues in which X = ASA or AcO, and

the leaving group was one of four different moieties, namely diethylphosphate [-$OP(O)(OEt)_2$], chloro (-Cl), hydroxyl (-OH) and nitrate (–ONO_2) (Fig 22). Since previous work with nitrate esters established the essential equivalence of the *ortho-* and *para-* positional isomers, we restricted our study to the *meta-* and *para-* isomers.

The *para* isomers are significantly more potent than the *meta* isomers. The *m-/p-* potency ratios ranged between 4.1 and >5.5 for the diethylphosphate derivatives, and between >4.5 and 29.6 for the nitrate derivatives; it was not possible to calculate such ratios for the –OH derivatives because the IC_{50}s of both isomers for all four cell lines were >500 μM. Indeed, the –OH compounds (**1d** and **1e**) had such a low potency that their IC_{50}s for cell growth could not be reliably established in our experimental system. Of the remaining three, the nitrates (**1f** and **1g**) and diethylphosphates (**1a** and **1b**), roughly equipotent, were much more potent than the –OH compounds. The potency of the corresponding -Cl derivative (**1c**) was considerably less, which could be due to lower solubility or other factors. There were individual variations in IC_{50}, based on the cell line. For example, in the case of HT-29 colon cancer cells, the nitrate and phosphate compounds were equipotent, whereas in the SW480 cell line the nitrate compound was 5.6-fold more potent than the diethylphosphate (**1b** and **1g**).

Thus, the leaving group had a clear effect on the potency of ABEs. Both the –$OP(O)(OEt)_2$ and ONO_2 groups are absolutely critical to their biological activity; their function as leaving groups determines the formation of drug intermediates. Of the four leaving groups that we examined, -$OP(O)(OEt)_2$ and –ONO_2 where roughly equivalent, whereas the –Cl was slightly less effective. The –OH group, a non-leaving group, appeared to eliminate the ability of ABEs to inhibit cancer cell growth.

3.3.4 The effect of the electron density of the spacer

To assess the importance of the spacer group (the benzyl moiety) on the pharmacological effect of ABEs, we studied a series of compounds based on X=ASA or AcO and LG=diethyl phosphate in which the spacer was modified by a second substituent (Y in Fig 19). This substituent was either an electron-donating methoxy group (-OMe, **1i**), or an electron-withdrawing chloro atom (-Cl, **1j**, **2c**) (Table 8). Most of these spacer modifications were positioned *ortho* to the benzyl ester group.

As seen in Table 8 and Fig 23, the electron density of the spacer had a profound effect on the potency of the ABE molecule. The -OMe group consistently and significantly reduced the potency of the compound (**1i** vs. **1b**). In contrast to the effect of the -OMe, the chloro group increased the potency of the compound, reducing its IC_{50} on average 3.3-fold (**1j** vs. **1b; 2c** vs. **2d**). The biological effects of additional substituents on the benzylic ring (-Cl or -OMe) reflect either differences in accommodation at the active site or differences in the rates of elimination of the diethylphosphate groups. It is conceivable that the electron density of the spacer affects the formation of the drug intermediate. –OMe, an electron-donating group, could stabilize a quinone methide; whereas –Cl, an electron-withdrawing group, could increase the reactivity of the quinone methide.

3.3.5 The effect of positional isomerism in the relationship of X to the leaving group

Positional isomerism plays an important role in determining the generation of the drug intermediate and thus drug potency. In all instances where direct

comparisons were possible, the *para* isomers were significantly more potent than the *meta* (Table 7 and 8, Fig 22 and 23). Overall, the *para* isomers were between 5-100 times more potent than the *meta* isomers in inhibiting the growth of pancreatic and colon cancer cells (**1a** vs. **1b** and **1f** vs. **1g**). The reason for this striking difference may be found in the general mechanism of action of these compounds, outlined in Fig 20. We have previously studied in detail the effect of positional isomerism on the pharmacological behavior of compounds **1f** and **1g** and also of their *ortho* isomer[133,134].

3.4 Discussion and Conclusion

We examined the contribution to the pharmacological activity of ABEs by their three structural components shown in Fig 19: LG (leaving group), X (usually ASA) and the spacer group linking the two. Our SAR findings can be viewed in the context of a mechanism of action recently proposed independently by Hulsmann *et al*[135] and by us[134] concerning ASA-based ABE compounds in which the leaving group is $–ONO_2$. The main feature of this mechanism is that it considers the spacer as the predominately active moiety (Fig 20). Briefly, the spacer forms a reactive intermediate, either a quinone methide (from its *para* and *ortho* positional isomers) or a carbocation (from the *meta* isomer). This drug intermediate can react with a nucleophile (i.e. glutathione or a suitable group of an enzyme), accounting for most, if not all, of the compound's biological activity. The properties of both the leaving group (LG) and the X group affect the formation of the drug intermediate of each ABE, and thus its biological activity. Fig 20 provides an illustrative example: compound **1b,** the *para* derivative of ASA, undergoes such a series of reactions. The first step is catalyzed by hydrolase(s), e.g., acetylsalicylate O-acetylhydrolase[136,137]. The next two steps forms the drug intermediate quinone methide, which then reacts with a nucleophile to generate a biological functionality. It is clear that in this formulation positional isomerism plays an important role in determining drug intermediate activity and thus drug potency (We have studied in detail the effect of positional isomerism on the pharmacological behavior of compounds **1f**, **1g** and also of their *ortho* isomer[133].

In conclusion, we have developed a series of novel aspirin derivatives (ABEs), some of which are active against several human cancer cell lines. We have identified the elements in these compounds critical to their biological activity, namely the nature of the acyloxy/salicyloxy function; the leaving group; and the electron density of the benzylic spacer, provided by

secondary substituents. This SAR study also provides clear evidence that positional isomerism of ABEs is influential with regard to their inhibitory action on cancer cell growth in vitro. Our findings suggest that optimizing the structural elements of these novel ABEs may enhance their anticancer properties and hopefully provide a class of compound useful in the prevention and/or treatment of cancer.

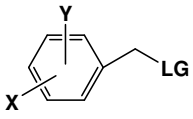

LG: Leaving group
X and **Y**: Spacer substitutes

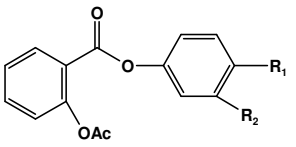

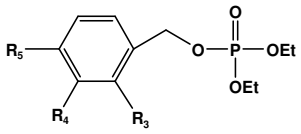

1a	$R_1 = H$	$R_2 = CH_2OP(O)(OEt)_2$	
1b	$R_1 = CH_2OP(O)(OEt)_2$	$R_2 = H$	
1c	$R_1 = CH_2Cl$	$R_2 = H$	
1d	$R_1 = H$	$R_2 = CH_2OH$	
1e	$R_1 = CH_2OH$	$R_2 = H$	
1f	$R_1 = H$	$R_2 = CH_2ONO_2$	
1g	$R_1 = CH_2ONO_2$	$R_2 = H$	
1h	$R_1 = OCH_3$	$R_2 = CH_2OP(O)(OEt)_2$	
1i	$R_1 = CH_2OP(O)(OEt)_2$	$R_2 = OCH_3$	
1j	$R_1 = CH_2OP(O)(OEt)_2$	$R_2 = Cl$	

2a	$R_3 = CH_3COO$	$R_4 = H$	$R_5 = H$
2b	$R_3 = H$	$R_4 = CH_3COO$	$R_5 = H$
2c	$R_3 = H$	$R_4 = H$	$R_5 = CH_3COO$
2d	$R_3 = Cl$	$R_4 = H$	$R_5 = CH_3COO$
3	$R_3 = H$	$R_4 = C_6H_5COO$	$R_5 = H$
4	$R_3 = H$	$R_4 = H$	$R_5 = CH_2OP(O)(OEt)_2$
5	$R_3 = H$	$R_4 = H$	$R_5 = F$
6	$R_3 = H$	$R_4 = H$	$R_5 = H$

7 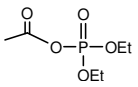

Figure 19. The chemical structure of ABEs. X represents the salicyloyl/acyloxy group; the benzyl group is regarded as the spacer; LG represents the leaving group; the X group is at the *meta* or *para* position with respect to the benzylic methylene and the Y group is a second substituent on the benzyl ring.

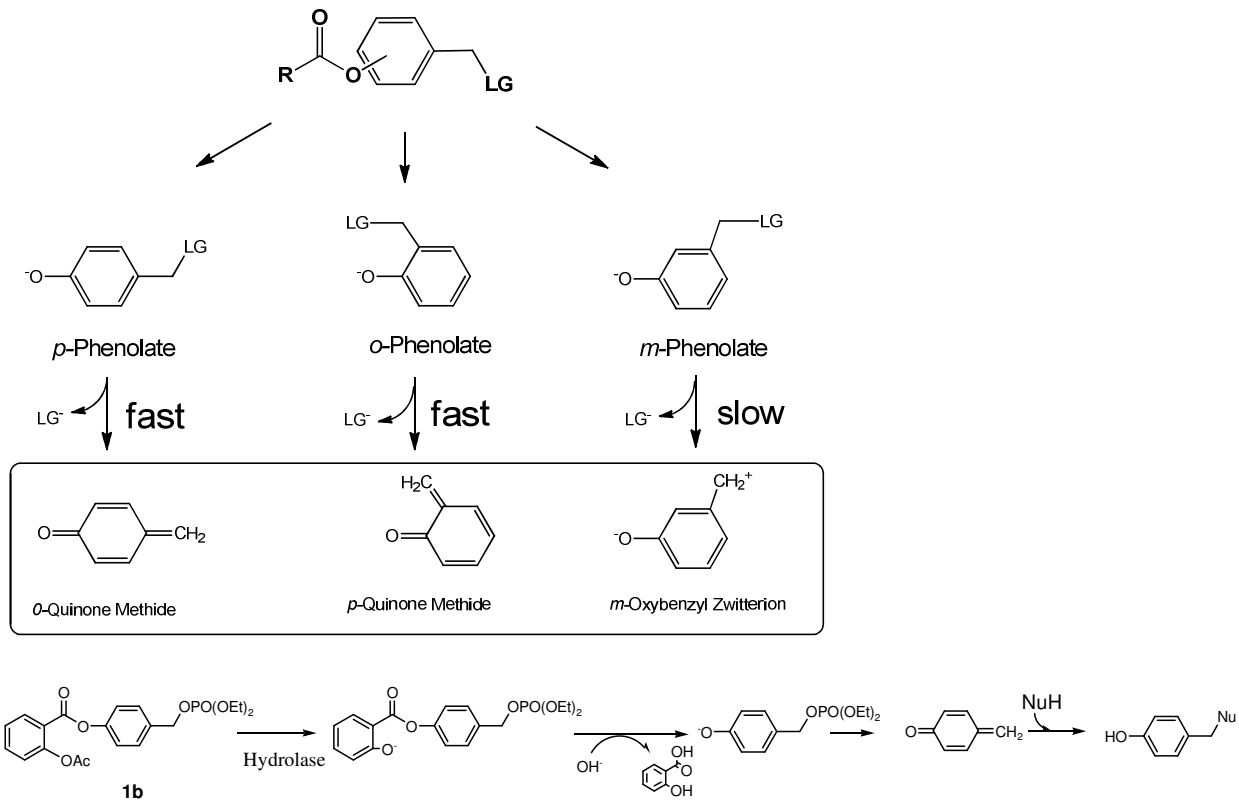

Figure 20. Proposed mechanism for the generation of ABE drug intermediates. *Upper panel:* Most ABEs generate one of the three intermediates, *para* or *ortho* quinone methide or a methylphenol zwitterion, as discussed in the text. *Lower panel:* The transformation of *para* phosphoaspirin (**1b**), these reactions follow the mechanism shown in the upper panel.

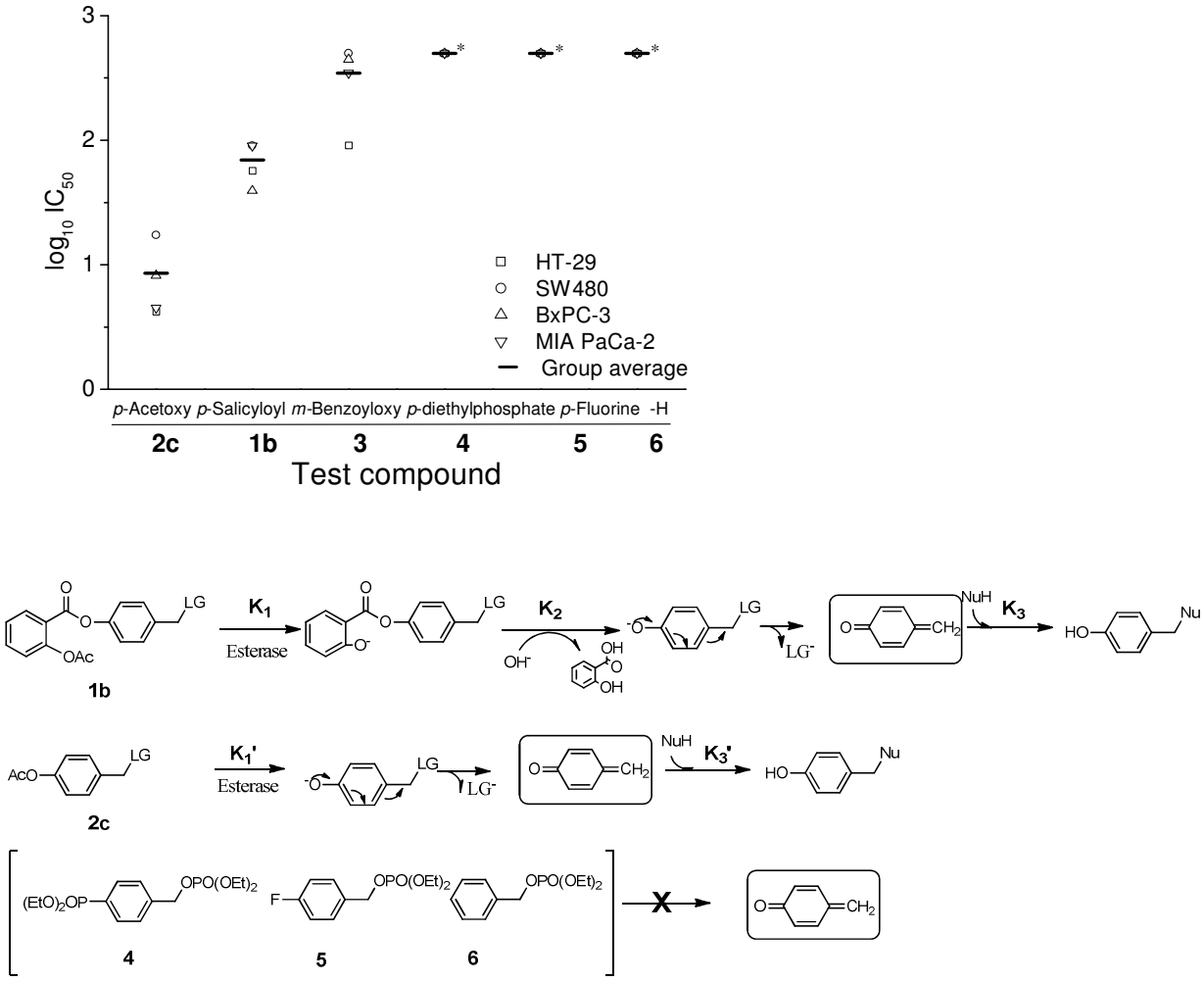

Figure 21. The effect of the X group on the IC_{50} for cell growth. *Upper panel:* The four different cell lines shown in the inset were treated with the compounds indicated in the abscissa for 24 h and their IC_{50} for cell growth (ordinate) was determined as in Methods. The average IC_{50} for each compound for all four cell lines is indicated by the horizontal line. * IC_{50}>500 μM; the results of several cell lines overlap and are not clearly delineated. *Lower panel:* Metabolic transformations of representative compounds. Compounds **1b** and **2c** proceed through the general pathway outlined in Figure 2 (the latter has one step less) to generate quinone methide (boxed) which reacts with a nucleophile giving the final product. Compounds **4**, **5** and **6** cannot generate quinone methides.

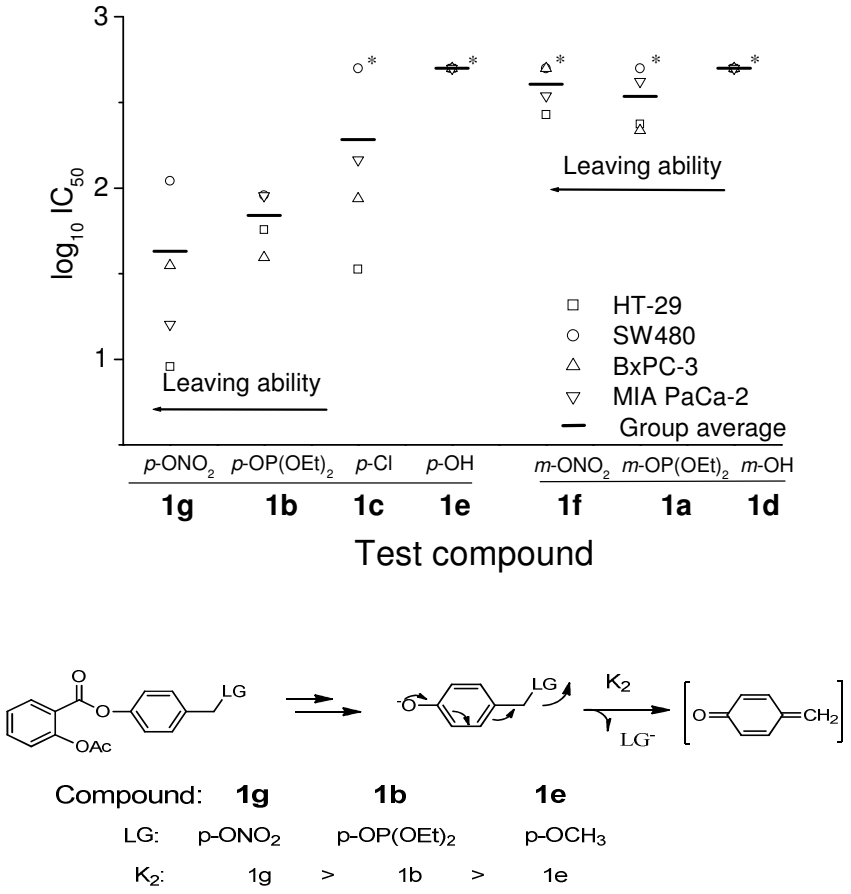

Figure 22. The effect of the leaving group on the IC_{50} for cell growth. *Upper panel:* The four different cell lines shown in the inset were treated with the compounds indicated in the abscissa for 24 h and their IC_{50} for cell growth (ordinate) was determined as in Methods. Compounds have been organized according to their positional isomerism (*para* vs. *meta*) and the leaving ability of their leaving groups (in decreasing order).The average IC_{50} for each compound in all four cell lines is indicated by the horizontal line. * IC_{50}>500 μM; in some cases the results of several cell lines overlap and are without clear demarkation. *Lower panel:* Metabolic transformations of *para* compounds generating quinone methide.

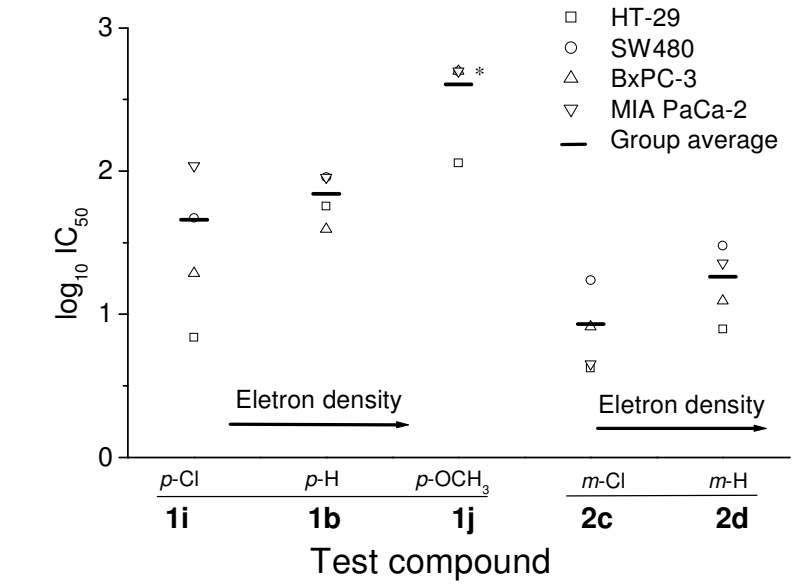

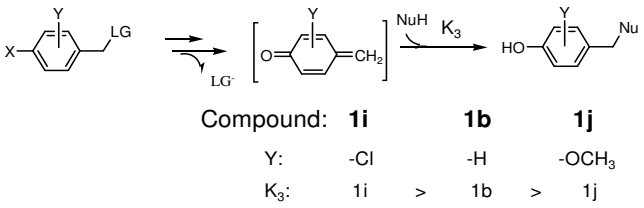

Figure 23. The effect of the benzyl ring electron density on the IC_{50} for cell growth. *Upper panel:* The four different cell lines shown in the inset were treated with the compounds indicated in the abscissa for 24 h and their IC_{50} for cell growth (ordinate) was determined as in Methods. Compounds have been ordered according to their positional isomerism (*para* vs. *meta*) and the electron density of their spacer (in increasing order).The average IC_{50} for each compound for all four cell lines is indicated by the horizontal line. * IC_{50}>500 μM; for **1j** the results of several cell lines overlap and are not clearly identified. *Lower panel:* Metabolic transformations of representative *para* compounds generating quinone methide followed by the addition of a nucleophile.

Table 6

The effect of the acyloxy group on the IC_{50} for cancer cell growth

Compound	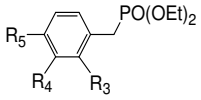			IC_{50}, μM			
				BxPC-3	MIA PaCa-2	HT-29	SW480
1b	R_3 = H	R_4 = H	R_5 = ASA	57.1±1.8	90.8±0.9	39.3±2.9	90.3±2.8
2a	R_3 = CH_3COO	R_4 = H	R_5 = H	>500	>500	>500	>500
2b	R_3 = H	R_4 = CH_3COO	R_5 = H	>500	>500	>500	>500
2c	R_3 = H	R_4 = H	R_5 = CH_3COO	4.2±0.7	17.3±2.2	8.2±1.2	4.5±0.5
3	R_3 = H	R_4 = C_6H_5COO	R_5 = H	91.2±0.5	>500	447±14.3	347±23.5
4	R_3 = H	R_4 = H	R_5 = P(O)(OEt)$_2$	>500	>500	>500	>500
5	R_3 = H	R_4 = H	R_5 = F	>500	>500	>500	>500
6	R_3 = H	R_4 = H	R_5 = H	>500	>500	>500	>500

Table 7

The effect of the leaving group on the IC_{50} for cancer cell growth

Compound	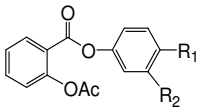		IC_{50}, μM			
			BxPC-3	MIA PaCa-2	HT-29	SW480
1a	$R_1 = H$	$R_2 = OP(O)(OEt)_2$	236±5.0	>500	207±9.5	418±33
1b	$R_1 = OP(O)(OEt)_2$	$R_2 = H$	57.1±1.8	90.8±0.9	39.3±2.9	90.3±2.8
1c	$R_1 = CH_2Cl$	$R_2 = H$	33.6 ± 0 .4	>500	86.7±3.9	146±8.0
1d	$R_1 = H$	$R_2 = CH_2OH$	>500	>500	>500	>500
1e	$R_1 = CH_2OH$	$R_2 = H$	>500	>500	>500	>500
1f	$R_1 = H$	$R_2 = CH_2ONO_2$	269±2.0	>500	>500	346±24.3
1g	$R_1 = CH_2ONO_2$	$R_2 = H$	9.1±0.1	110±3.8	35.4±2.8	16.0±1.3

Table 8

The effect of the electron density of the spacer on the IC_{50} for cancer cell growth

Compound	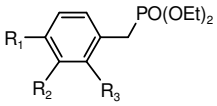			IC_{50}, μM			
				BxPC-3	MIA PaCa-2	HT-29	SW480
1b	R_1 = ASA	R_2 = H	R_3 = H	57.1±1.8	90.8±0.9	39.3±2.9	90.3±2.8
1i	R_1 = ASA	R_2 = H	R_3 = OCH_3	114±2.0	>500	>500	>500
1j	R_1 = ASA	R_2 = H	R_3 = Cl	6.9±1.8	47.2±3.5	19.3±0.5	109.3±0.8
2c	R_1 = OAc	R_2 = H	R_3 = H	4.2±0.7	17.3±2.2	8.2±1.2	4.5±0.5
2d	R_1 = OAc	R_2 = H	R_3 = Cl	7.9±0.5	30.1±4.5	12.4±1.7	22.8±3.5

Chapter 4. Control Drug Delivery Unit Part 1: Structure and Rheological Studies of Pluronic F127 Cross-linked Hydrogels

4.1 Introduction

Hydrogels are a class of material composed of hydrophilic polymer networks with high water retention capacity. In the medical field, biocompatible hydrogels have broad potential application, including surgical aids and drug delivery. In recent years, considerable effort has been made to understand the hydrogel properties of block polymers which consist of poly (ethylene oxide-poly (propylene oxide) (PEO-PPO). These polymers, commonly termed Pluronics, are widely used as nonionic polymeric surfactants. Various studies have been done to investigate the micelle formation, micelle structure and the gelation of PEO-PPO copolymer solution[138-142]. The incentive for these studies is due to its potential applications in biotechnology and drug delivery[143-147]. In dilute solution, the observed micellar behavior of PEO-PPO block polymers is now relatively clear. The block copolymers form micelles in aqueous solutions. These micelles are comprised of a hydrophobic compact core (PPO) and hydrophilic outer core or shell (PEO). The critical micelle concentration (CMC) and critical micelle temperature (CMT) strongly depends on the composition and architecture of the block copolymer. Generally, the CMC and CMT decreases with increasing content of the more hydrophobic block (PPO). The micelle structure also remains unchanged within certain concentration ranges, but with increasing temperature the aggregation of the number of micelle increase. For some systems, such as Pluronic F127, the packing of the micelles account for the gelation of copolymer[148-151].

Pluronic F127, an FDA approved biocompatible triblock copolymer, consist of PEO and PPO blocks (Fig. 24). Aqueous solutions of Pluronic F127, at 20% (w/v) or higher concentrations, exhibit a reverse thermal sol-gel transition. During this transition, temperature increase starting at 4^0C, Pluronic F127 is transformed from a mobile viscous solution to a semisolid gel. This gelation is reversible upon a decrease in temperature. This sol-gel phenomenon is attributed to the closed packed micellar structure described earlier[149,152-154]. The hydrogel formed by Pluronic F127 has been studied extensively in biomedical application such as drug delivery, specifically as an injectable system. However, when the physical gel formed is exposed to large volume of aqueous solutions, rapid dilution of the copolymer concentration occurs. This in turn leads to the immediate lost of the copolymer gel structure and integrity[145,155-160]. The sol-gel transition behavior of Pluronic F127 can also be affected by other factors. One factor that has been of interest is the cross-linking of the Pluronic F127. Cross-linking of the Pluronic F127 leads to the formation of a 3-D network, resulting in an improved retention of gel structure and integrity as described by Cohn et al[157]. Earlier rheological data has demonstrated that the modification of Pluronic F127 with di-methacrylate terminal group provides us with a method of cross-linking the hydrogel while only slightly changing the Pluronic F127 behavior. Swawheny et. al were able to show cross-linking of Pluronic F127-DMA in aqueous solution using the APS/sodium metabisulfite redox catalytic system as review by Cohn[157]. This system although quite capable of cross-linking the hydrogel system requires the use of toxic materials. Therefore, the need for a non-toxic material which would allow for the cross-linking of the Pluronic F127 hydrogel is required.

In this paper, we introduce a non-toxic method of cross-linking Pluronic F127 based on photo-polymerization. We also characterized the effect of photo-cross-linking on the gelation behavior of Pluronic F127 hydrogel using a photo-initiator (1-[-4-(2-Hydroxyethoxy)-phenyl]-2-hydroxy-2-methyl-1-propane-1-one). Photo-polymerization is used in a broad range of commercial and biological applications such as printing, dentistry, and optical materials[138,141,158,161,162]. These systems, because of their ability to rapidly convert liquid monomer or

macromer solutions to a cross-linked network under physiologic conditions, are also being used for an increasing number of biomedical applications[138,141,158,163]. The development of biocompatible photo-polymerizable polymers for application use in drug delivery has the potential to provide controlled release of therapeutic agents for diseases such as cancer. This is achieved due to the fact that photo-polymerization reactions are driven by chemicals that produce free radicals when exposed to specific wavelengths of light. A photon from a light source excites or dissociates the photo-initiator into a high-energy radical state. This radical then induces the polymerization of a macromer solution[161]. Thus, by using a photo-initiator and subjecting modified Pluronic F127 to a specific exposure time to UV irradiation we can generate a biomedical delivery system for medicinal agents. Thus, by varying treatment exposure time of UV irradiation the behavior of the photo-cross-linked hydrogel can be characterized based on its swelling, degradation, rheological and release profiles, as well as the cytotoxicity of the photo-initiator and Pluronic F127.

4.2 Experimental Methods and Materials

Pluronic F127 [$(PEO)_{99}(PPO)_{69}(PEO)_{99}$] and 1-[-4-(2-Hydroxyethoxy)-phenyl]-2-hydroxy-2-methyl-1-propane-1-one were gifts from BASF (Florham Park, NJ). Triethylamine, toluene, chloroform, petroleum ether, methacryloyl chloride, 3-(4,5-Dimethyl-2-thiazolyl)-2,5-diphenyl-2H-tetrazolium bromide (MTT), sodium dodecyl sulfate (SDS), hydrochloric acid (HCl) and Bovine Serum Albumin (BSA) were purchased from Sigma Aldrich (St. Louis, MO). All chemicals and reagents were of analytical quality.

Cell lines: The cell lines used in this study included HT-29 colon cancer cells (American Type Culture Collection Manassas, VA) and NCM 460 Cell Line (INCELL Corporation, San Antonio, TX).

Cell culture reagents: McCoy's 5A medium, Fetal bovine serum, penicillin-streptomycin solution (Mediatech, Manassas, VA) and M3:10TM medium (INCELL Corporation, San Antonio, TX) were used to grow and maintain cell cultured lines.

Synthesis of dimethacrylated Pluronic F127

Dimethacrylated Pluronic was synthesized and analyzed as previously described[157]. In brief, Pluronic F127 (50 g) was poured into a three-neck flask and dried at 120^0C under vacuum for 2 hours. The polymer was dissolved in 40 ml of dry chloroform and the solution cooled to 0^0C in an ice bath. Subsequently, Triethylamine (26 mmoles) was added to the mixture. Freshly distilled methacryloyl chloride (26 mmoles) was diluted in 10 ml of chloroform and added drop-wise for 2 hours into the cooled mixture. The reaction was allowed to proceed for 24 hours at room temperature. After 24 hours, the mixture was resuspended in 150 ml of toluene being heated on a hot plate. The triethylammonium hydrochloride salt generated by this procedure was removed by filtration of the hot mixture. The toluene mixture was subjected to precipitation in petroleum ether. The precipitate was isolated by vacuum filtration and washed

with petroleum ether. The white product, Pluronic F127 di-methacrylate was dried under vacuum at room temperature. . The extent of acrylation was determined by ^{1}H-NMR (Oxford, Oxfordshire, UK: 300 MHz) and FTIR (Nicolet iN10, Thermo Fisher Scientific Inc., Madison, WI).

Synthesis of Pluronic hydrogels

To fabricate Pluronic hydrogel, Pluronic F127 was dissolved in distilled water to make a 25% (w/v) solution. 1-[-4-(2-Hydroxyethoxy)-phenyl]-2-hydroxy-2-methyl-1-propane-1-one (molecular formula $C_{12}H_{16}O_4$), at a concentration of $^{2}/_{3}$% (w/v) relative to the polymer, was used as a photo-initiator. The sol-state solution was placed at 4^{0}C and mixed until the mixture became homogeneous. To fabricate gel-disks, 500 µl of solution per disk were poured into a mold at room temperature. After the gel state mixture equilibrated at room temperature, it was irradiated for 5, 10, 20 and 30 min by long-wavelength UV (365 nm) at 2745 µW/cm^2 intensity. Samples were UV irradiated in a UV cross-linker (Spectronics Corporation, Westbury, NY). All samples were placed 15 cm away from the bulb. After UV-induced polymerization, gel-disks were washed thoroughly to remove unreacted macromers and other impurities.

Determination of the extent of Swelling

Swelling ratios of hydrogels were obtained at 4, 25 and 37 ^{0}C. The initial masses of hydrogel were measured and the hydrogel disks were incubated in phosphate-buffered saline (10mM, pH 7.4) at the desired temperature. After 24h the final mass of the hydrogel disk were measured. At each temperature, the swelling ratios were calculated by the following equation:

- **Swelling ratio %: $[(W_s - W_d)/W_d] \times 100$**
- **(W_d: initial weight of hydrogel, W_s: final weight hydrogel)**

All experiments were performed in triplicates.

Determination of mass degradation

Mass degradation profile of hydrogels was obtained at 37^0C. The initial dry masses of the hydrogels were measured. Subsequently, the hydrogel disks were incubated in phosphate-buffered saline (10mM, pH 7.4) at 37 ^{0}C. At predetermined time points, the hydrogels were freeze dried and weighed. Mass erosion percent was calculated by the following equation:

- **Degradation ratio %: $[(W_I - W_F)/W_I] \times 100$**
- **(W_I: initial dry weight of hydrogel, W_F: final dry weight hydrogel)**

All experiments were performed in triplicates.

In vitro cytotoxicity of the photo-initiator and Pluronic F127

In vitro cytotoxicity of the Pluronic F127 polymer and the photo-initiator was quantitatively analyzed using the MTT assay. HT-29 colon cancer and NCM 460 normal colon cells were seeded in a 96-well plate at a density of $1x10^4$ cells per well and allowed to adhere by incubation overnight at 37^0C in a 5% CO_2 humidity chamber. To determine the possible *in vitro* effect of these agents, cells were treated with Pluronic F127 polymer solution and with 1-[-4-(2-Hydroxyethoxy)-phenyl]-2-hydroxy-2-methyl-1-propane-1-one (photo-initiator). Cells were treated with designated concentrations of Pluronic F127; 0.10, 0.25, 0.50, 1.00, 2.50, 5.00, 7.50 and 10.0 %w/v and photo-initiator ($x10^{-3}$); 0.1, 1.0, 2.5, 5.0, 7.5, 10.0. 50.0 and 100.0 %w/v for 24h. At this time point, 10 µl of MTT solution I (5mg/ml of MTT in PBS) was added to each well and incubated in a 5% CO_2 humidity chamber for 4h at 37^0C. The precipitant formed was dissolved in 100 µl of MTT 2 solution (10% SDS in 0.1% HCl) and incubated, again, in a 5% CO_2 humidity chamber overnight at 37^0C. Cell viability was determined spectrophotometrically at a wavelength of 595 nm and the data were handled

with SoftmaxPro Version 3.1.1 (Molecular Devices, Sunnyvale, CA). Cell viability was expressed as the ratio between the fluorescence intensity of cells incubated with test agent and that of cells incubated with culture medium alone.

Rheological study

Dynamic moduli of the hydrogels were measured by Bohlin Gemini HR Nano Rheometer (Malvern Instruments Inc., Westborough MA). Storage or elastic (G') and loss or viscous (G") moduli were measured as a function of stress, frequency and temperature. Rheological behaviors of physical and photo-cross-linked Pluronic hydrogel gels photo-cross-linked at different UV-irradiation times were evaluated at 25^0C for stress and frequency sweep and at 4-70^0C for temperature sweep. Samples were fabricated to match the diameter of the parallel plate. A force of 1N was applied to each sample.

Statistical analysis

Experimental values were expressed as mean ± SEM. Differences between mean values were evaluated using Student's t-test and the association between variables was determined using regression analysis; $p<0.05$ was considered statistically significant. All statistical analysis was performed using the GraphPad Software (LaJolla,CA)

4.3 Results

4.3.1 Preparation of Pluronic F127-DMA

Pluronic F127-DMA macromer was synthesized as the reaction of OH-terminated according to the method described in procedure 2.2 (Fig 25). The structure was confirmed by ^{1}H-NMR analysis (Fig 26A and 26B), which showed incorporation of methacrylic groups at both ends of the Pluronic polymer. The vinyl protons of the methacrylate group (=CH2) appeared at 5.58 ppm and 6.13 ppm. Whereas, the three protons of the methyl substituent (=CCH3) are shown at 1.95 ppm. The functionalization of Pluronic F127 was further determined by FTIR (Fig. 27A and 27B) which demonstrated the gradual peak appearance of weak peak at 1715.78 cm^{-1}. This peak corresponds to carbonyl vibration of the ester group. As determined by ^{1}H-NMR, the acrylation degree of Pluronic F127 was about 80.1%.

4.3.2 Synthesis of hydrogels

A 25% (w/v) solution of Pluronic F127-DMA, a clear viscous fluid at low temperature, was prepared in deionized water. At room temperature, due to the formation of micelles, the solution became a physical gel. Using 1-4-(2-Hydroxyethoxy)-phenyl-2-hydroxy-2-methyl-1-propane-1-one as a photo-initiator, cross-linked and non dissolving hydrogels were produced by UV irradiation. The photo-polymerization of the acrylate groups of the Pluronic micelles resulted in a network of chains; thus, forming a chemically cross-linked hydrogels (Fig 28).

4.3.3 Swelling

The effect of UV irradiation on swelling behavior was studied. Swelling ratio values of the hydrogels, obtained as a result of varying their exposure time to UV irradiation, are shown in Fig. 29. This figure demonstrates that the swelling ratio of the hydrogels gradually decreases with prolonged UV irradiation time. Thus, a more tightly cross-linked polymer gel structure is formed at a lesser exposure time. In addition, at incubations of higher temperatures, 25^0C and 37^0C, the swelling ratio significantly decreased. For example at 4^0C, as the UV irradiation time increase from 5 min to 10, 20 and 30 min, the ratio of swelling decreased by 24.8, 41.6 and 51.0%, respectively. Also, the swelling ratio of the hydrogels UV irradiated for 5 min from 4^0C to 25 and 37^0C decreased by 67.9 and 90.3% respectively. This indicates that these hydrogels, despite UV irradiation treatment, retained their thermo-responsive ability to respond to changes in temperature similar to that of the uncross-linked physical gel.

4.3.4 Degradation profile

The mass erosion profile of the cross-linked Pluronic F127 hydrogels irradiated with different UV times is presented in Fig 30. Due to gradual cleavage of the ester linkage in the polymerized site, the hydrogels degraded slowly as a function of time. Loosely cross-linked hydrogels prepared by a low dose of UV irradiation shows faster degradation than more cross-linked hydrogels prepared by prolonged UV irradiation times. Samples prepared using UV irradiation exposure times of 10, 20 and 30 min yielded degradation profile of 17.1, 27.6 and 35.0%, respectively. This degradation profile was slower compared to samples treated with 5 min UV irradiation. Thus, this demonstrates that the mass erosion

extent of the polymer gel network depends on the cross-linking density that directly affects the swelling ratio.

4.3.5 *In vitro* cytotoxicity of photo-initiator and Pluronic F127

A comparison of the *in vitro* cell viability of HT-29 colon cancer and NCM 460 normal colon cell lines after 24 h treatment with Pluronic F127 or the photo-initiator at varying concentrations is presented in Fig 31. Since these components are part of the drug delivery systems and are likely to be release it is crucial to determine whether they may exert a cytotoxic effect.

As the concentration of Pluronic F127 was increased, a concentration dependent effect on cytotoxicity was observed in both cancer and normal cells (Fig 31A). The effect of Pluronic F127 on the cell cytotoxicity of the cancer cells cell line was greater as compared to the normal colon treated at the same concentration. Consequently, the cell viability was 1.0 to 3.2 times higher for normal cells than that of cancer cells treated with Pluronic F127 (1.0 to 7.5%w/v, respectively). At concentrations of Pluronic F127 higher than 1%w/v, the differences in cell viability between normal and colon cells were statistically significant, $p<0.005$ in all cases.

The effect of the photo-initiator on cell viability for the normal colon (NCM 460) and colon cancer (HT-29) cells is shown in Fig 31B. NCM 460 cells were less sensitive than HT-29 cells to the photo-initiator. Thus, at the observed treatment concentrations, the photo-initiator had no cytotoxic effect on NCM 460 cells. However, the photo-initiator exhibited a concentration dependent cytotoxic effect on HT-29 cells. At the highest concentration of the photo-initiator (0.1%w/v), cytotoxicity increased by 1.2 times in cancer cells compared to normal cells. This increase in cytotoxicity was statistically significant, $p<0.01$. These cytotoxicity results emphasize the varying effect the cross-linking components exhibits on different cells.

Overall, the Pluronic F127 and the photo-initiator were more toxic to cancer cells than to normal cells. The lesser degree of cytotoxicity to normal cells treated with Pluronic F127 and 1-[-4-(2-Hydroxyethoxy)-phenyl]-2-hydroxy-2-methyl-1-propane-1-one (the photo-initiator) underscores the potential use of these compounds in drug delivery systems.

4.3.6. Rheological study

The dynamic moduli of the physical gel and the cross-linked hydrogel prepared at different UV exposure times were plotted and presented in Fig 32, 33 and 34. Each cross-linked hydrogel was measured as a function of frequency (at 25^0C:Fig.32), a function of stress (at 25^0C: Fig.33) and a function of temperature (at 4-70^0C: Fig.34).

As seen in Fig 32, indicating the frequency sweep, the hydrogels remained stable with increasing frequency. However, the dynamic moduli (G' and G") values were much higher than that of the physical hydrogel produced at 25^0C. G' and G" values gradually increased with prolong UV irradiation, revealing that the mechanical strength of the Pluronic hydrogel increased with increasing UV dose. This is due to the additional formation of cross-linked chain network structure. Over the entire range, the storage or elastic modulus (G') values were greater than the loss or viscous (G") values. This data indicates that the photo-cross-linked Pluronic hydrogels behaved as a viscous-elastic solid.

Stress sweeps, also referred to as amplitude sweeps, were used to characterize the stability of the physical gel and the cross-linked hydrogel. In general, the stability of a material increases as the linear visco-elastic range of the material widens. G' and G'' (data not shown for G") displayed the well known visco-elastic behavior. A standard amplitude sweep measured at a frequency of 1 Hz at a temperature of 25^0C is shown in Fig 33. This behavior reveals that in the linear visco-elastic range G' is constant with increasing stress. Whereas, at

the yield point, G' decreases at higher shear stress values. Over the entire range, the storage or elastic modulus (G') values were greater than the loss or viscous (G") values. This data indicates that the photo-cross-linked Pluronic hydrogels behave as a visco-elastic solid. The storage modulus were further analyzed at shear stress equal zero and at the yield point. The data was gathered and plotted against the UV irradiation exposure time (Fig. 33B). We observed that the shear stress at shear stress equal zero and at the yield point of the hydrogels increased with UV irradiation time exposure. This demonstrated that the degree of photo-cross-linking of the hydrogels is dependent on UV exposure time. This is in agreement with the frequency sweep results, which indicates as the degree of cross-linking increased the mechanical strength of the hydrogel increases due to the formation of a more densely formed polymeric network.

In our effort to further characterize the hydrogels, we explored the effect of temperature (Fig.34). In general, with an increase in temperature the dynamic moduli showed a build up regime followed by a plateau regime (Fig. 34A and 34B). The buildup of the dynamic moduli can be attributed to the increased formation of cross-linked networks. The elevation of temperature accelerates molecular motion and thus, increases the chance of inter or intra molecular interaction. Therefore, this association or reaction may lead to significant acceleration of gelation. Fig 34D shows the plot of transition temperature of the hydrogel versus the UV irradiation time. The plot demonstrates that there was no significant change in transition temperature of the different hydrogel with increased time exposure to UV irradiation. This demonstrated that the cross-linked hydrogels were able to maintain the gelation ability of the physical gel. Whereas, the values for dynamic moduli showed a UV treatment dependence where the G" and G" values increased with increasing UV irradiation dosage. The transition temperature values do not show a UV dependence. Comparing the initial and the final storage modulus (G'), the physical gel (uncross-linked) was found to have the highest change of 2,794.7 times increase between the maximum and minimum G' values. Interesting, as the exposure time to UV increased a decrease was observed in the change of storage modulus from the

minimum to the maximum G' values. The G' values increased 6.0, 1.6, 1.4 and 1.3 fold as the time of exposure to UV irradiation increased from 5, 10, 20 to 30 min, respectively.

Stress (amplitude), frequency and temperature sweeps were performed to evaluate the effect of UV irradiation dosage on the mechanical strength of the hydrogel. The visco-elastic material functions G' and G" of the hydrogels showed significant changes with UV treatment. An increase in UV irradiation time resulted in a corresponding increase in dynamic moduli. Temperature was seen as yet another key factor influencing dynamic moduli. Results generated from non-isothermal studies illustrates that physical interactions such as hydrogen bonding and a chemical interactions from the cross-linking process contribute to the visco-elastic property of the hydrogel. Indeed, we were able to show that increases in temperature resulted in an increase in dynamic moduli. Thus, the UV irradiation-dependent rheological properties of the photo-cross-linked Pluronic hydrogels are consistent with the swelling and mass erosion demonstrated in Fig 29 and 30.

4.4 Discussion and Conclusion

The thermo-reversible properties displayed in cross-linked hydrogels produced by functionalization of the Pluronic F127 triblock, aims to combine the reverse thermo-responsive behavior of the physical gel with the much improved mechanical properties of the cross-linked hydrogel. The method of synthesis utilized in this study resulted in a reverse thermo-responsive material that was able to immediately cross-link. By controlling the reaction parameter, various biodegradable Pluronic F127 hydrogels were synthesized using UV induced photo-polymerization. In accordance, earlier researchers synthesized and cross-linked dimethacrylated Pluronic macromer into a micellar gel state[141,158,163-166]. A diverse range of hydrogels with different cross-linking densities and mechanical strength could be produced by altering the UV exposure time.

Earlier rheological data has demonstrated that the presence of the two methacrylate terminal groups affects the Pluronic F127 behavior only slightly, with the native F17 triblock and the uncross-linked Pluronic F127-DMA showing very similar viscosity versus temperature behavior[139,167,168].

Previous method of cross-linking utilized ammonium persulfate (APS)/sodium metabisulfite redox catalytic system (Sawheny et al). The two reagents used in this cross-linking process are both toxic. Based on information obtained from the MSDS, APS, an oxidizing agent which is used as a polymerization initiator, was found to have has low dermal toxicity and was moderately toxic when ingested. On the other hand, the reducing agent sodium metabisulfite has been found to be toxic to humans. Sodium metabisulfite has also been shown to be carcinogenic, have reproductive and developmental toxicity, neurotoxicity, and acute toxicity. These toxic properties of these cross-linking agents limit their use for biological and drug delivery applications. The present study was initiated to determine whether a photo-initiator can be a potential alterative to cross-linking Pluronic F127. Pluronic F127-DMA aqueous

solution was cross-linked using a photo-initiator, a similar method used by Chun et al[138]. Numerous researchers have investigated photo-polymerization biological systems such as tissue engineering[144,158,169,170]. Earlier work done by Atsumi et al. studied the sensitivity of human submandibular-duct cells to two visible light sensitive photo-imitators, camphorquinone and 9-fluorenone. They showed that the photo-initiator induced intracellular reactive oxygen species (ROS). These species induced a ROS dependent cell death behavior, as the concentration of ROS increased cell viability decreased[171,172]. In yet another study, Bryant et al investigated the toxicity of multiple photo-initiators on The NIH 3T3 fibroblast cell line. They showed that indeed a few photo-initiators were particularly well tolerated by the fibroblast cells. Further work to determine the potential toxicity of photo-initiating agents for polymerization on different cell types was performed by Williams et al[173]. Their work demonstrated that different cell lines manifested significantly different responses to identical photo-initiator concentrations and light exposure. This work supports our finding with 1-[-4-(2-Hydroxyethoxy)-phenyl]-2-hydroxy-2-methyl-1-propane-1-one as a photo-initiator. We demonstrated no cytotoxcity to NCM 460 normal cells. We did, however, observe a slight increase of cytotoxicity in HT-29 colon cancer cells with increasing concentration of the photo-initiator. Since permeability through cellular membrane phospholipid bilayers increases with the hydrophobicity of compounds, the hydrophobicity characteristic of the photo-initiator is thought to explain part of its minor cytotoxic effect on HT-29. Due to its polar hydroxyl end groups, the hydrophobicity of 1-[-4-(2-Hydroxyethoxy)-phenyl]-2-hydroxy-2-methyl-1-propane-1-one has been found to be low. Thus, this particular property could explain the low cytotoxicity of 1-[-4-(2-Hydroxyethoxy)-phenyl]-2-hydroxy-2-methyl-1-propane-1-one.

Using 1-[-4-(2-Hydroxyethoxy)-phenyl]-2-hydroxy-2-methyl-1-propane-1-one to cross-link the Pluronic F127-DMA solution a diverse range of hydrogels with different cross-linking densities and mechanical strength could be produced by controlling the UV exposure time. In order to optimize the mechanical properties of these hydrogels, the UV exposure time of Pluronic F127-DMA was

varied from 0 to 30 min. First, the dynamic moduli were measured in a frequency sweep of varying frequency from 0.01 to 16 Hz. The different gels displayed only initial elasticity. The primary elasticity response observed by all hydrogels is quite evident by the fact the G' increased only slightly as the frequency increased. The G" values were substantially lower than the G' values over the entire frequency range being studied. This data is also substantiated by experiments report earlier by Cohn et al and Chun et al[138,157].

Cohn et al[157,174]reported that the physical Pluronic F127 gel begins to yield at very low stress. We demonstrated that this phenomenon was also seen by cross-linking hydrogels. An abrupt change can be seen in the shear stress plots as the hydrogels reach its yield point. The cross-linked hydrogels have also been shown to have higher storage modulus than the Pluronic F127 physical gel. Again, this behavior can be attributed to the cross-linking density characteristic to the UV exposure time.

The effect of temperature on hydrogels formation was also investigated. In accordance with earlier experiments by Cohn[157,174], we found that 25% Pluronic F127-DMA cross-linked hydrogels exhibited similar behaviors as the physical gel. As is apparent by the plot (Fig 34A and B) G' was higher than G" over the entire temperature sweep range from 4^0C to 70^0C. This behavior is in agreement with typical gel behavior. The higher storage modulus values demonstrated by the cross-linked hydrogels are mainly due to the reverse thermo-responsiveness of the Pluronic F127 building blocks. In contrast to the physical gel, the cross-linked hydrogel gels have limited mobility or flow of the of the cross-linked system as it undergoes temperature changes due to its cross-linked network[138,157,174,175]. This structural limitation resulted in the increase of the storage modulus. This was in turn dependent on the UV exposure treatment time.

These finding demonstrate that cross-linked density plays an important role on the mechanical strength of the hydrogel. This is reflected by the fact that the increase in UV exposure time generates an increasing stiffer gel as compared to the physical gel (uncross-linked). Evidently, when the temperature

of the hydrogel is reduced below the sol-gel transition temperature, the covalent bonds formed during the cross-link process prevented the hydrogels from reverting to its solution state. It is worth stressing, that the reverse thermo-responsive of the hydrogel is maintained regardless of the degree of cross-linking. The increase in the mechanical strength of the cross-linked gels shown in the rheological results is supported by the data from the swelling and degradation study (Fig. 29 and 30). The swelling behavior and the degradation of the cross-linked hydrogels gradually decrease with increased UV exposure time. This supports our rheological finding that increase UV exposure time produced a tighter cross-linked polymer gel structure which attributes to its increased mechanical strength. The thermo-responsive behavior of the cross-linked hydrogel, which is supported by the rheological findings, is consistent with the results from the swelling studies (Fig. 29). Our finding show that the swelling ratio substantially decreased with increasing temperature. This thermo-responsive property was also observed in the physical gel. If this hydrogel is to be used for drug delivery purposes, this thermo-responsive property is an important criterion.

Lastly, due to the degradation of the cross-linked hydrogel, the cytotoxicity of Pluronic F127 was measured. To investigate the cytotoxicity of Pluronic F127, NCM 460 normal colon and HT-29 colon cancer cells were treated with various concentration of Pluronic F127 for 24 hr. The cell viability was measure by standard MTT assay. MTT results confirmed that normal colon cells exhibited higher cell viability ratios in comparison to colon cancer cells. This could be explained by earlier work by Parnaud et al. In this study Parnaud et al[176] showed that dietary polyethylene-glycol (PEG) suppressed the occurrence of colorectal adenomas and carcinomas in an accelerated model of carcinogenesis. PEG also known as PEO, is the major monomer present in the Pluronic F127. This study showed the preventive effect of short-term PEG treatments in both male and female rats, when PEG was given in food or water. Taken together, these results suggest that PEG could be a potent anticancer agent in the post-initiation phase of carcinogenesis[176-181]. This finding supports our cytotoxicity behavior of Pluronic F127.

In conclusion, biodegradable Pluronic hydrogel were prepared by photo-cross-linking. Dimethacrylated Pluronic polymer was synthesized and cross-linked in a micellar gel state. We were able to generate a wide range of hydrogels with different cross-linking densities and mechanical strength as produced by controlling the UV irradiation exposure time. Through the investigation of swelling ratio, degradation and rheological studies, we demonstrated that the mechanical strength of the hydrogels was dependent on temperature and exposure time to UV irradiation. The data compiled in this study reveals that the mechanical strength of the Pluronic hydrogel increased with increasing UV dose due to the formation of a network of cross-linked chains and that these photo-cross-linked hydrogels maintained their visco-elastic properties. Based on the cytotoxicity data we demonstrated that the photo-initiator was non toxic and provides us with a safe procedure for cross-linking the Pluronic F127-DMA hydrogels. Hence, after making adjustment to different parameters of the hydrogel, photo-cross-linked Pluronic hydrogel could be utilized as a potential drug delivery system.

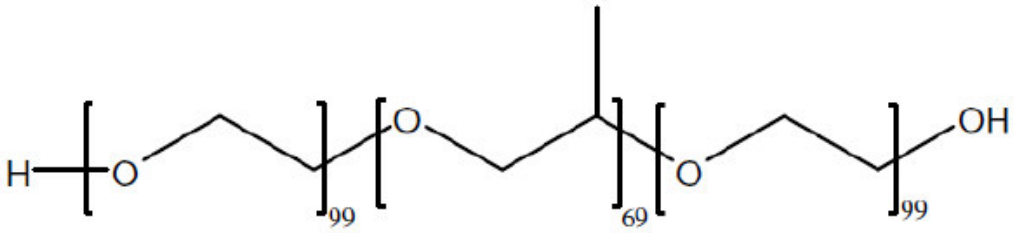

Figure 24. The chemical structure of Pluronic F127.

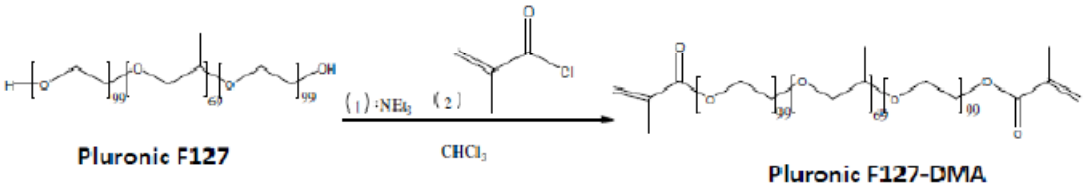

Figure 25. Schematic of the mechanism for the generation of Pluronic F127 Di-methacrylate (Pluronic F127-DMA).

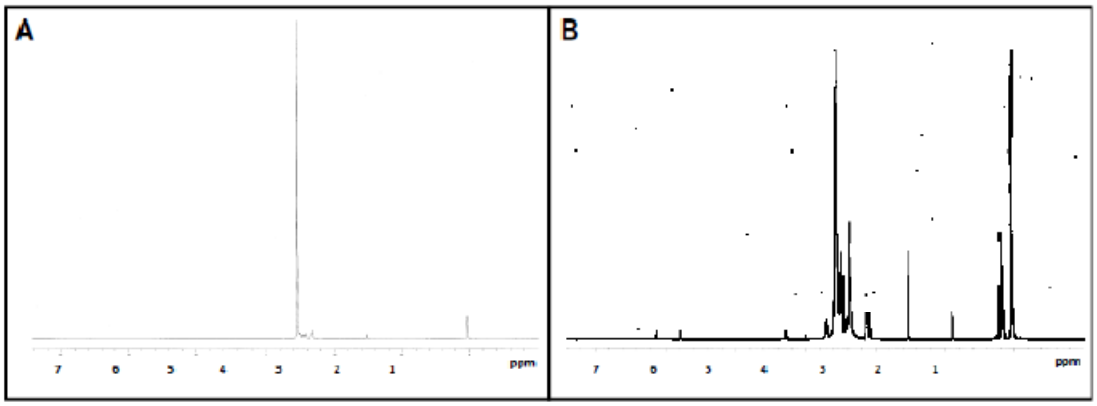

Figure 26. ^{1}H-NMR spectra ($CDCl_3$) of (a) Pluronic F127 and (b) Pluronic F127-DMA

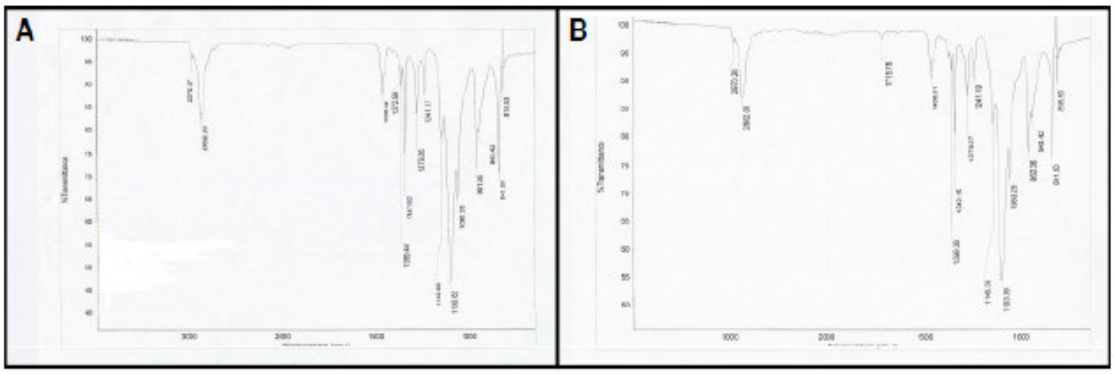

Figure 27. FTIR spectra of (a) Pluronic F127 and (b) Pluronic F127-DMA

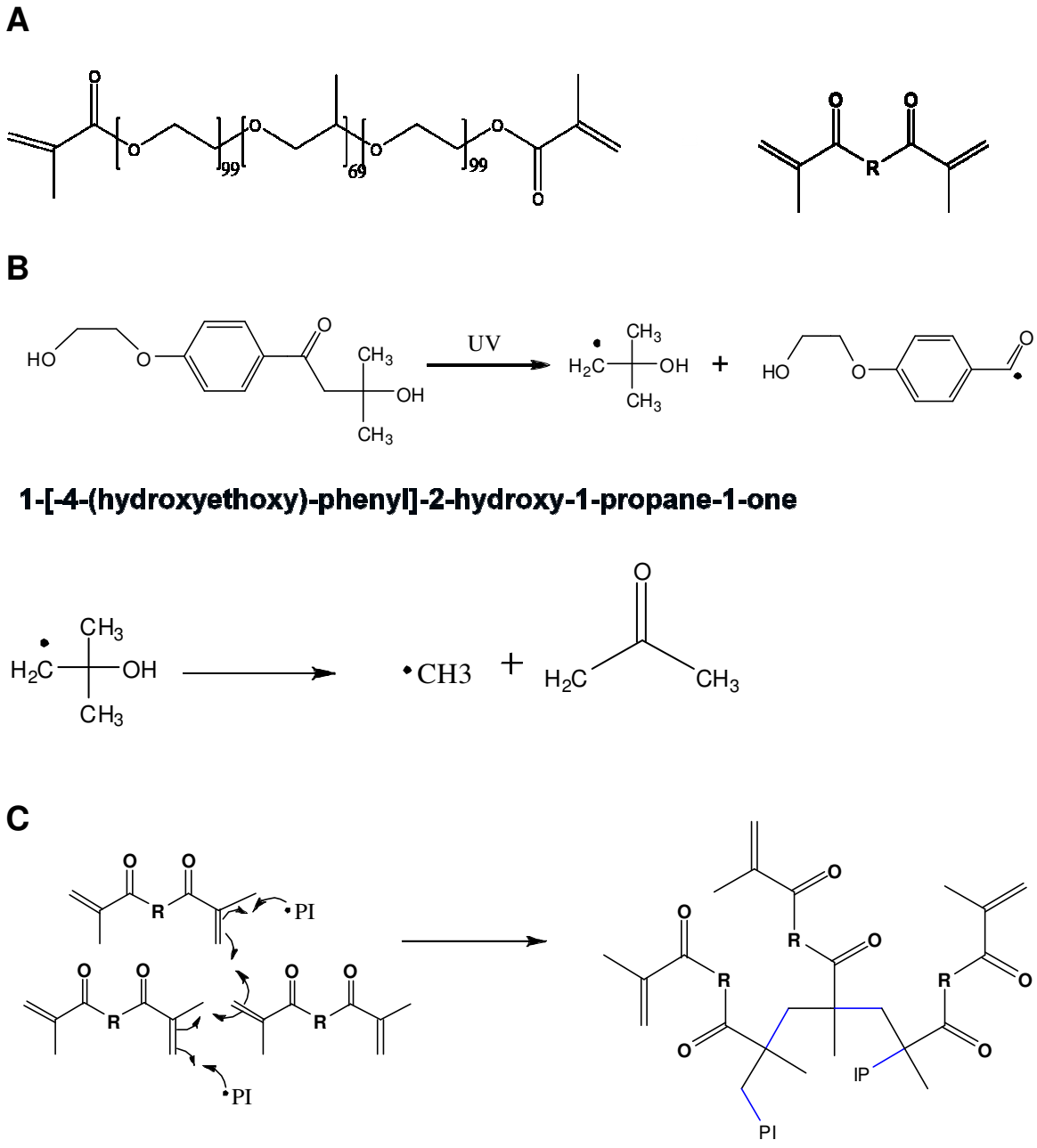

Figure 28. (a) Schematic representation of (a) Pluronic F127-DMA, (b) mechanism of photo-initiator and (c) mechanism of UV cross-linking of Pluronic F127-DMA for the cross-linking process of Pluronic F127-DMA solutions

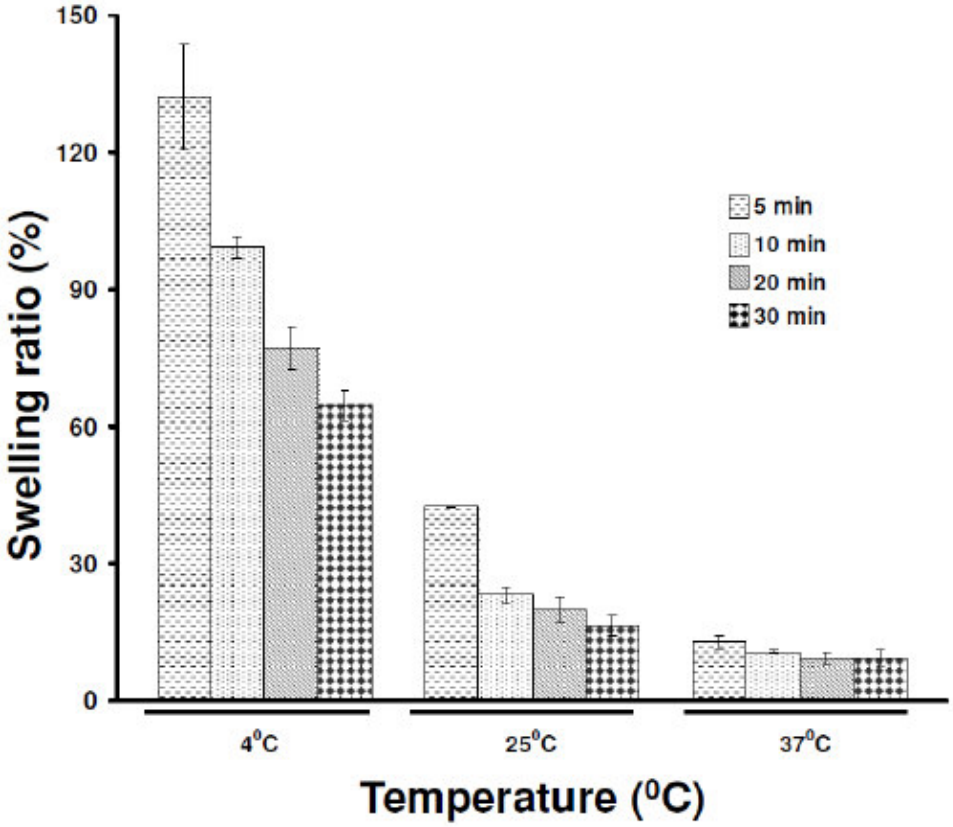

Figure 29. Swelling behaviors of Pluronic F127 hydrogels in PBS buffer as a function of UV irradiation. Samples were incubated at 4^0C, 25^0C and 37^0C

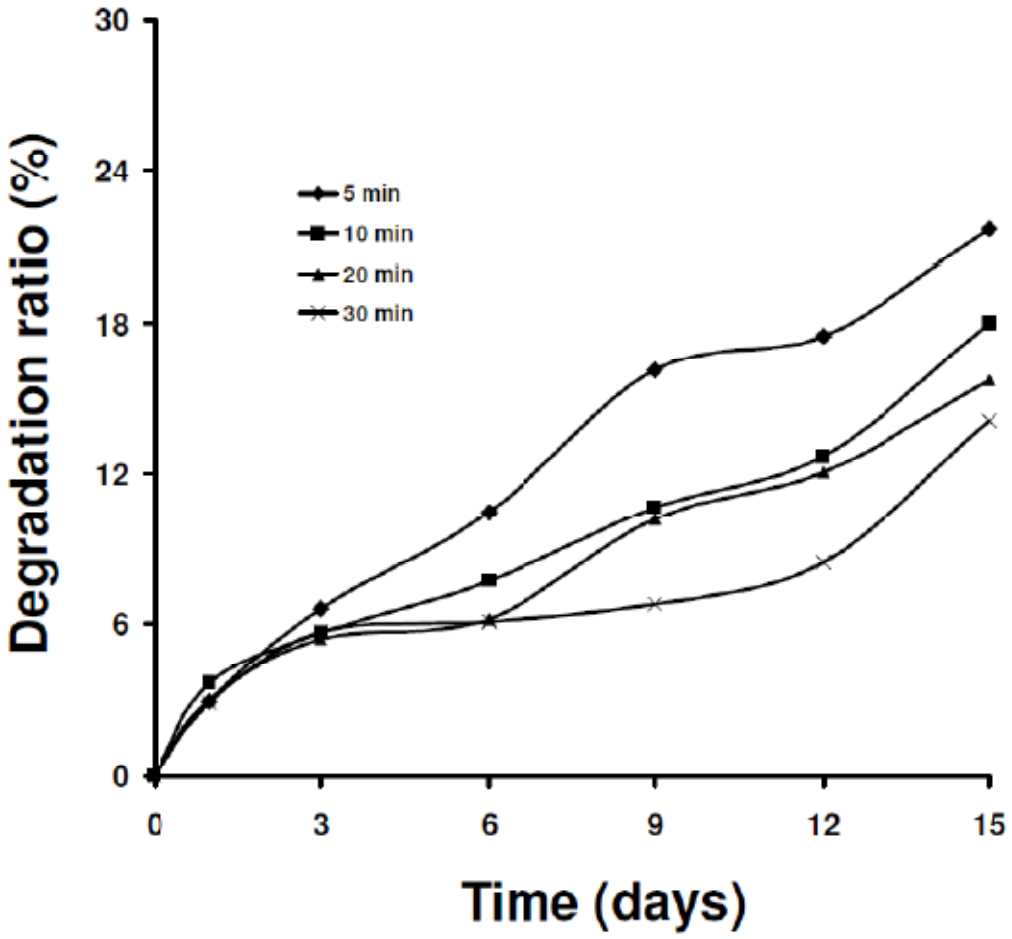

Figure 30. Degradation profiles of Pluronic F127 hydrogels prepared by exposure to UV for different periods. The samples were incubated at 37^0C

A

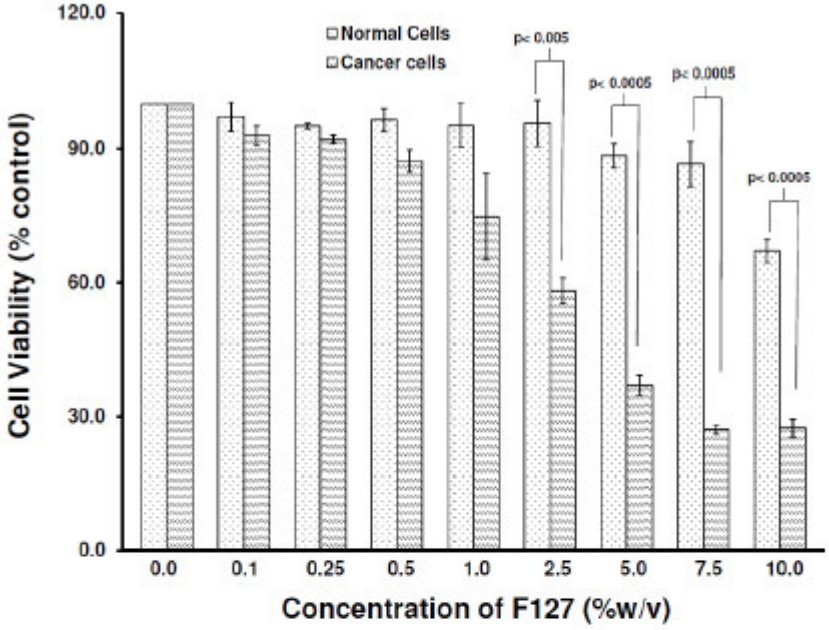

B

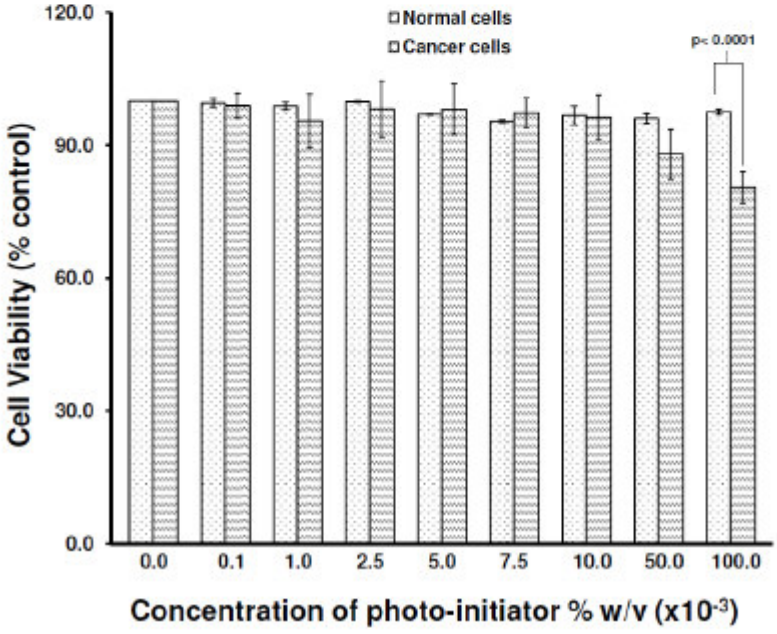

Figure 31. ***In vitro*** **viability of HT-2 colon cancer cells and NCM 460 normal colon cells treated with (a) Pluronic F127 solution and (b) 1-[-4-(2-Hydroxyethoxy)-phenyl]-2-hydroxy-2-methyl-1-propane-1-one(photo-initiator)** ***(n=3)***

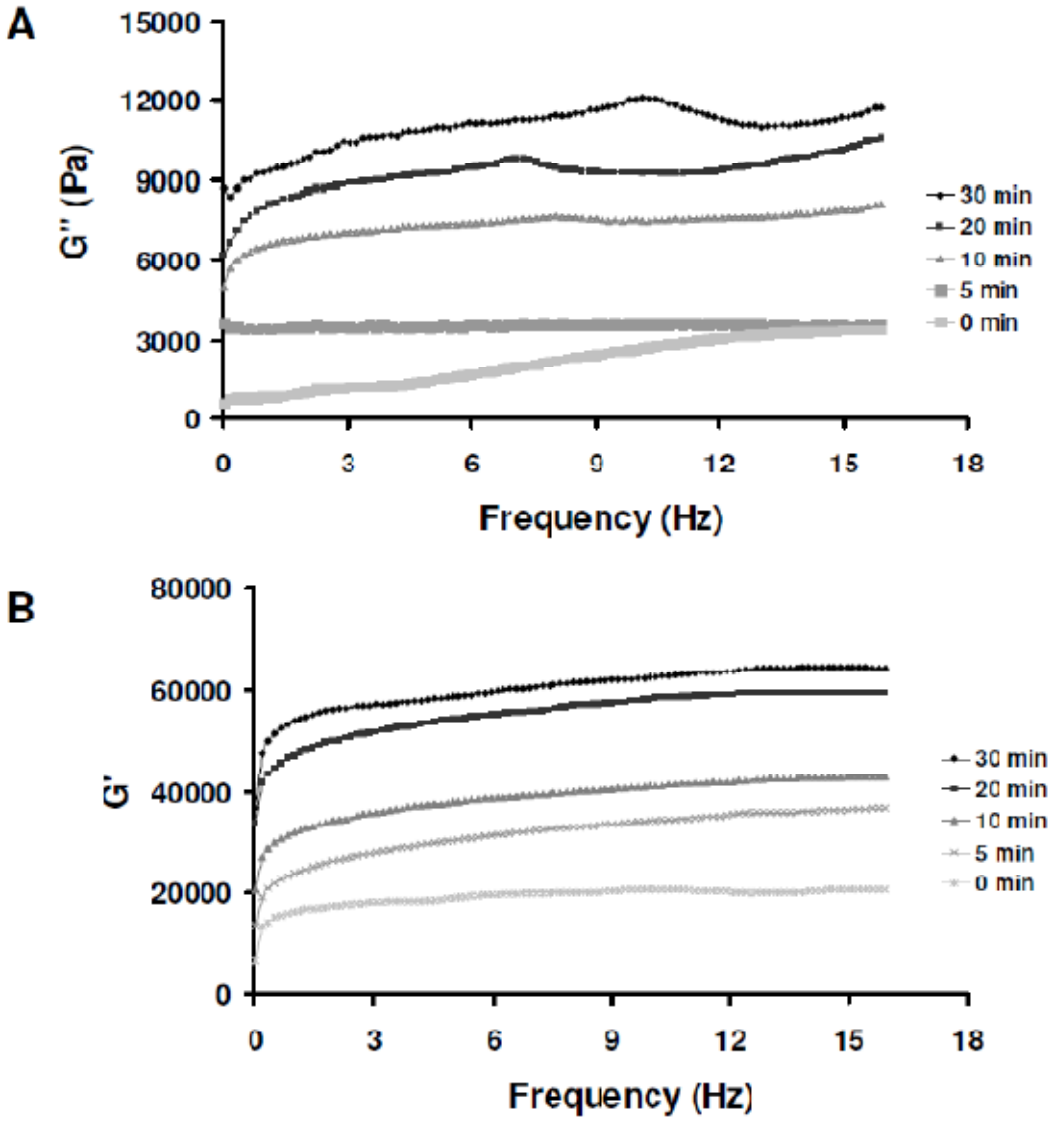

Figure 32. Frequency dependence of G' and G'' for 0, 5, 10, 20 and 30 min UV exposed cross-linked Pluronic F127-DMA exposed to UV irradiation for 0, 5, 10, 20 and 30 min at a Strain of 0.05 and 25^{0}C

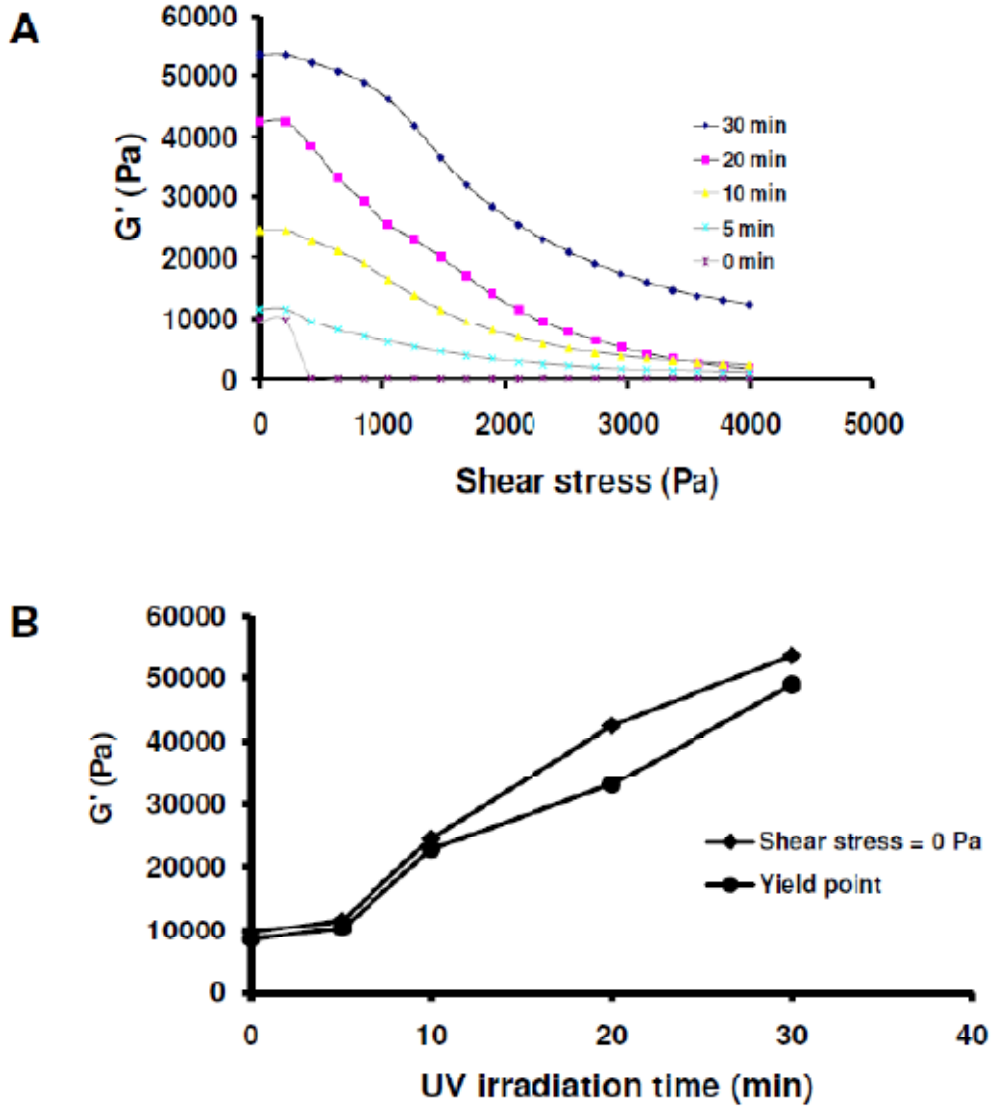

Figure 33. Amplitude sweep: (a) Loss modulus and (b) storage modulus as a function of temperature and (b) Maximum value of storage modulus (at shear stress equal zero and at yield point) as a function of UV exposure time for 25% w/v Pluronic F127 hydrogels exposed to UV irradiation for 0, 5, 10, 20 and 30 min at a frequency of 1Hz and 25^0C

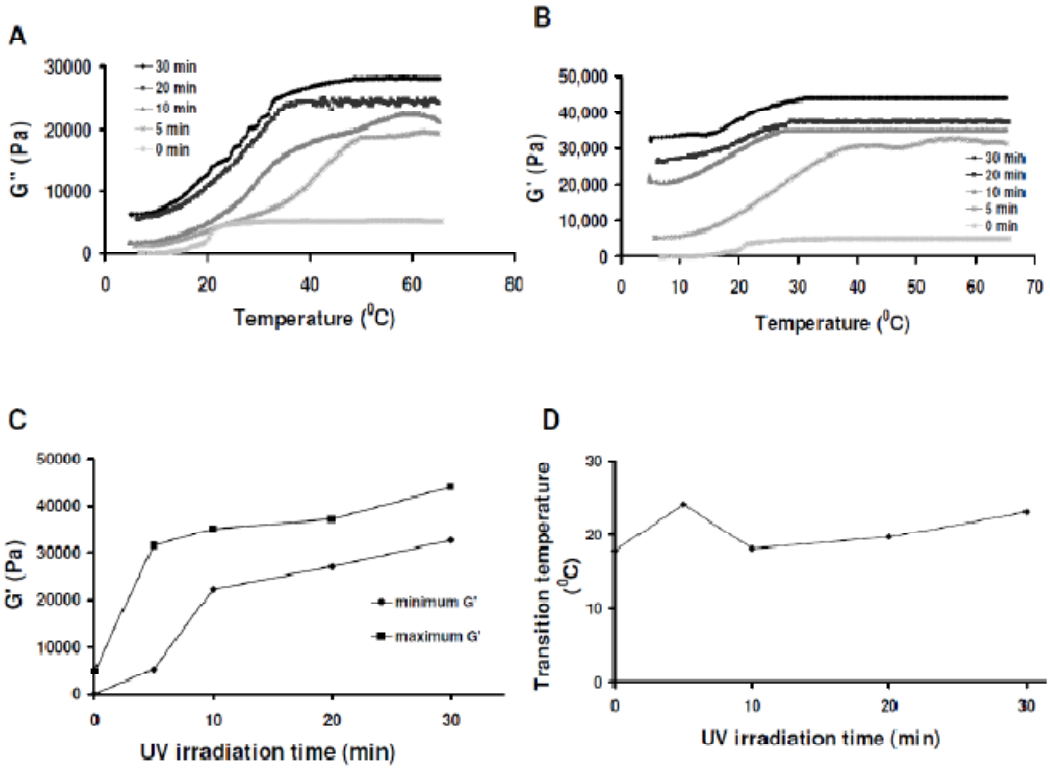

Figure 34. Temperature sweep: (a) Storage modulus a function of temperature, (b) loss modulus as a function of temperature, (c) maximum and minimum value of storage modulus as a function of UV exposure time and (d) Transition temperatures of the hydrogels as a function of UV exposure time for 25% w/v Pluronic F127 hydrogels exposed to UV irradiation for 0, 5, 10, 20 and 30 min at a frequency of 1Hz and strain amplitude of 0.05

Chapter 5. Controlled Release Drug Delivery Unit Part 2: Externally regulated controlled release of anticancer agents from photo-cross-linked Pluronic hydrogels

5.1 Introduction

A wide range of natural and synthetic polymeric hydrogels have been extensively used for drug-delivery carriers, tissue engineering templates, and as medical devices. Among them, much attention has been paid to stimuli-sensitive synthetic hydrogels for their unique properties (i.e., thermo-sensitivity). In particular, amphiphilic block copolymers, which show a reversible gel transition behavior in specific temperature ranges, have been used as injectable hydrogel materials. At high concentrations (critical micelle concentration) and below the critical temperature, they exist in a viscous solution state, but at the critical temperature they turn into a physically cross-linked gel state. These hydrogels have been exploited for use in controlled drug delivery[145,146,150]. Water-soluble tri-block copolymers of poly(ethylene oxide)-b-poly(propylene oxide)- b-poly(ethylene oxide), commercially known as Pluronics or Poloxamers, exhibit a similar thermal gelling property. Near room temperature and above a critical concentration (20% (w/v)) a once aqueous solution of Pluronic F127 transitions to a self assembled organized micelle gel structure[150-152,168,182], as described in the previous chapter

A growing interest has been focused on a sustained delivery system of anticancer agents. The use of biocompatible hydrogels appears to be a more attractive approach in achieving sustained drug release. Biocompatible polymers such as Pluronic F127 posses the ability to readily control the drug release rate by modulating the network structure with adjusting cross-linking density. The

cross-linking density of biocompatible polymers can be achieved by controlling the degree of chemically polymerization. One method of achieving effective cross-linked polymers is photo-polymerization, as characterized in the previous chapter (Chapter 4).

The development of biocompatible photo-polymerizable polymers for drug delivery applications has the potential to provide control release of therapeutic agents for diseases such as cancer. For instance, instead of taking therapeutics agents orally, physicians could potentially reduce cytotoxicity of therapeutic agents by externally controlling the release of these agents in a localized area. If fully developed into clinical practice, such a strategy could reduce the possibility of under or over dosing of therapeutic agents. In addition, this method would provide localized drug delivery at the site of the disease.

One potential disadvantage of the photo-polymerization processes the affect on the affect on the therapeutic agent. This process can potentially reduce the efficacy of the drug and inhibit the ability of the polymer to cross-link while the therapeutic agent is entrapped. Thus, to circumvent this problem, the drug loaded-poly(D,L-lactide –*co*-glycolide) (PLGA) nanoparticles (NPs) were formulated.

Nanoparticles of biodegradable polymers as drug delivery systems are widely investigated for controlled and targeted delivery of various drugs. Numerous studies have demonstrated that this formulation provides a way to avoid the addition of harmful adjuvant to the drug, confer the drug with reduced side effects and to achieve better therapeutic efficacy than the pure agent[183-186]. PLGA is a biodegradable and biocompatible polymer, which has been approved for human use by the US Food and Drug Administration (FDA)[183,187,188]. The protocols for preparation of drug/imaging-loaded PLGA NPs for various biomedical applications are numerous. Of these protocols, the solvent/extraction/evaporation technique was adopted for use in this study. Due to reproducibility, high drug loading capacity and high stability[189], this method was highly suitable for our study.

Some of the most promising pharmaceutical agents described to date for the prevention of cancer are nonsteroidal anti-inflammatory drugs (NSAIDs)[117,190]. The potential importance of NSAID derivatives in cancer control originates from their well-established efficacy in the prevention of human cancer and the accompanying understanding of their mechanisms of action. One such mode of action centers on the role of cyclooxygenase-2 (COX-2) overexpression in carcinogenesis; inhibition of COX enzymes is the best recognized mode of action of NSAIDs[191,192]. Of all the various NSAIDs reported to inhibit the development of tumors, sulindac sulfide seems to be one of the most effective in experimental animal models. Sulindac sulfide is a potent nonselective inhibitor of COX. Other NSAID derivatives have also emerged as a promising group of drugs for the prevention and treatment of cancer. NSAID derivatives consist of a releasing moiety covalently attached to conventional NSAIDs via a spacer. They have been shown to have significant promise as chemopreventive agents against a number of cancers. Several studies have shown NSAIDs derivatives such as NO-NSAIDs to be more tolerable than conventional NSAIDs, as well as several hundred times more potent in inhibiting the growth of cancer cell lines derived from a variety of human cancers including colon, pancreatic and breast cancer. For this study utilized a conventional NSAID, sulindac sulfide (Fig 35A) and a new derivative of NSAID containing a diethyl phospho-releasing group, Drug D (Fig 35B).

In this study we also examined the use of a thermoelectric (TE) module, a semiconductor based electronic component which functions as a small heat pump, as a controlled releasing mechanism. By applying a low voltage to the TE module, heat was transferred through the module from one side to the other. Therefore, one side was cool while the opposite side was simultaneously hot[193,194]. This phenomenon can be made reversible by changing the polarity of the applied voltage. This reversal causes the heat to be transferred to the opposite side of the TE module. Consequently, TE module can be used for both heating and cooling; thus, making it suitable for precise application for temperature control. Besides the ability to direct both heating and cooling with

the same module, other advantages of TE module that allow them to be suitable for temperature release application in drug delivery exist. These advantages include the fact that TE module contains no moving parts, is small and lightweight, has a wide variety of temperature ranges, is environmentally friendly and, based on the design of the module; can be cooled to very low temperatures[195-197].

Attaching the cross-linkable polymer onto the TE modules is crucial to enabling control release of the drug-loaded PLGA NPs from the polymer via thermo-stimulation. To enable the attachment of the drug-loaded thermo-reversible hydrogel to the TE module, we utilized poly(methyl methacrylate), PMMA. PMMA is a versatile polymeric material that is well suited for many imaging and non-imaging microelectronic applications[198-200]. It is most commonly used in x-ray and deep UV microlithographic processes. PMMA is also used as a protective coating for wafer thinning, and as a bonding adhesive[198]. In this study we exploited the interactive characteristic of PMMA with PEO moiety of Pluronic F127. This interaction is generally thought to be a weak interaction. The specific interaction may occur between the carbonyl carbon atoms of the PMMA and the oxygen atoms of the PEO. However, the exact nature of these interactions is still unknown[198]. This interaction facilitates the attachment of the cross-linkable hydrogel to the PMMA coated TE module.

In this study a novel drug delivery system has been developed utilizing a thermoelectric module acting as platform to initiate the thermo-responsiveness of the hydrogel. The drug formulation and *in vitro* release kinetic of a Pluronic system made of dimethacrylated Pluronic F-127 was examined as a function of ultra-violet (UV) irradiation dose. Particularly, sustained (1-15 days; UV exposure 0, 5, 10, 20 or 30 min) and externally regulated delivery (0, 10 or 30 min; UV exposure 10 min) of anticancer drug from the Pluronic hydrogels was investigated by using different UV irradiation doses. Here, we demonstrate our ability to generate such as system and to release into HT-29 colon cancer cells, in an externally regulated control manner, PLGA packaged chemopreventive agents.

5.2 Experimental Materials and Methods

Materials

Pluronics F-127 [$(PEO)_{99}(PPO)_{69}(PEO)_{99}$] and 1-[-4-(2-Hydroxyethoxy)-phenyl]-2-hydroxy-2-methyl-1-propane-1-one were gifts from BASF (Florham Park, NJ). Triethylamine, toluene, chloroform, petroleum ether, dichloromethane, acetonitrile, methacryloyl chloride, ethanol, hydrogen peroxide, sulfuric acid, formaldehyde, poly vinyl alcohol (PVA), sodium hydroxide, triton X-100, poly(lactic-co-glycolic acid) (PLGA L:G molar ration 50:50 MW 30,000-70,000), Poly(methyl methacrylate (PMMA, average M_w ~120,000g/mol) , coumarin-6, phalloidin-TRITC,3-(4,5-Dimethyl-2-thiazolyl)-2,5-diphenyl-2H-tetrazolium bromide (MTT), 4′,6-Diamidino-2-phenylindole dihydrochloride (DAPI) and sulindac sulfide were purchased from Sigma Aldrich (St. Louis, MO). 4-(diethoxyphosphoryoxy) butyl 2-(4-isobutyl phenyl) propamoate (Drug D) was manufactured and purchased from Chem-Master International, Inc (Stony Brook, NY). All chemicals and reagents were of analytical quality.

Cell lines: HT-29 colon cancer (**American Type Culture Collection Manassas, VA)** and NCM 460 cell Lines (INCELL Corporation, San Antonio, TX) were used in this study.

Cell culture reagents: Cell lines were grown and maintained in either McCoy's 5A medium supplemented with Fetal bovine serum and penicillin-streptomycin solution (Mediatech, Manassas, VA) and M3:10TM medium (INCELL Corporation, San Antonio, TX).

Synthesis of dimethacrylated Pluronic F-127

Dimethacrylated Pluronic was synthesized and analyzed as previously described[157]. In brief, Pluronic F127 (50 g) was poured into a three-neck flask and dried at 120^0C under vacuum for 2 hours. The polymer was dissolved in 40 ml of dry chloroform and the solution cooled to 0^0C in an ice bath. Subsequently, Triethylamine (26 mmoles) was added to the mixture. Freshly distilled methacryloyl chloride (26 mmoles) was diluted in 10 ml of chloroform and added drop-wise for 2 hours into the cooled mixture. The reaction was allowed to proceed for 24 hours at room temperature. After 24 hours, the mixture was resuspended in a solution of toluene (150 ml) which was being heated on a hot plate. The triethylammonium hydrochloride salt generated by this procedure was removed by filtration of the hot mixture. The toluene mixture was subjected to precipitation in petroleum ether. The precipitate was isolated by vacuum filtration and washed with petroleum ether. The white product, Pluronic F127 di-methacrylate was dried under vacuum at room temperature. The extent of acrylation was determined by ^{1}H-NMR (Oxford, Oxfordshire, UK: 300 MHz) and FTIR (Nicolet iN10, Thermo Fisher Scientific Inc., Madison, WI).

Synthesis of Pluronic hydrogels

To fabricate Pluronic hydrogel, Pluronic F127 was dissolved in distilled water to make a 25% (w/v) solution. 1-[-4-(2-Hydroxyethoxy)-phenyl]-2-hydroxy-2-methyl-1-propane-1-one (molecular formula $C_{12}H_{16}O_4$), at a concentration of $^2/_3$% (w/v) relative to the polymer, was used as a photo-initiator. The sol-state solution was placed at 4^0C and mixed until the mixture became homogeneous. To fabricate gel-disks, 500 µl of solution per disk were poured into a mold at room temperature. After equilibration at room temperature, the gel state mixture was irradiated for 5, 10, 20 and 30 min by long-wavelength UV (365 nm) at 2745

μW/cm^2 intensity in a UV cross-linker (Spectronics Corporation, Westbury, NY). All samples were placed 15 cm away from the bulb. After UV-induced polymerization, gel-disks were washed thoroughly to remove unreacted macromers and other impurities.

To make hydrogel discs encapsulated with drug-loaded NPs the above procedure was used with the exception that the drug-loaded NPs were added to the dissolved F127 DMA solution after adding the photo-initiator. This was mixed until the solution became homogenous.

Preparation of nanoparticles

Sulindac sulfide and Drug D -loaded PLGA nanoparticles were prepared using a solvent evaporation method described by Dong and Feng[185,187]. In brief, a solution of 4 ml of dichloromethane (DCM) containing 100 mg of PLGA and 5 mg of sulindac sulfide was poured into a 1% (w/v) aqueous solution of polyvinyl alcohol (PVA). The mixture was subjected to sonication (Ultrasonic sonicator, Fisher Scientific, Pittsburg, PA) for 5 min. To promote evaporation of the organic solvent, the resulting emulsion was stirred overnight at room temperature. Subsequently, the mixture was centrifuged at 11,500 rpm for 30 min. The nanoparticles were resuspended by sonication into 50 ml of distilled water followed by centrifugation at 11,500 rpm for 30 min. The nanoparticles were washed three times, and then freeze-dried. Fluorescent coumarin-6 (0.05%(w/v)) loaded NPs were prepared in the same manner.

Characterization of nanoparticles

Particle size and size distribution

The size and size distribution of the PLGA NPs with and without sulindac sulfide and Drug D were measured using a Particle Sizer Brookhaven Instrument (Holtsville, NY). The value recorded was based on the mean of ten measurements. The size distribution unit is defined as the polydispersity index (PI). PI ranges from 0 to 1 where 1 indicated a large variation in particle size.

Surface charge

The zeta potential of PLGA NPs with (sulindac sulfide or Drug D) and without drug was detected using laser doppler anemometry (Zeta plus, zeta potential analyzer, Brookhaven Corporation, Holtsville, NY). Before measurement, the samples were prepared by dilution in 0.1µm filtered deionized water.

Surface morphology

The surface morphology of the PLGA NPs with and without drug (sulindac sulfide or Drug D) was investigated by scanning electron microscopy (SEM) (JEOL, Tokyo, Japan: Model# JSM-35CF). The samples were prepared by placing a suspension of the NPs on silicon wafer and dried overnight at room temperature. The samples were coated with a gold layer for 30 s before imaging using SEM.

Drug encapsulation efficiency and drug content

For quantification of sulindac sulfide or Drug DD via HPLC (Waters Corporation, Milford, MA), 2 mg of each of the drug encapsulated NPs were resuspended and dissolved in 1 ml of acetonitrile: water (50:50). The drug encapsulation efficiency was determined as the ratio of the amount of drug encapsulated versus the amount of drug added. The drug content was determined as the ratio of the amount of drug encapsulated versus the mass of NPs used for the analysis.

In vitro drug release

To study the release rate of the drug-loaded NPs, *in vitro* drug release of drug-loaded NPs entrapped in cross-linked F127 DMA and drug-loaded PLGA NPs were measured in triplicate. Drug-loaded PLGA NPs were dispersed by mixing in PBS at 37 ^{0}C. In addition, 2 mg of drug-loaded NP was dispersed into each hydrogel disc before photo-cross-linking. The drug encapsulated hydrogels were immersed in 5 ml of PBS at 4 ^{0}C and 37 ^{0}C. At the designated time intervals, the supernatant was isolated and the pellet (drug-loaded NPs) or hydrogel was resuspended in fresh PBS medium. The drug released in the supernatant was extracted with DCM. After the removal of DCM by nitrogen flow, the deposited drug was dissolved in 1 ml acetonitrile: water (50:50) and analyzed via HPLC.

Determination of the integrity of the anticancer agents

The chemical integrity of the drug (sulindac sulfide) encapsulated in PLGA NPs was investigated using FTIR spectra. FTIR analysis of void PLGA NPs, native sulindac sulfide and sulindac sulfide-loaded PLGA NPs was performed in the range between 4000-500cm^{-1}. FTIR analysis was also performed on Pluronic F127 DMA hydrogel with or without either sulindac sulfide or sulindac-loaded

PLGA NPs. To further determine the effect of UV irradiation on the integrity of the anticancer agent, native and PLGA encapsulated sulindac sulfide as well as a sulindac-sulfide/DMSO solution were UV irradiated for 30 min in the presence of photo-initiator. These samples were analyzed before and after UV irradiation by HPLC as described above.

In vitro cellular uptake of NPs

Ht-29 cells (10,000 cell per well) were seeded onto a 96-well plate and left to attach overnight. The cells were treated with 100µl of 0.25mg/ml of coumarin-6 loaded NPS for 0.5, 1, 2 and 4 h respectively. At the designated interval, samples in each well were washed three times with 50 µl cold PBS; thus, eliminating traces of the NPs left in the wells. To lyse cells, 50 µl of 0.5% Trition-X-100 in 0.2M NaOH was added to samples in each well. The fluorescence intensity of each sample was measured using a microplate reader (Molecular Devices, Sunnyvale, CA) with excitation wavelength at 430nm and emission wavelength at 485 nm.

To provide direct evidence of cellular uptake of the NPS rather than cellular attachment, confocal laser scanning microscopy was used to visually monitor the internalization of the NPs in HT-29 cells. The HT-29 colon cancer cells were seeded and grown overnight in 35mm plates. The cells were incubated with 3 ml of 0.25 mg/ml coumarin-6-loaded PLGA NPs or coumarin-6 for 2 h. After this time the medium was removed and the cells were washed three times with cold PBS. The cells were fixed by incubation for 5 min in an appropriate amount of 3.7% formaldehyde solution. The cell were washed three times with PBS and permeabilized with 0.1% Triton-X for 5 min. Subsequently, the cells were washed three times with PBS and actin filaments were attained by incubation in the dark for 40 min with 50µg/ml Phalloidin-TRITC. Cells were washed three times and nuclei stained with DAPI. Cells were washed, left in PBS and observed under confocal laser scanning microscopy **(**Zeiss LSM 510 META

NLO Two-Photon Laser Scanning Confocal Microscope System, Thornwood, NY**).**

In vitro cytotoxicity of the different formulations of PLGA NPs

In vitro cytotoxicity of the PLGA NPs (no drug), sulindac sulfide-loaded NPs, and Drug D-loaded NPs was quantitatively analyzed using the MTT assay. In brief, HT-29 colon cancer cells were seeded in 96-well tissue culture plates at a density of $1x10^4$ cells per well, divided into two groups for treatment and allowed to adhere overnight. Cells were treated for 24, 48 or 72 h with PLGA NPs (no drug; relative to the concentration of Drug D and sulindac sulfide), Drug D-loaded PLGA NPs suspension (relative to the concentration of Drug D), Drug D (1 to 50µg/ml), sulindac sulfide- loaded PLGA NPs suspension (relative to the concentration of sulindac sulfide) or sulindac sulfide (1 to 200 µg/ml). At the designated time, 10 µl of MTT reagent I was added to the culture media and the samples incubated for 4h at 37^0C in a 5% humidity chamber. At the appointed time, 100 µl of the solubilization solution (MTT reagent II) was added and incubation continued overnight. Cellular viability was determined spectrophotometrically using microplate reader (Molecular Devices, Sunnyvale, CA) plate reader at 595 nm.

Meanwhile, the determine the possible effect of PLGA NPs on the *in vitro* therapeutic effect, the *in vitro* cytotoxicity of PLGA NPs void of any drugs was examined. MTT assay, described above, was conducted using HT-29 colon cancer and NCM 460 normal colon cells. PLGA NPs suspension at concentrations ranging from 1- 200µg/ml was utilized in this experiment.

The cell viability was expressed as the ratio between the fluorescence intensity of cells incubated with test agent and that of cells incubated with culture medium only. IC_{50}, the drug concentration at which inhibition of 50% cell growth was observed in comparison to that of the control sample, was calculated from cell viability versus the drug concentration curve at a given time point.

All experiments were performed in triplicates.

Characterization of the thermoelectric module

The temperature change associated with the applied voltage was assessed for the thermoelectric (TE) module (Custom Thermoelectric, Bishopville, MD Cat# 07111-5L31-06CL). The TE module was placed on a heat sink (metal plate) or immersed in PBS. Various voltages were applied to the unit using DC power supply (Hewlett Packard, Santa Clara, CA) and the change in temperature on both the cold and hot side of the TE module was measured using a Fluke Digital Thermometer (Everett, WA).

Attachment of Pluronic F127 DMA to thermoelectric module/silicon wafer

Silicon wafers were cleaned in piranha solution (7/3v/v conc. H_2S0_4/35wt% H_20_2), washed thoroughly with deionized (DI) water, and dried under nitrogen gas. The cleaned wafers were coated with 50 and 100 mg/ml of poly(methyl methacrylate) (PMMA) solution by spin casting process. The coated wafer was annealed overnight at 100^0C in a vacuum oven. After the wafer was cooled to room temperature, the thickness of the PMMA film was measured and Pluronic F127 DMA containing photo-initiator was applied to the coated side of the module. The unit was irradiated with UV for 10 min to attach the hydrogel to the thermoelectric module. The unit was immersed in water with mixing to determine whether or not the hydrogel annealed. To determine the strength of attachment, using flowing water, a force was applied to the attached hydrogel.

All subsequent experiments utilized the TE module coated with100mg/ml of poly(methyl methacrylate) (PMMA) solution.

In Vitro Study of Drug delivery unit

In vitro cytotoxicity of the constructed drug delivery unit was quantitatively analyzed via cell count viability. In brief, HT-29 colon cancer cells were seeded in 100 mm culture plates at a density of $2.5x10^6$ cells per plate, and allowed to adhere overnight. On the following day, the hydrogel with or without drug-loaded NPs were attached to the thermoelectric module. The unit was then immersed in 10 ml of McCoy media and a voltage output of 4.5V was applied for 0, 10 or 30 min. At predetermined time points, HT-29 cells were treated with the collected media and incubated for 24 h at 37^oC in 5% CO_2 humidity chamber. After the incubation period cells were collected and counted to determine cell viability. This experiment was performed in triplicate.

Statistical analysis

Experimental values were expressed as mean ± SEM. Differences between mean values were evaluated using Student's t-test and the association between variables was determined using regression analysis; $p<0.05$ was considered statistically significant. All statistical analysis was performed using Graph Pad software (La Jolla, Ca).

5.3 Results

5.3.1 Preparation of Pluronic F127-DMA

Pluronic F127-DMA macromer was synthesized as the reaction of OH-terminated according to the method described in procedure. Confirmation of the structure by ^{1}H-NMR analysis revealed the incorporation of methacrylic groups at each ends of the Pluronic polymer. The vinyl protons of the methacrylate group (=CH2) appeared at 5.58 ppm and 6.13 ppm. Whereas, the three protons of the methyl substituent (=CCH3) are shown at 1.95 ppm. The functionalization of Pluronic F127 was further determined by FTIR. There was a gradual peak appearance of a weak peak at 1715.78 cm^{-1}. This peak corresponds to carbonyl vibration of the ester group. As determined by ^{1}H-NMR, the acrylation degree of Pluronic F127 was about 80.1%.

5.3.2 Synthesis of hydrogels

Thirty percent (w/v) Pluronic F127 DMA was prepared in deionized water. At room temperature and above, the solution converted from a clear viscous liquid to a physical gel due to the formation of Pluronic micelles at increased temperatures. Using 1-4-(2-Hydroxyethoxy)-phenyl-2-hydroxy-2-methyl-1-propane-1-one as a photo-initiator, cross-linked and non dissolving hydrogels were produced by UV irradiation. The photo-polymerization of the acrylate groups of the Pluronic micelles resulted in a network of chains which formed a chemically cross-linked hydrogels.

5.3.3 Characterization of nanoparticles

5.3.3.1 Surface charge, particle size and distribution, encapsulation efficiency and drug content of PLGA NPs

The size, size distribution, and encapsulation efficiency of the nanoparticles with and without drug (PLGA NPs, Drug D-loaded PLGA NPs and sulindac sulfide-loaded PLGA NPs) are listed in Table 9. The drug-loaded PLGA NPs exhibit an average size of around 280 nm with a polydispersity value less than 0.200. The PLGA NPs (no drug) exhibited an average size of 217 nm with a polydispersity value less than 0.050. This data indicates that the particles devoid of drug are smaller and more uniformed in size compared to the drug-loaded NPs.

Zeta potential of the PLGA nanoparticles with and without drug was measured to be approximately -22.00 mV. This attribution may be due to the presence of the carboxyl group in the PLGA polymer. Incorporation of a positively charged antibody specific to the type of cancer model being targeted can be facilitated by the charge of the nanoparticles; thus, making this an excellent candidate for targeted delivery.

The drug encapsulation efficiency of the sulindac sulfide- loaded PLGA NPS and the Drug D-loaded PLGA was approximately 63.01% and 61.14%, respectively. There was no significant difference between the two drugs in respect to the amount of drug encapsulated. However, the drug content of the sulindac sulfide- loaded PLGA NPS and the Drug D-loaded PLGA was approximately 5.8% and 14.7%, respectively. The quantity of drug contained in Drug D- loaded PLGA NPs was higher than the amount of drug per mg of PLGA

NPs contained in sulindac sulfide-loaded PLGA NPs. Drug D-loaded PLGA NPs had 2.5 times more drug than sulindac sulfide-loaded PLGA NPs.

5.3.3.2 Surface morphology

Surface morphology of the PLGA NPs with and without anticancer agent was studied by SEM. It found from Fig. 36 that both NPs exhibit circular smooth surface (Data only shown for placebo PLGA NPs). The smooth surface may result in slower drug release, as it decrease the surface area compared to a rougher surface.

5.3.4 *In vitro* drug release from PLGA NPs and photo-cross-linked hydrogel

The *in vitro* drug release profile of the Drug D-loaded PLGA NPs and sulindac sulfide-loaded PLGA NPs are shown in Fig 37. The anticancer agents were released from the drug-loaded PLGA NPs in PBS buffer (pH 7.4) at 37^0C. We observed that Drug D-loaded PLGA NPs and sulindac sulfide PLGA NPs exhibited similar biphasic drug release kinetics, with an initial burst up to 4.4±0.7% and 20.5±0.3% in the first day, followed by accumulative release of 19.2±1.4 % and 56.7±5.9% after 15 days, respectively. The drug release of Drug D- loaded NPs was 3.0 times slower than for sulindac sulfide-loaded PLGA NPs.

To achieve sustained release of the anticancer agents from the photo-cross linked Pluronic hydrogels, we examined the use of drug-loaded PLGA NPs.

Drug-loaded PLGA NPs were homogeneously mixed with di-methacrylated Pluronic F127 solution at 4^0C and the mixture was UV irradiated at room temperature at different exposure times. *In vitro* release profiles of anticancer agents -loaded PLGA NPs from the Pluronic hydrogel are shown in Fig. 38. For Pluronic hydrogels analyzed at 4^0C, entrapped anticancer agent was quickly released at an early incubation stage followed by a subsequent steady release rate up to 15 days. For Drug D-loaded PLGA NPs, entrapped in the hydrogel after 5 min UV irradiation, there was an initial burst release of 33.0% of the entrapped Drug D and a cumulative release of 98.7% after 15 days. Under the same conditions, a similar trend was observed for sulindac sulfide-loaded PLGA NPs sample. This initial burst release are attributed to the temperature and the loose cross linking network structure that do not sufficiently retard the rapid diffusion of entrapped anticancer agent. Also, the gradual degradation of the hydrogel also contributes to the rapid anticancer agent release. The initial burst and the extent of cumulative release were reduced with prolong UV irradiation time. Comparing the release rate of Drug D-loaded PLGA NPs after 10, 20 and 30 min UV irradiation, there was 8.2, 23.0 and 44.2% reductions in the initial release rate and 22.1, 34.7 and 43.6% reduction in the cumulative release rate compared to the 5 min UV irradiation treatment time. When the release profile of anticancer agents from hydrogel was analyzed at 37^0C, similar trends were observed as seen at 4^0C in regards to the initial burst and cumulative release of anticancer agents at the different UV irradiation times. However, at 37^0C, the observed initial burst release of anticancer agents from the hydrogel was considerably reduced and a more sustained release patterns, relative to the hydrogels at 4^0C, was observed with increase UV irradiation time. For example, Drug D-loaded PLGA NPs samples treated with 5 min UV irradiation showed a 82.1% reduction in initial burst release and a 74.6%% reduction in cumulative release when the testing temperature was increase from 4^0C to 37^0C. This means that the degree of cross-linking dictating the swelling ratio, the degradation ratio and the mechanical strength of the hydrogel, as well as the

temperature played a key role in determining the release pattern of anticancer agent.

5.3.5. The effect of UV irradiation of the integrity of the anticancer agents

By varying the exposure time of UV irradiation, the cross-linking density of the Pluronic hydrogel changes, which in turn, allows for controlled release of the anticancer agent. Thus, after UV irradiation, it is questionable that the anticancer agents in or out of the drug-loaded PLGA NPs were structurally intact after entrapment within the hydrogels. Therefore, the structural integrity of the UV irradiated anticancer agents was examined by FTIR and HPLC. Firstly native sulindac sulfide, sulindac-sulfide/DMSO solution and sulindac-sulfide-loaded PLGA NPs were suspended in photo-initiator solution, UV irradiated for 30 min and examined by HPLC. The degradation of sulindac sulfide before and after UV treatment, as determined by HPLC analysis is depicted in Fig 39. In samples that were not UV irradiated, the presence of sulindac, sulindac sulfone and sulindac sulfide were detected. The only samples affected by UV irradiation were those samples solubilized in DMSO. In this case, the presence of sulindac sulfide, sulindac and sulindac sulfone was 1.1 times less, 2.4 and 25.7 times more than the untreated samples, respectively.

The chemical integrity of sulindac sulfide and characterization of any chemical changes in the polymeric matrix was also investigated using FTIR spectra (Fig 40). FTIR spectra of void PLGA NPs, native sulindac sulfide, sulindac sulfide-loaded PLGA NPs, Pluronic F127DMA hydrogel and sulindac sulfide-loaded PLGA NPs or sulindac entrapped in hydrogel were scanned in the range between 4000-500 cm^{-1}. Spectral analysis of native sulindac sulfide and

void PLGA NPs showed characteristic due to different functional groups. Sulindac sulfide has distinct bands at 1694cm^{-1} corresponding to the carbonyl group and bands at 1602cm^{-1} and 1589cm^{-1} both corresponding to the aromatic ring (C=C). Whereas, PLGA NPs had a distinct band at 1751cm^{-1}. This band corresponded to the carbonyl group. The bands occurring in void PLGA NPs are similar to the bands in the sulindac sulfide-loaded PLGA NPs with the addition to some extra bands due to the sulindac sulfide (Fig 42A).

FTIR analysis of the photo-cross-linked with or without sulindac sulfide (native of PLGA NP formulated) was inconclusive. All three spectra were identical. This may be due to the large volume of water present in the hydrogels which mask the remaining bands (sulindac sulfide bands (Fig 40B).

When cross-linking the native drug entrapped in the hydrogel we observed an inhibition if the cross-linking ability. The inhibition may be due to the oxidative free radicals generated from the photo- initiator by UV irradiation interacting with the native anticancer agents, quenching the cross-linking action of the hydrogel. Protection of the anticancer agents from the UV light by the PLGA shell enables the hydrogel to be cross-linked and maintain the integrity of the anticancer agent. We have also determined by HPLC of sulindac sulfide and sulindac sulfide-loaded PLGA NPs that the Integrity of the anticancer agents is not affected by the internal acidic microenvironment created as a byproduct of the degradation of the PLGA polymer. This observation is supported by HPLC analysis of the native drug and drug-loaded PLGA NPs (Fig 39) and the cumulative release results.

5.3.6 Cellular uptake of nanoparticles by HT-29 cells

Due to its biocompatibility, high fluorescence activity, low dye loading (<0.5% w/w) and low leaking rate, Coumarin-6 has been widely used as a

fluorescence marker in experiment of cellular uptake of NPs. In an effort to visualize and measure the cellular uptake of the polymeric NPs, coumarin-6 is often used to replace the drug in the NP formulation[187,201-204]. In this study, HT-29 colon cancer cells were used to investigate the cellular uptake of the fluorescent PLGA NPs. The cellular uptake of the coumarin-6 loaded PLGA NPs (0.25 mg/ml nanoparticles) into HT-29 cells after 0.5, 1, 2 and 4 h incubation is presented in Fig 41. The cellular uptake of the NPs was expressed as the fluorescence strength of the internalized NPs relative to that of the NP concentration. This study demonstrated that coumarin-6-loaded PLGA NPs were into HT-29 cells more readily than the native dye. On average cellular uptake of coumarin-6 loaded PLGA NPs was approximately 1.6 times (1/2 h to 2h) and 2.5 times (4h) more compared the cellular uptake of the native dye.

In addition to the formulation of the coumarin-6, the duration of incubation is also an important factor for determining the efficiency of cellular uptake. Our study shows that the cellular uptake of coumarin-6-loaded PLGA NPs was 1.3, 2.2 and 3.4 times more after 1, 2, and 4h of treatment respectively compared to the 30 min of treatment. From this data we conclude that the formulation of the anticancer agent and an extended time of incubation lead to a higher efficiency of cellular uptake.

HT-29 cells were incubated with 0.25mg/ml native coumarin-6, and coumarin-6 loaded PLGA NPs suspension for 2 hours at 37^0C and analyzed by Confocal microscopy (Fig 42). The red actin filament (TRITC stained) indicates the boundary and shape of the cells (Fig 42 A and E), the blue stained area (DAPI) indicates the nucleus (Fig. 42 B and F) and the green stained areas indicates the presence of coumarin-6 (Fig. 42 C and G). In the cytoplasm, the green coumatin-6 loaded PLGA NPs aggregate in and around the nucleus, indicating the NPs have been internalized by the cells. This data also supports the findings of the cellular uptake which demonstrated that there was a higher uptake of coumarin-6 loaded PLGA NPs than of the native dye.

5.3.7 *In vitro* cytotoxicity of the different formulations of PLGA NPs

The *in vitro* cytotoxicity of HT-29 cells after incubation for 24 (upper), 48 (middle), 72 (lower) h culture with native drug and drug-loaded PLGA NPs is shown in Fig 43. The viability was measured by MTT assay. Various concentrations of sulindac sulfide, sulindac sulfide-loaded PLGA NPS, Drug D and Drug D-loaded PLGA NPs were utilized. The *in vitro* effect of the different anticancer agent formulations can be quantitatively compared by IC_{50} values. The IC_{50} values given in Table 10 are obtained from the data generated and depicted in Fig 45. HT-29 cells with sulindac sulfide- loaded PLGA NPs for 24, 48 and 72 h have IC_{50} values which are1.5, 2.5 and 1.5 times, respectively, lower than native sulindac sulfide. A similar trend is observed for Drug D IC_{50} values. We observed that the viability of HT-29 colon cancer cells decreased with increased drug concentration and time of incubation. We also observed that the greatest negative effect on cell viability was exhibited by Drug D and the sulindac-loaded PLGA NPs. Thus, It can this be concluded that the sulindac sulfide or Drug D-loaded PLGA NPs formulations can increase the *in vitro* therapeutics effect in comparison to sulindac sulfide or Drug D respectively. To achieve better targeting effect the NPs would have to be tagged with a specific antibody.

A comparison of *in vitro* cellular viability after 24 h treatment with PLGA NPs (varying concentration) of HT-29 colon cancer cell and NCM 460 normal colon cell is shown in Fig 44. Since PLGA NPs are part of the drug delivery systems and are released it is crucial to determine whether they may independently exert a cytotoxic effect on normal cells. The placebo PLGA NPs (without anticancer agent) exhibits no significant cytotoxicity at the studied NPs concentration levels used for normal cells. This implies that the polymer is biocompatible. In addition, the observed cell viability of HT-29 cancer cells treated with placebo PLGA had on average 1.1 times lower compared to the

normal cells at corresponding concentrations of PLGA NPs. At higher concentrations (180 and 200µl/ml), the difference in cell viability was statistically significant, $p<0.005$ and $p< 0.001$, respectively.

5.3.8 Characterization of TE module

A depiction of the major components of the thermoelectric or peltier module used in this study is shown in Fig 45. The module consists of the N and P-type thermoelectric materials sandwiched between two electrical insulators. The cold end carries the heat load, thereby, creating a temperature difference across the device. As a result of this temperature difference, a heat flux occurs. The heat is transferred from the cold end, where the hydrogel will be placed, to the hot end via conduction.

The TE module was attached to a DC power supply and various voltages were applied to the unit to determine the current output. As seen in Fig 46B, there is a direct relationship between the voltage and the current. As the voltage applied to the TE module increased the output current also increased. Another parameter measured at various voltages was the temperature of the hot and cold side to the TE module in air and PBS (37^0C). The temperature of the hot and cold side of the TE module was measured in air and PBS (Fig 46A). When exposed to air, there was an increase in the temperature of the hot side and a decrease in the temperature of the cold side of the TE module as the voltage increased. At a voltage of 4.0V, the net temperature change in air was 72.5^0C and 9.1^0C for the hot and cold side of the TE module, respectively. In comparison, the TE module immersed in PBS at 37^0C followed the same trend. Again, at 4.0V, the net temperature change in PBS was 34.3^0C and 18.5^0C for the hot side the cold side of the TE module, respectively. This data indicates the hot side of the TE module was much cooler in PBS than air. Also, we observed that the change in temperature seen for the cold side of the TE module was greater in PBS than in air. Even though the temperature of the TE module

increased with increasing voltage, the temperature of the PBS solution did not change. This data indicated that PBS, which acts as a heat sink and represents the physiological conditions in the body, is capable of dispersing the heat to prevent increases in temperature.

5.3.9. Attachment of hydrogel and TE module

The cooling capacity of the TE module is proportional to the magnitude of the applied current and the thermal conditions of each side of the TE module. By varying the applied current, it is possible to regulate the heat flow and control the surface temperature. In order to external regulate the control release from the Pluronic hydrogel, the hydrogels needs to be attached to the cold side of the TE module.

5.3.9.1. Film thickness

The spin casting of the PMMA on the silicon wafer was an efficient method to evenly coat the silicon wafer. The thickness of the film was measured after the silicon wafer was spun casted with 50 and 100mg/ml of PMMA solution (Table 11). Results showed that the thickness of the film depended on the concentration of the PMMA; a thicker the spin casted film corresponded to a higher PMMA concentration.

5.3.9.2 Strength of attachment

To determine whether the hydrogel would remain attached to the PMMA silicon wafer, the attached hydrogel/silicon wafer units were immersed in PBS. At designated time intervals, to determine whether the hydrogel remained attached to the silicon wafer or whether the bond (the adhesion) between the silicon wafer and hydrogel was broken, the units were monitored and photographed. After monitoring for 21 days, we were able to demonstrate that

the bond between the silicon wafer and hydrogel remained intact (Fig 47). After 1-6 days of attachment using PMMA concentrations below 50mg/ml, the bond between the hydrogel and silicon wafer was destroyed (data not shown). Thus, indicating that the strength of the attachment of the hydrogel to the TE module is dependent on the concentration of PMMA. The adhesive property of PMMA is greater at concentrations of 50mg/ml and higher.

We further examined the strength of the attachment of the hydrogel to the TE module. To achieve this, a constant force, the flow of water, was applied to the attached hydrogel/silicon wafer unit. A flow rate of 10 L/min or 1.67 x 10^{-4} m^3/sec was applied to the attached gel. This applied flow was greater than 5.6 L/min; the normal blood flow rate in an average sized adult. The type of flow was first classified by calculating the Reynold's number (equation 1). The Reynold's number characterizes the type of flow; a stable laminar flow is characterized by $R_n < 2000$, while $R_n \geq 2000$ is indicative of unstable laminar or turbulent flow. The Reynold's number was determined to be 10,565. Based on the flow rate and the size of the tubing, the flow of water was expected to be non laminar. Using equation 2, the force being applied by the flow of water onto the attached hydrogel was determined to be 74.5 μN. This force was exerted on the attached hydrogel continuously for 6.5 days, without detachment for the silicon wafer.

$$\text{Re}\,ynold's\ number(Rn) = \frac{\rho V d}{\mu} \qquad \text{Equation 1}$$

$$Force = \frac{\mu A V}{h} \qquad \text{Equation 2}$$

fluid density (ρ fluid velocity (V) coefficient of viscosity (μ)

height of gel (h) area of wafer (A) diameter (d)

5.3.10 *In vitro* release from drug delivery unit

In vitro release of the drug from the prepared drug delivery units was evaluated by cell viability assay using HT-29 cancer cells. Results of the cellular viability of cells exposed to the drug delivery unit harboring different anticancer agents for various time periods are presented in Fig 48. As shown in Fig 50A, when the units contained either only cross-linked Pluronic F127 hydrogel or sulindac sulfide-loaded PLGA NPs entrapped cross-linked Pluronic F127 hydrogel with no voltage applied, there was no significant change in cells viability compared to the control cells. There was no significant change in cellular viability for cells treated in the presence of units containing either only cross-linked Pluronic F127 hydrogel (4.5 V applied) or sulindac sulfide-loaded PLGA NPs/cross-linked Pluronic F127 hydrogel (no voltage applied) as compared to the control cells (cells grown in media alone). However, the viability of cells in the presence of the "complete drug delivery unit" (sulindac sulfide-loaded PLGA NPs/cross-linked Pluronic F127 hydrogel with an applied voltage of 4.5V) was significantly lower than that of the control. As seen in Fig 48A, the viability of cell grown in the presence of the "complete unit" decreased as the duration of treatment increased. Cellular viability of cells treated with the "complete unit" was 1.8 times lower when cell were treated at 30 min compared to cells treated at 10 min. This difference between cells treatment time is statistically significant ($p<0.05$). The same trend is observed for drug delivery units prepared with Drug D-loaded PLGA NPs (Fig 48B).

Therefore, we conclude that the effect of the release of anticancer agent from the drug delivery unit on the viability of cells was dependent on the presence of voltage ad duration of treatment. Thus, the prototype drug delivery unit that we prepared could be regarded as a safe drug delivery carrier and is promising device for externally regulated controlled drug delivery.

5.4 Discussion and Conclusion

One of the greatest challenges of chemoprevention or chemotherapy involves localized distribution of the therapeutic agent for selective and successful transport to the site of the disease, such as cancer. There are numerous studies aimed at developing more efficient systems for the site specific delivery of drugs. One such study involves the use of response stimulated hydrogels, such as Pluronic F127. Biocompatible Pluronic F127 hydrogels, capable of releasing anticancer agents in a sustained and controlled manner, are prepared by UV irradiation. By this method, di-methacrylated Pluronic macromer are synthesized and cross-linked forming a gel state. As we previously reported, a diverse range of hydrogels with different cross-linking densities and mechanical strengths were produced by controlling their exposure to UV irradiation. Through the investigation of swelling ratio and degradation it was demonstrated that the degree of cross-linking and mechanical strength were directly dependent on the duration of exposure to UV irradiation and to temperature. We observed that the cross-linked hydrogels, while maintaining its cross-linked structure, retained the ability to respond to changes in temperature similar to that of the physical gel. Another essential property of the polymer that was essential was its ability to release anticancer agent from the cross-linked hydrogel. In order to protect the anticancer agents from UV irradiation, the agents were formulated into PLGA NPs before entrapment into the hydrogel.

The nanoparticle system is multifunctional. It can provide a way to formulate anticancer drugs without the use of harmful adjuvants and can promote synergistic therapeutic effects. The drug-loaded PLGA NPs were prepared by a solvent extraction/evaporation technique. PLGA NPs were characterized as to determine the particle size, size distribution, surface morphology, chemical integrity, drug encapsulation efficient and loading content. In addition, the release profiles of the nanoparticles were investigated. The characterization of the PLGA

NPs is important because the fate of the drug after it is administered depends on the physiochemical properties as well as the chemical structure of the drug [205]. Particle size is an important parameter as it directly affects the physical stability, biodistribution, cellular uptake and the release of the entrapped drug from the nanoparticles[187,201-204]. In this study we developed drug loaded PLGA NPs which average in size of 280 nm with a negative zeta potential (-22.00mV); a highly stable drug carrier which has be found to be capable of escaping the reticuloendothelial system in the body[184,185,206]. Characterization of the physiochemical properties of the drug encapsulated in the PLGA NPs and entrapped in the hydrogel provides useful information about the integrity of the drug. Using FTIR and HPLC analysis helped in determining the integrity of the drug. This data confirmed that the drug retained its properties after encapsulated and UV irradiation. *In vitro* release experiments were developed to measure the release of encapsulated drugs (sulindac sulfide and Drug D) in PBS buffer from the PLGA NPs and the cross-linked hydrogels. We observed an initial burst of drug from the drug-loaded PLGA NPs followed by a slower steady release. The initial burst observed may be attributed to drug being weakly bonded to the large surface area of the PLGA NPs than to the drug encapsulated inside the nanoparticle. This, the slower steady release that followed may be attributed to the surface morphology of the PLGA NPs. The spherical and smooth surface morphology of the nanoparticles helps to determine their *in vitro* and *in vivo* performance. Whereas, the release of anticancer agent from the cross-linked hydrogel was found to be dependent on two factor, the degree of cross-linking and the applied temperature. The therapeutic potency of the PLGA NPs formulation was proven in HT-29 cells treated with sulindac sulfide, sulindac sulfide-loaded PLGA NPs, Drug D, Drug D-loaded PLGA NPs and placebo PLGA NPs. MTT assays confirmed that the drug-loaded PLGA NPs exhibited lower IC_{50} values compared to the native drugs and the placebo PLGA NPs. This can be explained by the degree of cellular uptake and by the efficacy of the therapeutic agent. In previous studies, coumarin-6 has been proven to be a useful fluorescence/confocal dye[202-204]. Here using the properties of coumarin-6, we

demonstrated that the internalization of the dye into HT-29 cells was higher for coumarin-6-loaded PLGA NPs compared to native dye. This evidence serves to indicate that, potentially, we can generate a system that could promote the effective intracellular delivery of drugs. In our observation, the intracellular uptake of uptake of coumarin-6-loaded PLGA NPs was 1.6-2.5 times higher than native dye. It is known that the uptake of native drug(s) in solution may be due to the diffusion of the drug molecules across the cellular membrane. Therefore, the drug's efficacy is limited to how much of the native drug is able to enter the cell. An advantage of the PLGA NPs is that cellular internalization of the PLGA NPs is mediated by non specific endocytosis. It has been demonstrated that the nanoparticles readily exit the endolysosomes and enter the cytoplasm under cellular *in vitro* condition[183,184,203,205,207,208]. The fractions of nanoparticle that enter the cytoplasm seem to release the encapsulated therapeutic agent in a sustained manner as the PLGA slowly degrades. This was also demonstrated by us as seen in Fig 39. The placebo PLGA, which did not contain any therapeutic, also entered the cell via non specific endocytosis but did not have a significant anti-proliferative effect compared to the drug-loaded PLGA NPs. Not done in this study bit of interest would be the attachment of a targeting moiety onto the PLGA NPs surface. Thus, the anti-proliferative activity expected would be achieved through receptor mediated endocytosis of the particle binding to the targeted receptor on the cell membrane aiding in the intracellular accumulation of nanoparticles[203,206,207]. When evaluating the cytotoxicity of drugs formulated in the PLGA NPS, the cytotoxic effect of the drug carrier (PLGA NPs) alone must be taken into account. Here we have shown that the viability of normal and cancer colon cells treated with placebo (200µg/ml) was 93.7 ±2.5% and 74.9±0.0% for 24 h respectively at. Thus, the cytotoxicity of the placebo PLGA NPs to NCM 460 normal colon cells was almost negligible. However, the placebo PLGA NPs did exhibit a marginal cytotoxic effect on HT-29 colon cancer cells. With this factor in mind, we can still conclude that PLGA NPs formulated sulindac sulfide or Drug D can achieve higher *in vitro* therapeutic effect than the native or pristine drug.

Controlled release has proven to be useful in areas such as food and cosmetics. Controlled release has had its largest impact in the field of drug delivery[145,209]. The method by which a drug is delivered can have a significant effect on its therapeutic efficacy. Most drugs have an optimum concentration within which they retain the maximum therapeutic benefits. Drug concentration above and below the optimal concentration can be toxic or produce no therapeutic effect. Conventional drug delivery methods, such as oral and injectible devices, are typically marked by a high increase in concentration followed by a rapid decrease in concentration until the drug concentration falls below therapeutic range. Therefore the time spent optimizing the drug concentration for treatment is useless, as the optimal concentration may be short lived. In the field of controlled sustained release the initial focus is on achieving a controlled release of drug over an extended period of time. Most of the work on sustained drug delivery is centered on the use of biocompatible polymers. These polymers are capable of releasing the drug at a nearly constant rate, due to diffusion out of the polymer or by degradation of the polymer over time. In numerous studies however, sustained release is not the optimal method of drug delivery. Instead delivery by pulses of drug at variable time periods, termed pulsatile release, works better in certain cases and is the sometimes preferred method. This is because the pulsating mechanism of delivery mimics the way in which the human body naturally produces some compounds, such as insulin. Previous work on methods of achieving pulsatile release has focused on developing polymers that respond to specific stimuli: such as exposure to ultrasound, enzymes and changes in pH or temperature. Pulsatile release systems can be self regulated (use of enzymes) or externally regulated (use of temperature).

In this study, to our drug delivery system, a thermo-responsive polymer (Pluronic F127-DMA) of which we photo-cross-link to entrap drug-loaded PLGA NPs, a thermoelectric module was employed as an external regulator. Based on the release profile of the hydrogel containing drug-loaded PLGA NPs (Fig 38),

this system was capable of sustained controlled release over 15 days, the longest time period examined. We demonstrated that this sustained release from the hydrogel was dependent on the degree of photo-cross-linking as well as the degradation of the hydrogel.

A thermoelectric (TE) module is a semiconductor based electronic component which functions as a small heat pump. TE modules have been and are currently being used for cooling of computer components and thermal cyclers used in polymerase chain reactions (PCRs). Besides the ability to operate both heating and cooling within the same module, there are a few advantages of TE module that allow them to be suitable for temperature release application in drug delivery. The TE module contains no moving parts, is small and lightweight, has a wide variety of temperature ranges, environmentally friendly and can be cooled to very low temperatures based on the design of the module[193,194]. Due to the fact that the modules were to be inserted in cell culture media, it is necessary to seal the TE modules. Therefore, a moisture sealant (i.e., silicone based in nature) is applied to the edge of the device. The ceramic substrates or faces of the modules are made of Alumina ceramic (Al_2O_3). Less frequently they are made of more thermally conductive ceramics such as berrylium oxide (BeO) or aluminum nitride (AlN). Attached to the ceramic substrates are interconnectors, both N and P type pellets, made of copper. They are arranged in an alternating pattern, much like a chess board, and form one long series circuit through the entire thermoelectric module. A schematic representative of a TE module is shown in Fig 45. By applying a low voltage to the TE module, heat was transferred through the module from one side to the other, depending on polarity of the applied voltage. Thus, we were able to obtain a TE module that can be used for both heating and cooling, making it a suitable mechanism for precise temperature control applications. If desired, the temperature of the thermoelectric module device can be controlled to vary in a pulsatile manner or the temperature can be maintained at a steady level over a period of time. The temperature change that is required for controlling the thermal response of the cross-linked

hydrogel is average to be 20.6^{0}C (Chapter 4). By applying a voltage of 4.0V to the thermoelectric, the recorded temperature was 18.8^{0}C, which is sufficient to induce the transition change required for release of the drug from the hydrogel.

To stimulate the thermo-responsiveness of the hydrogel, the drug-loaded PLGA NPs entrapped hydrogel was attached to a TE module device. Attaching the cross-linkable polymer onto the TE modules is crucial for enabling the control release of the drug-loaded PLGA NPs from the polymer via thermo-stimulation. Poly(methyl methacrylate) (PMMA), a versatile polymeric material, is well suited for many imaging and non-imaging microelectronic applications[198]. PMMA is most commonly used in x-ray and deep UV microlithographic processes. PMMA is also used as a protective coating for wafer thinning, and as a bonding adhesive[198,200]. In our study PMMA interaction with PEO block of Pluronic F127. This interaction is generally thought to be a weak interaction. The specific interaction may occur between the carbonyl carbon atoms of the PMMA and the oxygen atoms of the PEO; however, the exact nature of these interactions is still unknown. This interaction allows for the PMMA facilitated attachment of the cross-linkable hydrogel to the cold-side of the TE module. Therefore, the degree of attachment is dependent on the concentration of PMMA used. Hence, with this in mind, we were able to devise a method that facilitated a sturdy attachment of the hydrogel to the TE module.

Overall, we have developed a new drug delivery system utilizing a thermoelectric module acting as platform to initiate the thermo-responsiveness of the hydrogel containing drug-loaded PLGA NPs. This hydrogel was synthesized by utilizing photo-polymerization methods, which allowed for the quick and efficient cross-linking of hydrogel. The mechanical strength of cross-linked hydrogel increased as the UV exposure time increased. The formulation of the drug had many advantages which included protecting the drug from UV degradation and enabling more efficient uptake of the drug. Lastly, as proof of concept, the fully constructed drug delivery (UV exposed for 10 min) was utilized for the release of anticancer drug to treat HT-29 colon cancer cells. Under all the

conditions examined, only fully constructed DDS with drug-loaded PLGA NPs given a voltage output of 4.5V was the difference in cell viability statistically significance as compared to control. Cell viability results imply that the anticancer agent release from our drug delivery unit is dependent on the presence of voltage and the treatment time. Therefore our prototype drug delivery unit could be regarded as a safe drug delivery carrier and is promising for controlled externally regulated drug delivery.

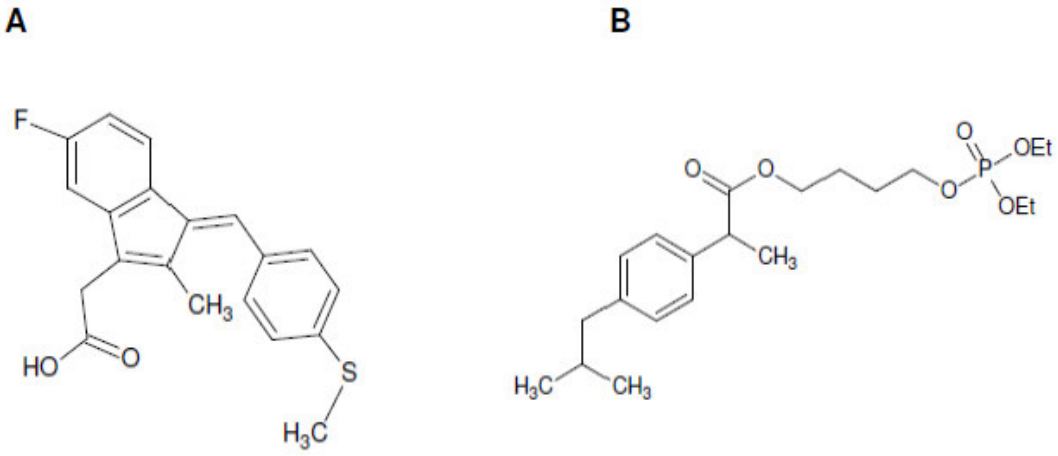

Figure 35. Structure of chemopreventive compounds (a) Sulindac sufide and (b) Drug D (4-(diethoxyphosphoryoxy) butyl 2-)4-isobutyl phenyl)propamoate)

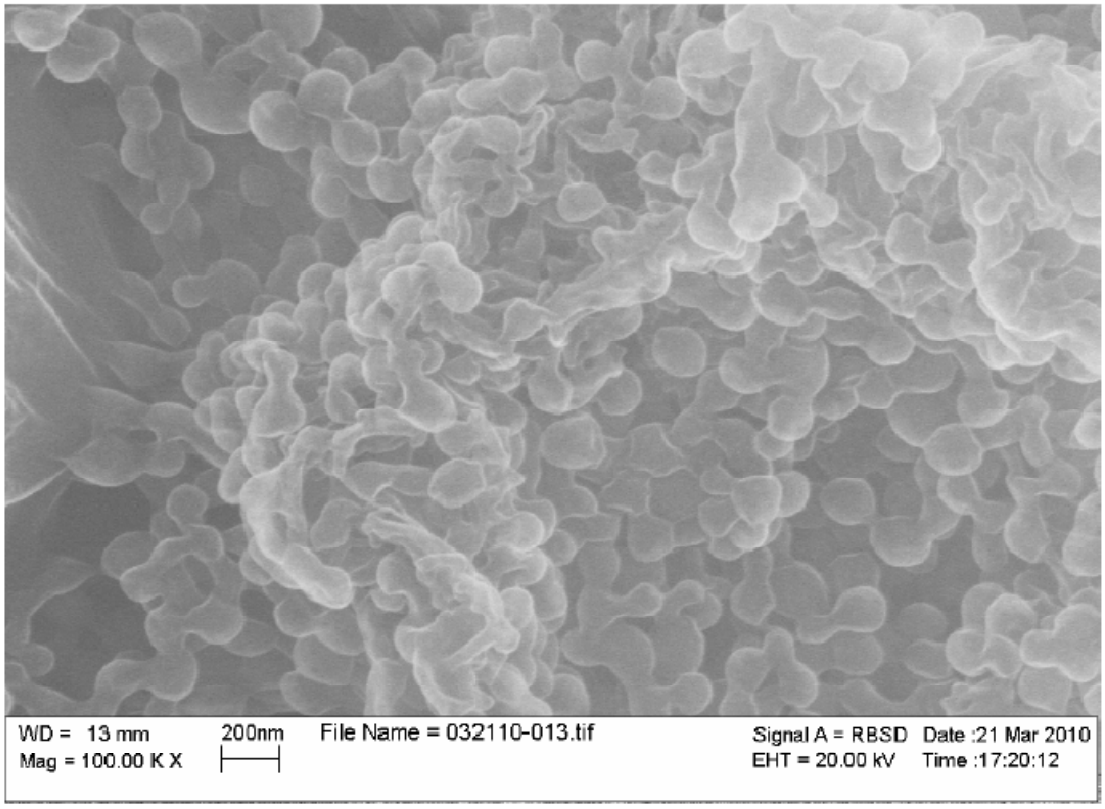

Figure 36. SEM image of PLGA nanoparticles.

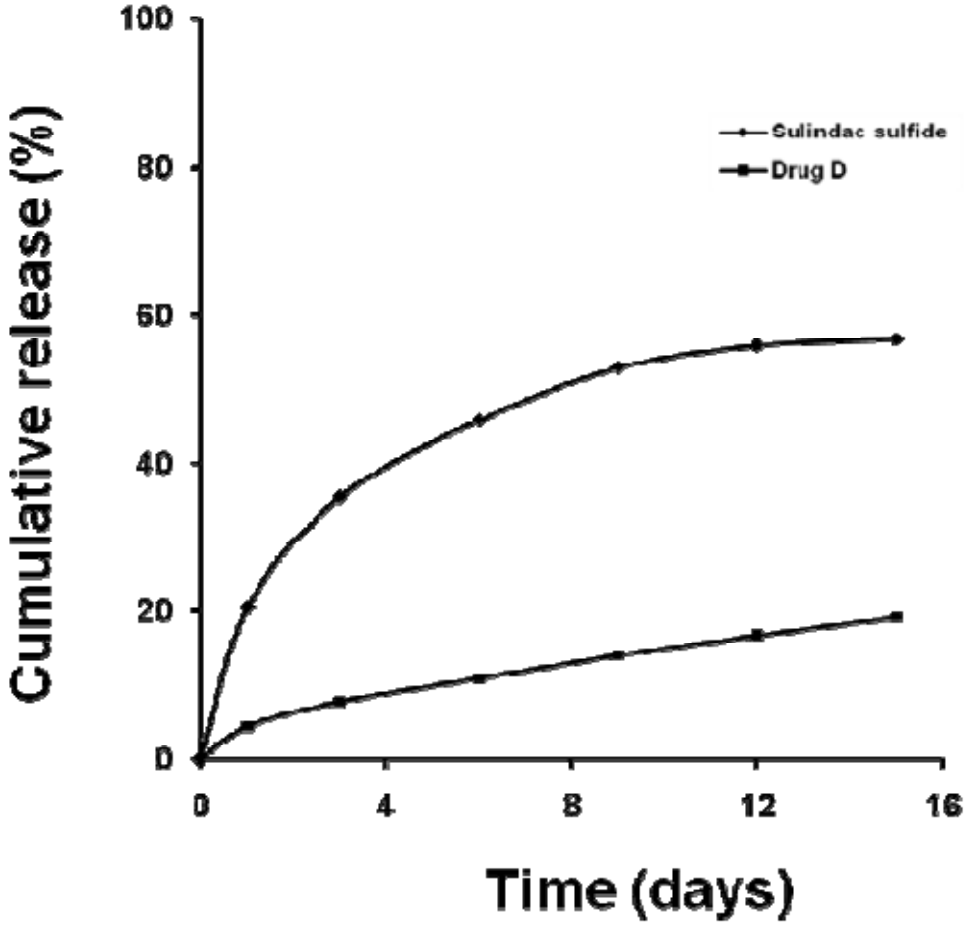

Figure 37. Cumulative release of sulindac sulfide and Drug D from PLGA nanoparticles in PBS as a function of time. Results are shown as mean (n=3)

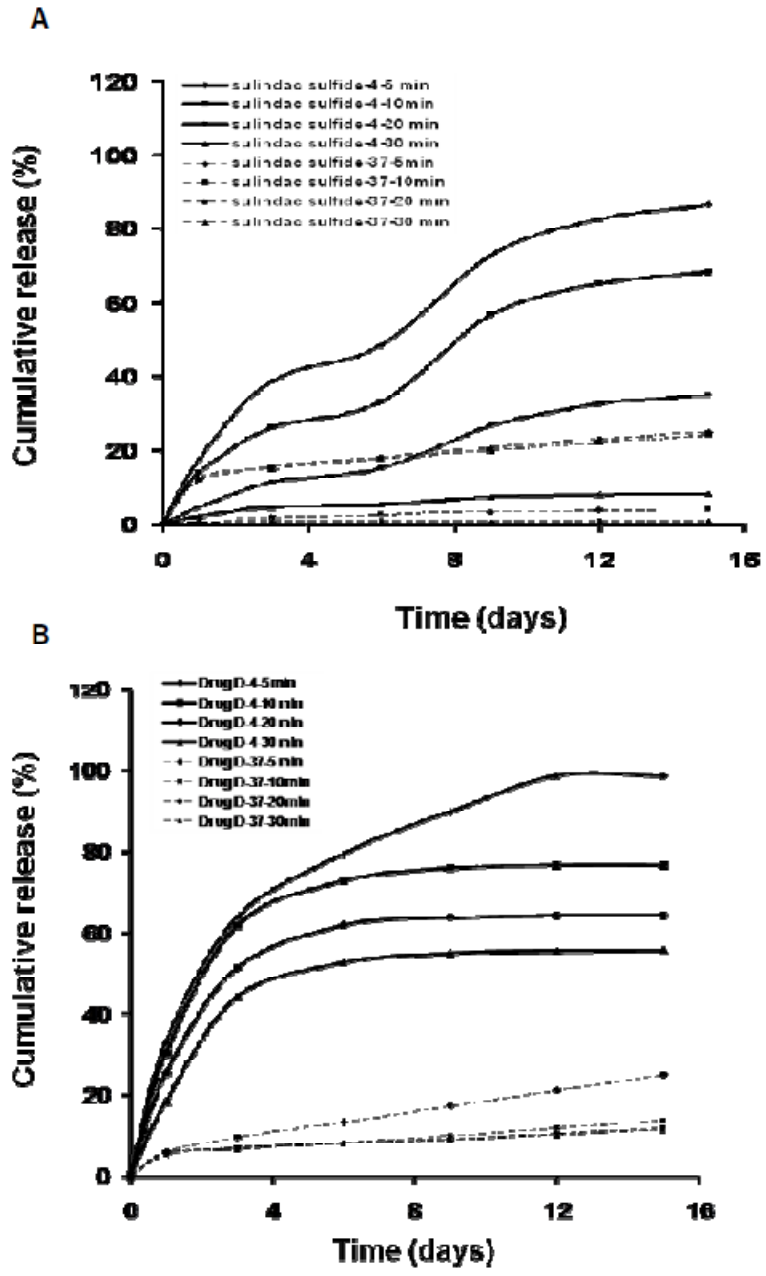

Figure 38. Cumulative release profiles from hydrogels. A) Sulindac sulfide and B) Drug D are released from Pluronic hydrogels in PBS as a function of time. Results are shown as mean (n=3)

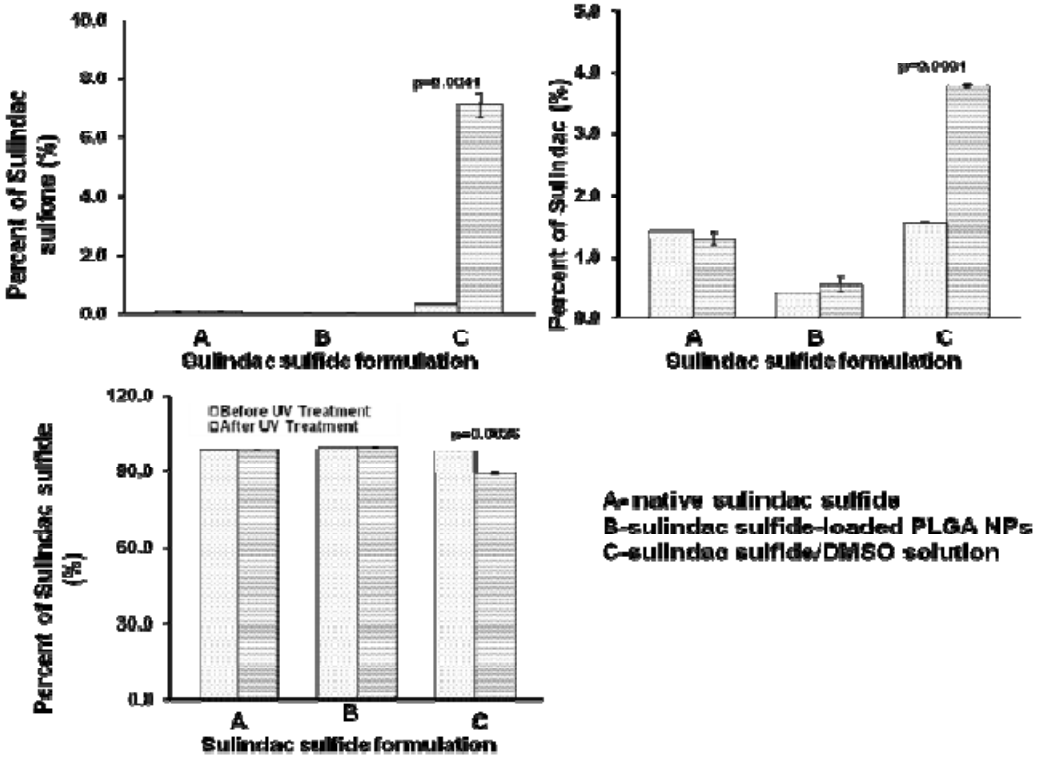

Figure 39. Chemical integrity of native and PLGA formulated sulindac sulfide, sulindac and sulindac sulfone before and after 30 min UV exposure.

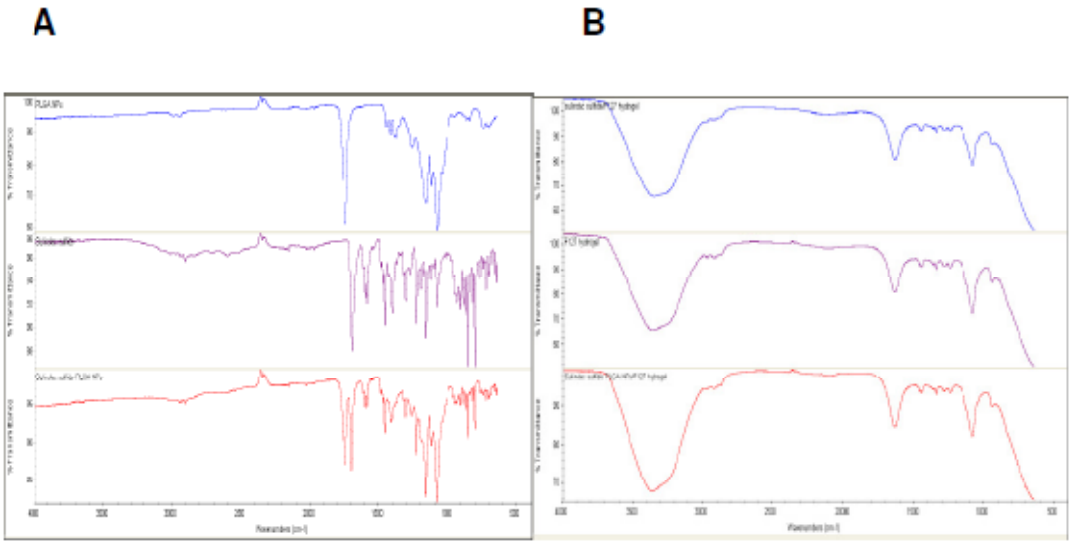

Figure 40. FTIR spectra of A) PLGA, sulindac sulfide and sulindac sulfide-loaded PLGA nanoparticles and B) Pluronic F127 photo-cross-linked hydrogels with either sulindac sulfide, placebo (no drug) and sulindac sulfide-loaded PLGA nanoparticles

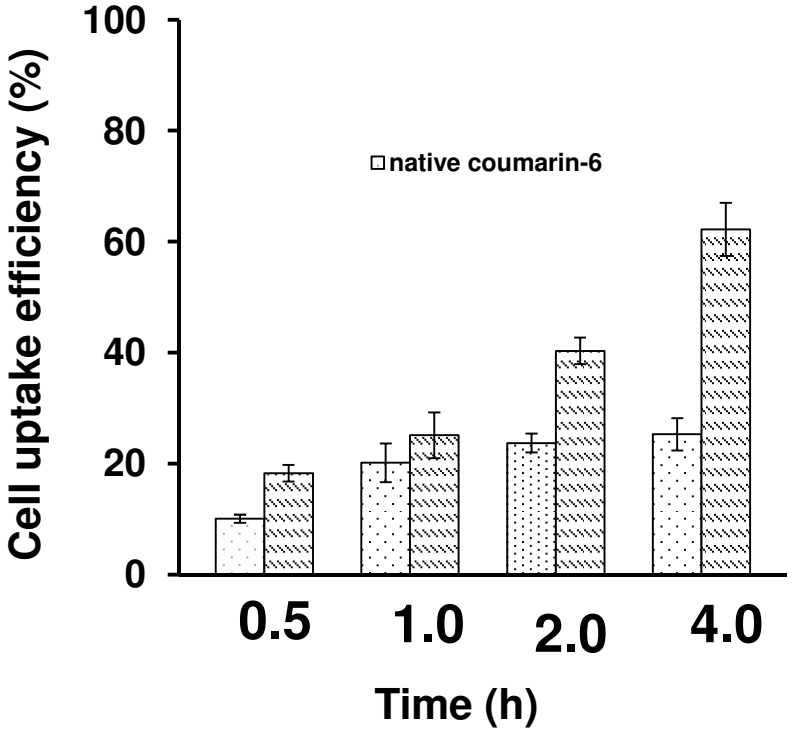

Figure 41. Cellular uptake of the coumarin-6-loaded PLGA nanoparticles and native coumarin-6 after 0.5, 1, 2, 4 h incubation at 0.250mg.ml nanoparticles concentration by HT-29 colon cancer cells

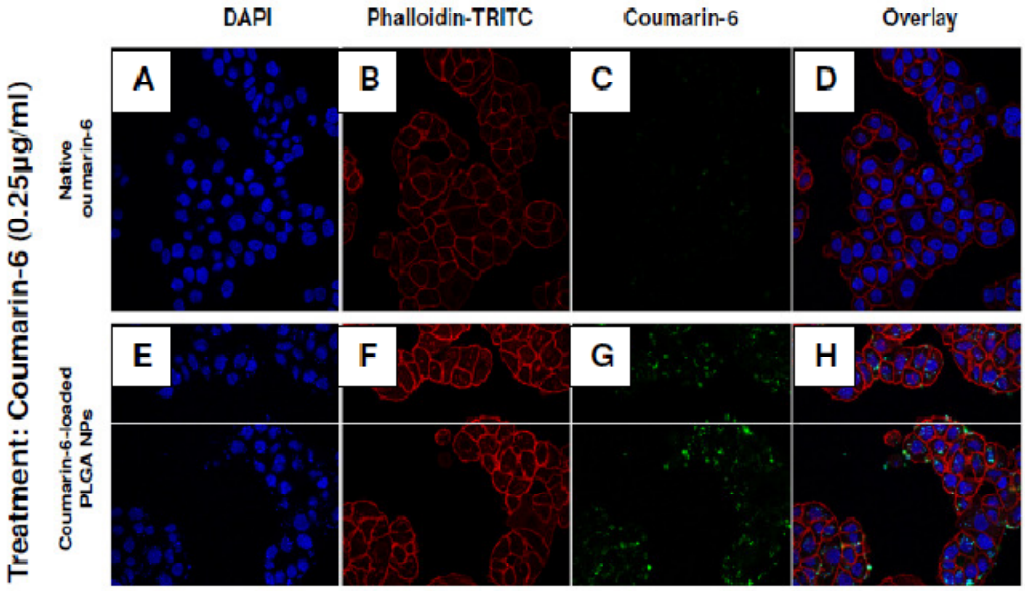

Figure 42. Laser scanning microscopy of HT-29 colon cancer cells after 2h incubation with native coumarin-6 and coumarin-6-loaded PLGA nanoparticles at 0.250mg/ml concentration

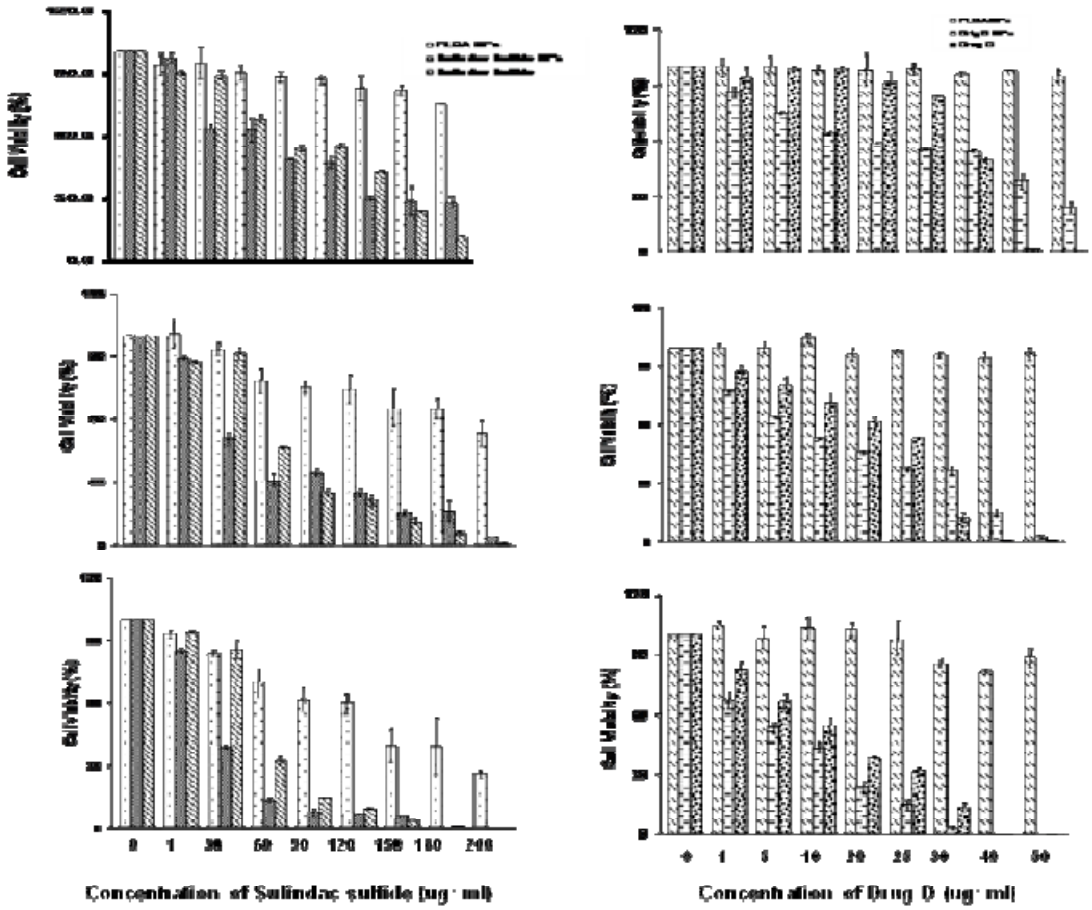

Figure 43. ***In vitro*** **viability of HT-29 colon cancer cells treated with placebo PLGA, sulindac sulfide-loaded PLGA nanoparticles and Drug D-loaded PLGA nanoparticles at varying concentrations after 24 (upper), 48 (middle), 72(lower)h culture, respectively (n=3)**

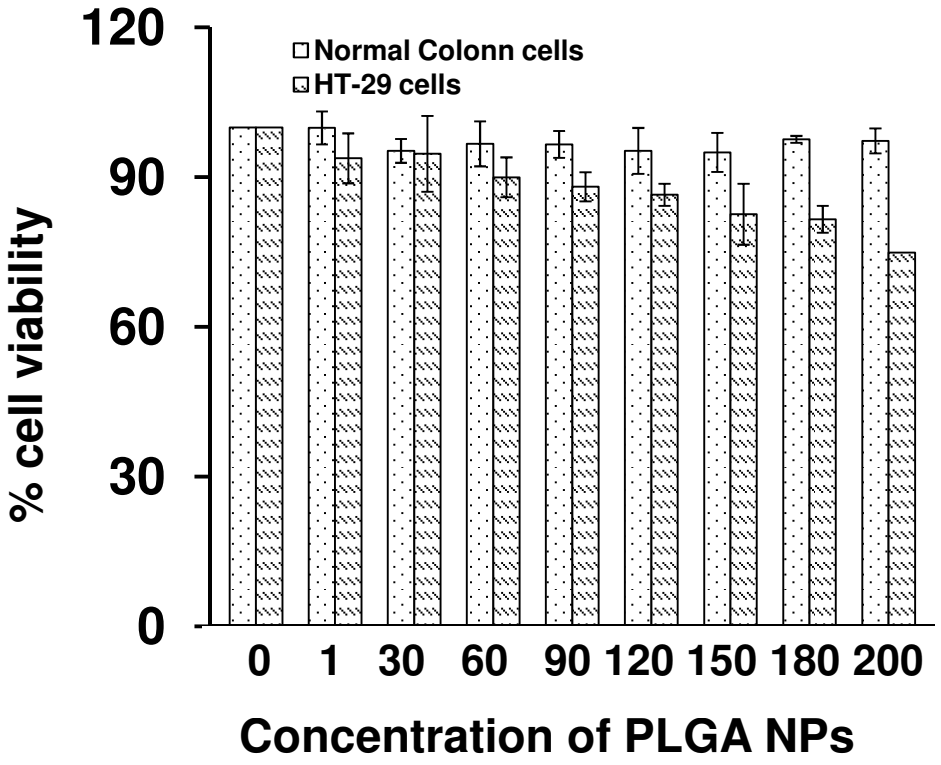

Figure 44. *In vitro* viability of HT-29 colon cancer cells and NCM 460 normal colon cells treated with placebo PLGA nanoparticles at the same 1, 30, 60, 90, 120, 150, 180, 200µg/ml nanoparticles concentration after 24h culture (n=3)

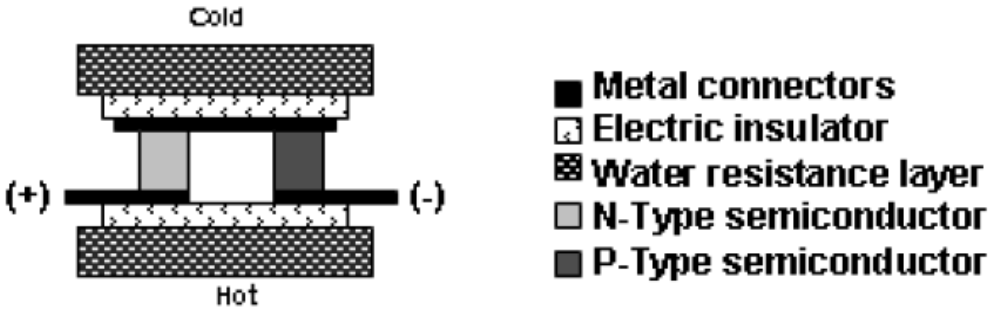

Figure 45. Schematic of a thermoelectric (TE) module

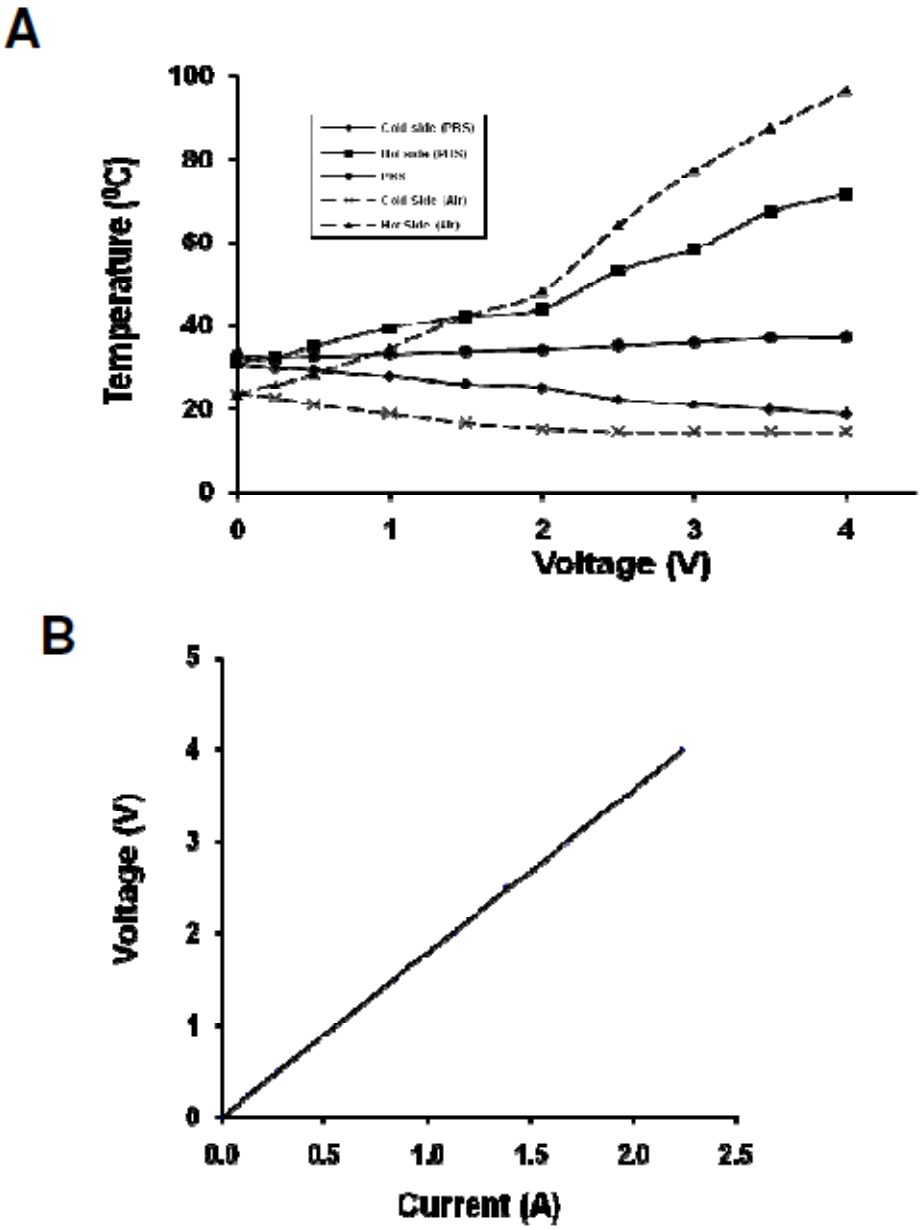

Figure 46. Characterization of thermoelectric module. The above graph depicts A) the change in temperature of the hot and cold side of the TE module in air and PBS as a function of voltage applied, and B) the change in current output as a function of voltage applied.

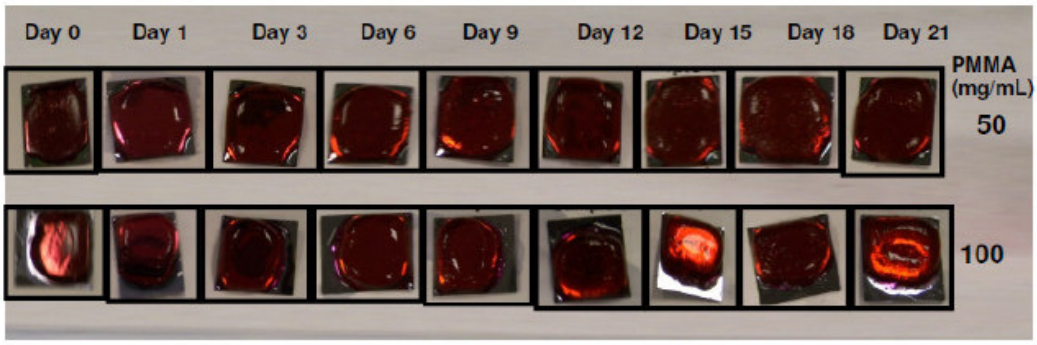

Figure 47. Attachment of Pluronic F127 to silicon wafer coated with 50 and 100mg/ml PMMA

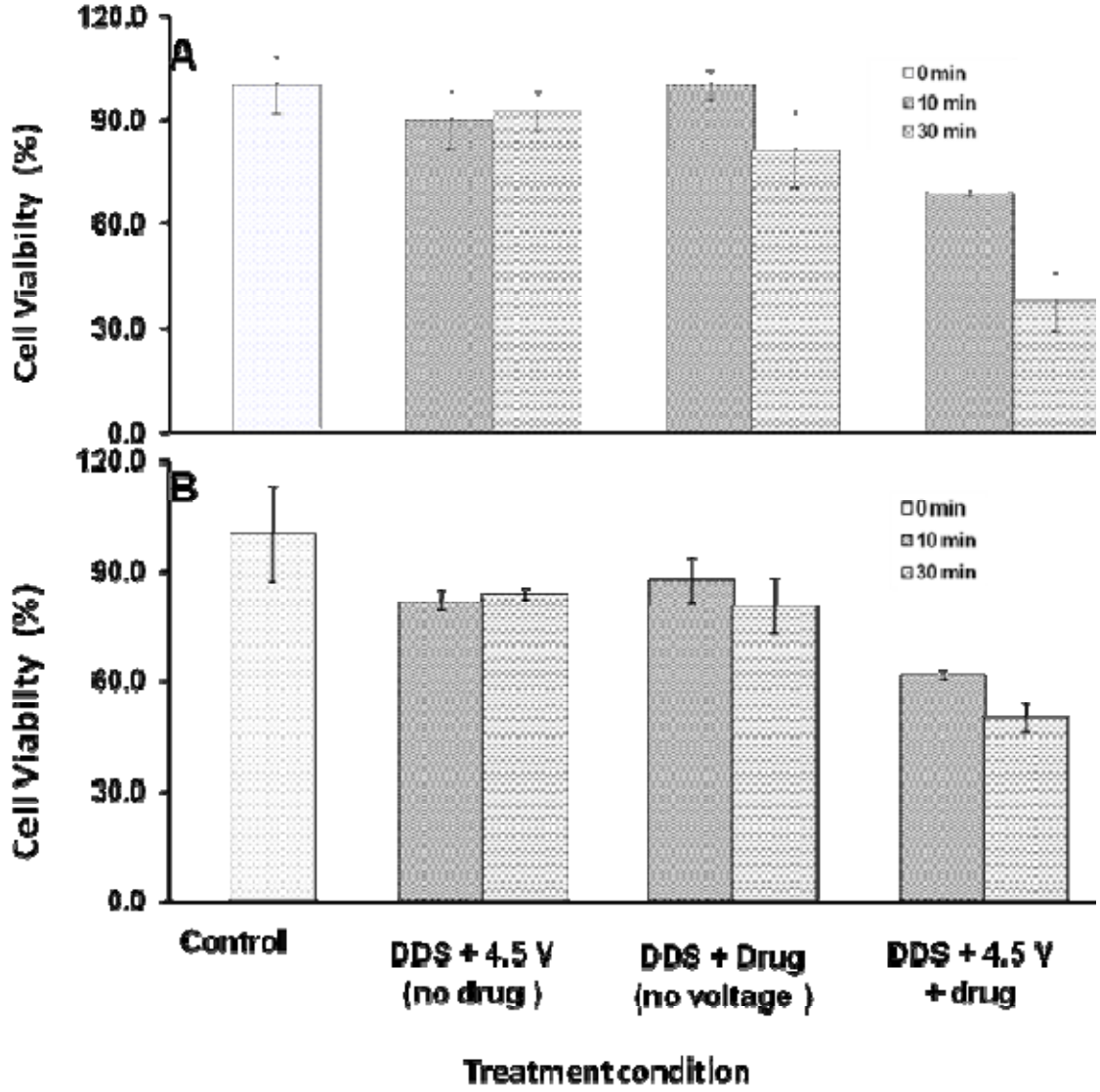

Figure 48. *In vitro* viability of HT-29 colon cancer cells treated with Pluronic F127 drug delivery system (DDS) containing no drug (4.5V), drug (sulindac sulfide- or Drug D-loaded PLGA NPs) (0V) and drug (sulindac sulfide- or Drug D-loaded PLGA NPs) (4.5V) . Drug treatment: A) sulindac-sulfide-loaded PLGA NPS and B) Drug –loaded PLGA NPs

Table 9.

Size, polydispersity, charge, drug encapsulation efficiency and drug content of PLGA nanoparticles with Drug D, sulindac sulfide or placebo (no drug)

Formulation	Particle size (nm)	Polydispersity Index (PDI)	Zeta potential (mV) ± SEM	% Drug Encapsulation ±SEM	%Drug content ±SEM
PLGA NPs	216.5 ±2.9	0.041 ±0.016	-20.36± 1.29	---	---
Sulindac sulfide loaded PLGA NPs	279.1± 2.9	0.160 ± .007	-23.43± 0.90	63.01± 0.47	5.8 ± 0.04
Drug D Loaded PLGA NPs	281.8 ±4.2	0.113 ± 0.015	-22.35± 0.73	61.14± 0.11	14.7 ± 0.03

Table 10.

IC_{50} values of native sulindac sulfide, native Drug D and PLGA nanoparticles with sulindac sulfide, Drug D or without drug (placebo) after 24, 48, 72 h incubation with HT-29 colon cancer cells (n=3)

	IC_{50} (µg/ml)± SEM		
Drug Formation	**24 h**	**48h**	**72 h**
Sulindac sulfide	**126.0 ± 0.5**	**52.4 ± 0.8**	**46.1 ± 1.6**
Sulindac sulfide loaded PLGA NPs	**84.5 ± 1.0**	**21.9 ± 0.5**	**30.3 ± 2.6**
Drug D	**30.2 ± 0.2**	**24.8 ± 0.5**	**15.6 ± 3.2**
Drug D loaded PLGA NPS	**28.7 ± 0.4**	**15.7 ± 0.6**	**7.6 ± 1.2**
PLGA NPs	**---**	**---**	**131.7± 6.0**

Table 11.

Thickness of PMMA film as a function of PMMA concentrations

PMMA concentration (mg/ml)	Thickness (Å)
50	1117.3 ±12.3
100	2415.5 ±95.7

References

1 Society, A. C. Cancer Facts & Figures 2009. (2009).

2 Masayo, Y., Kiyonaga, F., Koji, K., Setsuo, H. & Tadashi, K. The Proteomic Profile of Pancreatic Cancer Cell Lines Corresponding to Carcinogenesis and Metastasis. *Journal of Proteomics & Bioinformatics* **2** (2009).

3 Gronborg, M. *et al.* Biomarker discovery from pancreatic cancer secretome using a differential proteomic approach. *Mol Cell Proteomics* **5**, 157-171 (2006).

4 Hruban, R. H., Goggins, M., Parsons, J. & Kern, S. E. Progression model for pancreatic cancer. *Clinical cancer research : an official journal of the American Association for Cancer Research* **6**, 2969-2972 (2000).

5 Hruban, R. H., Wilentz, R. E. & Kern, S. E. Genetic progression in the pancreatic ducts. *The American journal of pathology* **156**, 1821-1825 (2000).

6 Kern, S. *et al.* A white paper: the product of a pancreas cancer think tank. *Cancer Res* **61**, 4923-4932 (2001).

7 Sommers, S. C., Murphy, S. A. & Warren, S. Pancreatic duct hyperplasia and cancer. *Gastroenterology* **27**, 629-640 (1954).

8 Colon and Rectal Cancer. (2009).

9 Cordon-Cardo, C. & Prives, C. At the crossroads of inflammation and tumorigenesis. *J Exp Med* **190**, 1367-1370 (1999).

10 Cotran, R., Kumar V, Collins T, Kellof GJ. Robbins Pathologic Basis of Disase. (1999).

11 Konturek, S. J., Konturek, P. C., Hartwich, A. & Hahn, E. G. Helicobacter pylori infection and gastrin and cyclooxygenase expression in gastric and

colorectal malignancies. *Regul Pept* **93**, 13-19, doi:S0167011500001737 [pii] (2000).

12 El-Sheikh, S. S. *et al.* Cyclooxygenase-2: a possible target in schistosoma-associated bladder cancer. *BJU Int* **88**, 921-927, doi:2477 [pii] (2001).

13 Boyle, P. & Ferlay, J. Cancer incidence and mortality in Europe, 2004. *Ann Oncol* **16**, 481-488, doi:mdi098 [pii]
10.1093/annonc/mdi098 (2005).

14 Wolff, R. A. Chemoprevention for pancreatic cancer. *Int J Gastrointest Cancer* **33**, 27-41 (2003).

15 Sporn, M. B. & Suh, N. Chemoprevention of cancer. *Carcinogenesis* **21**, 525-530 (2000).

16 Das, D., Arber, N. & Jankowski, J. A. Chemoprevention of colorectal cancer. *Digestion* **76**, 51-67 (2007).

17 Doucas, H., Garcea, G., Neal, C. P., Manson, M. M. & Berry, D. P. Chemoprevention of pancreatic cancer: a review of the molecular pathways involved, and evidence for the potential for chemoprevention. *Pancreatology* **6**, 429-439 (2006).

18 Thatcher, G. R. An introduction to NO-related therapeutic agents. *Current topics in medicinal chemistry* **5**, 597-601 (2005).

19 Thatcher, G. R., Nicolescu, A. C., Bennett, B. M. & Toader, V. Nitrates and NO release: contemporary aspects in biological and medicinal chemistry. *Free Radic Biol Med* **37**, 1122-1143 (2004).

20 Velazquez, C., Praveen Rao, P. N. & Knaus, E. E. Novel nonsteroidal antiinflammatory drugs possessing a nitric oxide donor diazen-1-ium-1,2-diolate moiety: design, synthesis, biological evaluation, and nitric oxide release studies. *J Med Chem* **48**, 4061-4067 (2005).

21 Ignarro, L. J. Nitric oxide as a unique signaling molecule in the vascular system: a historical overview. *J Physiol Pharmacol* **53**, 503-514 (2002).

22 Govoni, M., Casagrande, S., Maucci, R., Chiroli, V. & Tocchetti, P. In vitro metabolism of (nitrooxy)butyl ester nitric oxide-releasing compounds: comparison with glyceryl trinitrate. *J Pharmacol Exp Ther* **317**, 752-761 (2006).

23 Carini, M. *et al.* Nitric oxide release and distribution following oral and intraperitoneal administration of nitroaspirin (NCX 4016) in the rat. *Life Sci* **74**, 3291-3305 (2004).

24 Gao, J., Kashfi, K. & Rigas, B. In vitro metabolism of nitric oxide-donating aspirin: the effect of positional isomerism. *J Pharmacol Exp Ther* **312**, 989-997 (2005).

25 Fiorucci, S. *et al.* Gastrointestinal safety of NO-aspirin (NCX-4016) in healthy human volunteers: a proof of concept endoscopic study. *Gastroenterology* **124**, 600-607. (2003).

26 Iconomou, G., Kalofonos, H. P., Koutras, A. K., Vagenakis, A. G. & Rigas, B. Pilot study of nitric oxide-donating aspirin in patients with pancreatic cancer pain. *J Support Oncol* **4**, 168 (2006).

27 Muscat, J. E., Dyer, A. M., Rosenbaum, R. E. & Rigas, B. Nitric oxide-releasing medications and colorectal cancer risk: the framingham study. *Anticancer Res* **25**, 4471-4474 (2005).

28 Rigas, B. & Kashfi, K. Nitric-oxide-donating NSAIDs as agents for cancer prevention. *Trends Mol Med* **10**, 324-330 (2004).

29 Kashfi, K. *et al.* Positional isomerism markedly affects the growth inhibition of colon cancer cells by nitric oxide-donating aspirin in vitro and in vivo. *J Pharmacol Exp Ther* **312**, 978-988 (2005).

30 Gao, J., Liu, X. & Rigas, B. Nitric oxide-donating aspirin induces apoptosis in human colon cancer cells through induction of oxidative stress. *Proc Natl Acad Sci U S A* **102**, 17207-17212 (2005).

31 Tesei, A. *et al.* In vitro and in vivo evaluation of NCX 4040 cytotoxic activity in human colon cancer cell lines. *J Transl Med* **3**, 7 (2005).

32 Kashfi, K. & Rigas, B. The mechanism of action of nitric oxide-donating aspirin. *Biochem Biophys Res Commun* **358**, 1096-1101 (2007).

33 Kashfi, K. & Rigas, B. Molecular targets of nitric-oxide-donating aspirin in cancer. *Biochemical Society transactions* **33**, 701-704 (2005).

34 Hundley, T. R. & Rigas, B. Nitric oxide-donating aspirin inhibits colon cancer cell growth via mitogen-activated protein kinase activation. *J Pharmacol Exp Ther* **316**, 25-34 (2006).

35 Spiegel, A. *et al.* NO-donating aspirin inhibits both the expression and catalytic activity of inducible nitric oxide synthase in HT-29 human colon cancer cells. *Biochem Pharmacol* **70**, 993-1000 (2005).

36 Rao, C. V. *et al.* Nitric oxide-releasing aspirin and indomethacin are potent inhibitors against colon cancer in azoxymethane-treated rats: effects on molecular targets. *Mol Cancer Ther* **5**, 1530-1538 (2006).

37 Williams, J. L. *et al.* Growth inhibition of human colon cancer cells by nitric oxide (NO)-donating aspirin is associated with cyclooxygenase-2 induction and beta-catenin/T-cell factor signaling, nuclear factor-kappaB, and NO synthase 2 inhibition: implications for chemoprevention. *Cancer Res* **63**, 7613-7618 (2003).

38 Williams, J. L. *et al.* Growth inhibition of human colon cancer cells by nitric oxide (NO)-donating aspirin is associated with cyclooxygenase-2 induction and beta-catenin/T-cell factor signaling, nuclear factor-kappaB, and NO synthase 2 inhibition: implications for chemoprevention. *Cancer Res* **63**, 7613-7618. (2003).

39 Corazzi, T., Leone, M., Maucci, R., Corazzi, L. & Gresele, P. Direct and irreversible inhibition of cyclooxygenase-1 by nitroaspirin (NCX 4016). *J Pharmacol Exp Ther* **315**, 1331-1337 (2005).

40 Herschman, H. R. Primary response genes induced by growth factors and tumor promoters. *Annu Rev Biochem* **60**, 281-319, doi:10.1146/annurev.bi.60.070191.001433 (1991).

41 Wallace, J. L. Prostaglandins, NSAIDs, and cytoprotection. *Gastroenterol Clin North Am* **21**, 631-641 (1992).

42 Seibert, K. *et al.* Pharmacological and biochemical demonstration of the role of cyclooxygenase 2 in inflammation and pain. *Proc Natl Acad Sci U S A* **91**, 12013-12017 (1994).

43 Bennett, A. *et al.* Prostaglandins and breast cancer. *Lancet* **2**, 624-626, doi:S0140-6736(77)92496-5 [pii] (1977).

44 Rigas, B., Goldman, I. S. & Levine, L. Altered eicosanoid levels in human colon cancer. *J Lab Clin Med* **122**, 518-523, doi:0022-2143(93)90010-V [pii] (1993).

45 Hida, T. *et al.* Non-small cell lung cancer cycloxygenase activity and proliferation are inhibited by non-steroidal antiinflammatory drugs. *Anticancer Res* **18**, 775-782 (1998).

46 Howe, L. R., Subbaramaiah, K., Brown, A. M. & Dannenberg, A. J. Cyclooxygenase-2: a target for the prevention and treatment of breast cancer. *Endocr Relat Cancer* **8**, 97-114 (2001).

47 Liu, X. H., Yao, S., Kirschenbaum, A. & Levine, A. C. NS398, a selective cyclooxygenase-2 inhibitor, induces apoptosis and down-regulates bcl-2 expression in LNCaP cells. *Cancer Res* **58**, 4245-4249 (1998).

48 Marrogi, A. *et al.* Human mesothelioma samples overexpress both cyclooxygenase-2 (COX-2) and inducible nitric oxide synthase (NOS2): in

vitro antiproliferative effects of a COX-2 inhibitor. *Cancer Res* **60**, 3696-3700 (2000).

49 Mohammed, S. I. *et al.* Expression of cyclooxygenase-2 (COX-2) in human invasive transitional cell carcinoma (TCC) of the urinary bladder. *Cancer Res* **59**, 5647-5650 (1999).

50 Rodriguez-Burford, C. *et al.* Effects of nonsteroidal anti-inflammatory agents (NSAIDs) on ovarian carcinoma cell lines: preclinical evaluation of NSAIDs as chemopreventive agents. *Clin Cancer Res* **8**, 202-209 (2002).

51 Shiff, S. J., Koutsos, M. I., Qiao, L. & Rigas, B. Nonsteroidal antiinflammatory drugs inhibit the proliferation of colon adenocarcinoma cells: effects on cell cycle and apoptosis. *Exp Cell Res* **222**, 179-188, doi:S0014-4827(96)90023-3 [pii] 1006/excr.1996.0023 (1996).

52 Zimmermann, K. C. *et al.* Cyclooxygenase-2 expression in human esophageal carcinoma. *Cancer Res* **59**, 198-204 (1999).

53 Gately, S. The contributions of cyclooxygenase-2 to tumor angiogenesis. *Cancer Metastasis Rev* **19**, 19-27 (2000).

54 Kojima, M. *et al.* Association of enhanced cyclooxygenase-2 expression with possible local immunosuppression in human colorectal carcinomas. *Ann Surg Oncol* **8**, 458-465 (2001).

55 Sheng, H., Shao, J., Morrow, J. D., Beauchamp, R. D. & DuBois, R. N. Modulation of apoptosis and Bcl-2 expression by prostaglandin E2 in human colon cancer cells. *Cancer Res* **58**, 362-366 (1998).

56 Tsujii, M. & DuBois, R. N. Alterations in cellular adhesion and apoptosis in epithelial cells overexpressing prostaglandin endoperoxide synthase 2. *Cell* **83**, 493-501, doi:0092-8674(95)90127-2 [pii] (1995).

57 Tsujii, M. *et al.* Cyclooxygenase regulates angiogenesis induced by colon cancer cells. *Cell* **93**, 705-716, doi:S0092-8674(00)81433-6 [pii] (1998).

58 Watson, A. J. Chemopreventive effects of NSAIDs against colorectal cancer: regulation of apoptosis and mitosis by COX-1 and COX-2. *Histol Histopathol* **13**, 591-597 (1998).

59 Tardieu, D. *et al.* The COX-2 inhibitor nimesulide suppresses superoxide and 8-hydroxy-deoxyguanosine formation, and stimulates apoptosis in mucosa during early colonic inflammation in rats. *Carcinogenesis* **21**, 973-976 (2000).

60 Elder, D. J., Halton, D. E., Hague, A. & Paraskeva, C. Induction of apoptotic cell death in human colorectal carcinoma cell lines by a cyclooxygenase-2 (COX-2)-selective nonsteroidal anti-inflammatory drug: independence from COX-2 protein expression. *Clin Cancer Res* **3**, 1679-1683 (1997).

61 Smigel, K. Arthritis drug approved for polyp prevention blazes trail for other prevention trials. *J Natl Cancer Inst* **92**, 297-299 (2000).

62 Liu, C. H. *et al.* Overexpression of cyclooxygenase-2 is sufficient to induce tumorigenesis in transgenic mice. *J Biol Chem* **276**, 18563-18569, doi:10.1074/jbc.M010787200M010787200 [pii] (2001).

63 Cao, Y., Pearman, A. T., Zimmerman, G. A., McIntyre, T. M. & Prescott, S. M. Intracellular unesterified arachidonic acid signals apoptosis. *Proc Natl Acad Sci U S A* **97**, 11280-11285, doi:10.1073/pnas.200367597200367597 [pii] (2000).

64 Aggarwal, S. *et al.* Indomethacin-induced apoptosis in esophageal adenocarcinoma cells involves upregulation of Bax and translocation of mitochondrial cytochrome C independent of COX-2 expression. *Neoplasia* **2**, 346-356 (2000).

65 Zhang, L., Yu, J., Park, B. H., Kinzler, K. W. & Vogelstein, B. Role of BAX in the apoptotic response to anticancer agents. *Science* **290**, 989-992, doi:8940 [pii] (2000).

66 Chan, T. A., Morin, P. J., Vogelstein, B. & Kinzler, K. W. Mechanisms underlying nonsteroidal antiinflammatory drug-mediated apoptosis. *Proc Natl Acad Sci U S A* **95**, 681-686 (1998).

67 Yin, M. J., Yamamoto, Y. & Gaynor, R. B. The anti-inflammatory agents aspirin and salicylate inhibit the activity of I(kappa)B kinase-beta. *Nature* **396**, 77-80, doi:10.1038/23948 (1998).

68 Saunders, F. R. & Wallace, H. M. On the natural chemoprevention of cancer. *Plant Physiol Biochem*, doi:S0981-9428(10)00057-4 [pii]10.1016/j.plaphy.2010.03.001 (2010).

69 Odian, G. & Tsay, J. Radiation Graft-Polymerization of Styrene to Cellulose Acetate-Butyrate. *Makromol Chem* **182**, 1481-1489 (1981).

70 Odian, G. Basic Concepts in Elastomer Synthesis. *Abstr Pap Am Chem S* **182**, 15-Poly (1981).

71 Mcgrath, J. E. Chain-Reaction Polymerization. *J Chem Educ* **58**, 844-861 (1981).

72 Cornelissen, J. J. L. M., Fischer, M., Sommerdijk, N. A. J. M. & Nolte, R. J. M. Helical superstructures from charged poly(styrene)-poly(isocyanodipeptide) block copolymers. *Science* **280**, 1427-1430 (1998).

73 Discher, B. M., Hammer, D. A., Bates, F. S. & Discher, D. E. Polymer vesicles in various media. *Curr Opin Colloid In* **5**, 125-131 (2000).

74 Burke, S., Shen, H. W. & Eisenberg, A. Multiple vesicular morphologies from block copolymers in solution. *Macromol Symp* **175**, 273-283 (2001).

75 Discher, D. E. & Eisenberg, A. Polymer vesicles. *Science* **297**, 967-973 (2002).

76 Hajduk, D. A., Kossuth, M. B., Hillmyer, M. A. & Bates, F. S. Complex phase behavior in aqueous solutions of poly(ethylene oxide)-poly(ethylethylene) block copolymers. *Journal of Physical Chemistry B* **102**, 4269-4276 (1998).

77 Kabanov, A. V. & Alakhov, V. Y. Pluronic (R) block copolymers in drug delivery: From micellar nanocontainers to biological response modifiers. *Crit Rev Ther Drug* **19**, 1-72 (2002).

78 Shen, H. W. & Eisenberg, A. Control of architecture in block-copolymer vesicles. *Angew Chem Int Edit* **39**, 3310-+ (2000).

79 Alexandridis, P. Amphiphilic copolymers and their applications. *Curr Opin Colloid In* **1**, 490-501 (1996).

80 Antipov, A. A., Sukhorukov, G. B. & Mohwald, H. Influence of the ionic strength on the polyelectrolyte multilayers' permeability. *Langmuir* **19**, 2444-2448, doi:Doi 10.1021/La026101n (2003).

81 Soo, P. L. & Eisenberg, A. Preparation of block copolymer vesicles in solution. *J Polym Sci Pol Phys* **42**, 923-938, doi:Doi 10.1002/Polb.10739 (2004).

82 Borsali, R. *et al.* From "sunflower-like" assemblies toward giant wormlike micelles. *Langmuir* **19**, 6-9, doi:Doi 10.1021/La026125u (2003).

83 Breulmann, M., Forster, S. & Antonietti, M. Mesoscopic surface patterns formed by block copolymer micelles. *Macromol Chem Physic* **201**, 204-211 (2000).

84 Antonietti, M. & Forster, S. Vesicles and liposomes: A self-assembly principle beyond lipids. *Adv Mater* **15**, 1323-1333, doi:DOI 10.1002/adma.200300010 (2003).

85 Balsara, N. P., Tirrell, M. & Lodge, T. P. Micelle Formation of Bab Triblock Copolymers in Solvents That Preferentially Dissolve the a-Block. *Macromolecules* **24**, 1975-1986 (1991).

86 Zhang, L. F. & Eisenberg, A. Multiple Morphologies of Crew-Cut Aggregates of Polystyrene-B-Poly(Acrylic Acid) Block-Copolymers. *Science* **268**, 1728-1731 (1995).

87 Zhang, L. F. & Eisenberg, A. Multiple morphologies and characteristics of "crew-cut" micelle-like aggregates of polystyrene-b-poly(acrylic acid) diblock copolymers in aqueous solutions. *J Am Chem Soc* **118**, 3168-3181 (1996).

88 Ha, J. C., Kim, S. Y. & Lee, Y. M. Poly(ethylene oxide)-poly(propylene oxide)-poly(ethylene oxide) (pluronic)/poly(epsilon-caprolactone) (PCL) amphiphilic block copolymeric nanospheres - I. Preparation and characterization. *J Control Release* **62**, 381-392 (1999).

89 Barenholz, Y. Liposome application: problems and prospects. *Curr Opin Colloid In* **6**, 66-77 (2001).

90 Paphadjopoulos, D., Wilson, T. & Taber, R. Liposomes as Vehicles for Cellular Incorporation of Biologically-Active Macromolecules. *In Vitro Cell Dev B* **16**, 49-54 (1980).

91 Weinstein, J. N. Liposomes as Targeted Drug Carriers - a Physical-Chemical Perspective. *Pure Appl Chem* **53**, 2241-2254 (1981).

92 Hristova, K. & Needham, D. Phase-Behavior of a Lipid Polymer-Lipid Mixture in Aqueous-Medium. *Macromolecules* **28**, 991-1002 (1995).

93 Woodle, M. C. & Lasic, D. D. Sterically Stabilized Liposomes. *Biochimica Et Biophysica Acta* **1113**, 171-199 (1992).

94 Kreuter, J. Nanoparticle-Based Drug Delivery Systems. *J Control Release* **16**, 169-176 (1991).

95 Langer, R. New Methods of Drug Delivery. *Science* **249**, 1527-1533 (1990).

96 Patri, A. K., Majoros, I. J. & Baker, J. R. Dendritic polymer macromolecular carriers for drug delivery. *Curr Opin Chem Biol* **6**, 466-471, doi:Doi 10.1016/S1367-5931(02)00347-2 (2002).

97 Anderson, B. C., Pandit, N. K. & Mallapragada, S. K. Understanding drug release from poly(ethylene oxide)-b-poly(propylene oxide)-b-poly(ethylene oxide) gels. *J Control Release* **70**, 157-167 (2001).

98 Torchilin, V. P. Structure and design of polymeric surfactant-based drug delivery systems. *J Control Release* **73**, 137-172 (2001).

99 Breitenbach, A., Li, Y. X. & Kissel, T. Branched biodegradable polyesters for parenteral drug delivery systems. *J Control Release* **64**, 167-178 (2000).

100 Cammas, S. *et al.* Thermo-responsive polymer nanoparticles with a core-shell micelle structure as site-specific drug carriers. *J Control Release* **48**, 157-164 (1997).

101 Gao, C. Y., Leporatti, S., Moya, S., Donath, E. & Mohwald, H. Swelling and shrinking of polyelectrolyte microcapsules in response to changes in temperature and ionic strength. *Chem-Eur J* **9**, 915-920 (2003).

102 Qiu, X. P., Leporatti, S., Donath, E. & Mohwald, H. Studies on the drug release properties of polysaccharide multilayers encapsulated ibuprofen microparticles. *Langmuir* **17**, 5375-5380 (2001).

103 Sukhorukov, G. B., Antipov, A. A., Voigt, A., Donath, E. & Mohwald, H. pH-controlled macromolecule encapsulation in and release from polyelectrolyte multilayer nanocapsules. *Macromol Rapid Comm* **22**, 44-46 (2001).

104 Alexandridis, P. & Hatton, T. A. Poly(Ethylene Oxide)-Poly(Propylene Oxide)-Poly(Ethylene Oxide) Block-Copolymer Surfactants in Aqueous-Solutions and at Interfaces - Thermodynamics, Structure, Dynamics, and Modeling. *Colloid Surface A* **96**, 1-46 (1995).

105 Saeki, S., Kuwahara, N., Nakata, M. & Kaneko, M. Upper and Lower Critical Solution Temperatures in Poly (Ethyleneglycol) Solutions. *Polymer* **17**, 685-689 (1976).

106 Alexandridis, P., Athanassiou, V., Fukuda, S. & Hatton, T. A. Surface-Activity of Poly(Ethylene Oxide)-Block-Poly(Propylene Oxide)-Block-Poly(Ethylene Oxide) Copolymers. *Langmuir* **10**, 2604-2612 (1994).

107 Guo, C., Wang, J., Liu, H. Z. & Chen, J. Y. Hydration and conformation of temperature-dependent micellization of PEO-PPO-PEO block copolymers in aqueous solutions by FT-Raman. *Langmuir* **15**, 2703-2708 (1999).

108 Husseini, G. A., Myrup, G. D., Pitt, W. G., Christensen, D. A. & Rapoport, N. A. Y. Factors affecting acoustically triggered release of drugs from polymeric micelles. *J Control Release* **69**, 43-52 (2000).

109 Nivaggioli, T., Tsao, B., Alexandridis, P. & Hatton, T. A. Microviscosity in Pluronic and Tetronic Poly(Ethylene Oxide) Poly(Propylene Oxide) Block-Copolymer Micelles. *Langmuir* **11**, 119-126 (1995).

110 Yeh, R. K. *et al.* NO-donating nonsteroidal antiinflammatory drugs (NSAIDs) inhibit colon cancer cell growth more potently than traditional NSAIDs: a general pharmacological property? *Biochem Pharmacol* **67**, 2197-2205 (2004).

111 Rigas, B. The use of nitric oxide-donating nonsteroidal anti-inflammatory drugs in the chemoprevention of colorectal neoplasia. *Curr Opin Gastroenterol* **23**, 55-59 (2007).

112 Rao, C. V. *et al.* Nitric oxide-releasing aspirin and indomethacin are potent inhibitors against colon cancer in azoxymethane-treated rats: effects on molecular targets. *Mol Cancer Ther* **5**, 1530-1538 (2006).

113 Chell, S., Kaidi, A., Kadi, A., Williams, A. C. & Paraskeva, C. Mediators of PGE2 synthesis and signalling downstream of COX-2 represent potential targets for the prevention/treatment of colorectal cancer. *Biochim Biophys Acta* **1766**, 104-119 (2006).

114 Samuelsson, B., Morgenstern, R. & Jakobsson, P.-J. Membrane prostaglandin E synthase-1: a novel therapeutic target. *Pharmacol Rev* **59**, 207-224 (2007).

115 Flavahan, N. A. Balancing prostanoid activity in the human vascular system. *Trends Pharmacol Sci* **28**, 106-110 (2007).

116 Carini, M., Aldini, G., Orioli, M. & Maffei Facino, R. In vitro metabolism of a nitroderivative of acetylsalicylic acid (NCX4016) by rat liver: LC and LC-MS studies. *J Pharm Biomed Anal* **29**, 1061-1071 (2002).

117 Carini, M. *et al.* Nitric oxide release and distribution following oral and intraperitoneal administration of nitroaspirin (NCX 4016) in the rat. *Life Sci* **74**, 3291-3305 (2004).

118 Carini, M. *et al.* Chemiluminescence and LC-MS/MS analyses for the study of nitric oxide release and distribution following oral administration of nitroaspirin (NCX 4016) in healthy volunteers. *J Pharm Biomed Anal* **35**, 277-287 (2004).

119 Gao, J., Kashfi, K. & Rigas, B. In vitro metabolism of nitric oxide-donating aspirin: the effect of positional isomerism. *J Pharmacol Exp Ther* **312**, 989-997 (2005).

120 Keeble, J. E. & Moore, P. K. Pharmacology and potential therapeutic applications of nitric oxide-releasing non-steroidal anti-inflammatory and related nitric oxide-donating drugs. *Br J Pharmacol* **137**, 295-310 (2002).

121 Rao, C. V., Rivenson, A., Simi, B. & Reddy, B. S. Chemoprevention of colon carcinogenesis by dietary curcumin, a naturally occurring plant phenolic compound. *Cancer Res* **55**, 259-266 (1995).

122 Ukawa, H., Yamakuni, H., Kato, S. & Takeuchi, K. Effects of cyclooxygenase-2 selective and nitric oxide-releasing nonsteroidal antiinflammatory drugs on mucosal ulcerogenic and healing responses of the stomach. *Dig Dis Sci* **43**, 2003-2011 (1998).

123 Kashfi, K. & Rigas, B. Non-COX-2 targets and cancer: expanding the molecular target repertoire of chemoprevention. *Biochem Pharmacol* **70**, 969-986 (2005).

124 Rigas, B. & Kozoni, V. The novel phenylester anticancer compounds: Study of a derivative of aspirin (phoshoaspirin). *Int J Oncol* **32**, 97-100 (2008).

125 Zhao, W., Mackenzie, G. G., Murray, O. T., Zhang, Z. & Rigas, B. Phosphoaspirin (MDC-43), a novel benzyl ester of aspirin, inhibits the growth of human cancer cell lines more potently than aspirin: a redox-dependent effect. *Carcinogenesis* **30**, 512-519 (2009).

126 Baron, J. A. Epidemiology of non-steroidal anti-inflammatory drugs and cancer. *Prog Exp Tumor Res* **37**, 1-24 (2003).

127 Baron, J. A. What now for aspirin and cancer prevention? *J Natl Cancer Inst* **96**, 4-5 (2004).

128 Baron, J. A. *et al.* A randomized trial of aspirin to prevent colorectal adenomas. *N Engl J Med* **348**, 891-899 (2003).

129 Rayyan, Y., Williams, J. & Rigas, B. The role of NSAIDs in the prevention of colon cancer. *Cancer Invest* **20**, 1002-1011 (2002).

130 Penning, T. D. *et al.* Synthesis and biological evaluation of the 1,5-diarylpyrazole class of cyclooxygenase-2 inhibitors: identification of 4-[5-(4-methylphenyl)-3-(trifluoromethyl)-1H-pyrazol-1-yl]benze nesulfonamide (SC-58635, celecoxib). *J Med Chem* **40**, 1347-1365 (1997).

131 Bernard, M. P., Bancos, S., Sime, P. J. & Phipps, R. P. Targeting cyclooxygenase-2 in hematological malignancies: rationale and promise. *Curr Pharm Des* **14**, 2051-2060 (2008).

132 Wang, D. & DuBois, R. N. Pro-inflammatory prostaglandins and progression of colorectal cancer. *Cancer Lett* **267**, 197-203 (2008).

133 Kashfi, K. *et al.* Positional isomerism markedly affects the growth inhibition of colon cancer cells by nitric oxide-donating aspirin in vitro and in vivo. *J Pharmacol Exp Ther* **312**, 978-988 (2005).

134 Kashfi, K. & Rigas, B. The mechanism of action of nitric oxide-donating aspirin. *Biochem Biophys Res Commun* **358**, 1096-1101 (2007).

135 Hulsman, N. *et al.* Chemical insights in the concept of hybrid drugs: the antitumor effect of nitric oxide-donating aspirin involves a quinone methide but not nitric oxide nor aspirin. *J Med Chem* **50**, 2424-2431 (2007).

136 Ali, B. & Kaur, S. Mammalian tissue acetylsalicylic acid esterase(s): identification, distribution and discrimination from other esterases. *J Pharmacol Exp Ther* **226**, 589-594 (1983).

137 Kim, D. H., Yang, Y. S. & Jakoby, W. B. Aspirin hydrolyzing esterases from rat liver cytosol. *Biochem Pharmacol* **40**, 481-487 (1990).

138 Chun, K. W., Lee, J. B., Kim, S. H. & Park, T. G. Controlled release of plasmid DNA from photo-cross-linked pluronic hydrogels. *Biomaterials* **26**, 3319-3326, doi:DOI 10.1016/j.biomaterials.2004.07.055 (2005).

139 Lee, S. Y., Lee, Y., Kim, J. E., Park, T. G. & Ahn, C. H. A novel pH-sensitive PEG-PPG-PEG copolymer displaying a closed-loop sol-gel-sol transition. *J Mater Chem* **19**, 8198-8201, doi:Doi 10.1039/B912540j (2009).

140 Sosnik, A. & Cohn, D. Reverse thermo-responsive poly(ethylene oxide) and poly(propylene oxide) multiblock copolymers. *Biomaterials* **26**, 349-357, doi:10.1016/j.biomaterials.2004.02.041S0142961204001796 [pii] (2005).

141 Yoon, J. J., Chung, H. J. & Park, T. G. Photo-crosslinkable and biodegradable pluronic/heparin hydrogels for local and sustained delivery of angiogenic growth factor. *J Biomed Mater Res A* **83A**, 597-605, doi:Doi 10.1002/Jbm.A.31271 (2007).

142 Zhao, S. P., Cao, M. J., Wu, J. & Xu, W. L. Synthesis and Characterization of Biodegradable Thermo- and pH-Sensitive Hydrogels Based on Pluronic F127/Poly(epsilon-caprolactone) Macromer and Acrylic Acid. *Macromol Res* **17**, 1025-1031 (2009).

143 Bromberg, L. E. & Ron, E. S. Temperature-responsive gels and thermogelling polymer matrices for protein and peptide delivery. *Adv Drug Deliver Rev* **31**, 197-221 (1998).

144 Drury, J. L. & Mooney, D. J. Hydrogels for tissue engineering: scaffold design variables and applications. *Biomaterials* **24**, 4337-4351, doi:Doi 10.1016/S0142-9612(03)00340-5 (2003).

145 Jeong, B., Bae, Y. H., Lee, D. S. & Kim, S. W. Biodegradable block copolymers as injectable drug-delivery systems. *Nature* **388**, 860-862 (1997).

146 Peppas, N. A., Bures, P., Leobandung, W. & Ichikawa, H. Hydrogels in pharmaceutical formulations. *Eur J Pharm Biopharm* **50**, 27-46, doi:S0939-6411(00)00090-4 [pii] (2000).

147 Rokhade, A. P., Shelke, N. B., Patil, S. A. & Aminabhavi, T. M. Novel hydrogel microspheres of chitosan and pluronic F-127 for controlled release of 5-fluorouracil. *J Microencapsul* **24**, 274-288, doi:Doi 10.1080/02652040701281365 (2007).

148 Alexandridis, P., Athanassiou, V. & Hatton, T. A. Pluronic-P105 Peo-Ppo-Peo Block-Copolymer in Aqueous Urea Solutions - Micelle Formation, Structure, and Microenvironment. *Langmuir* **11**, 2442-2450 (1995).

149 Alexandridis, P., Holzwarth, J. F. & Hatton, T. A. Micellization of Poly(Ethylene Oxide)-Poly(Propylene Oxide)-Poly(Ethylene Oxide) Triblock Copolymers in Aqueous-Solutions - Thermodynamics of Copolymer Association. *Macromolecules* **27**, 2414-2425 (1994).

150 Kabanov, A. V. *et al.* A New Class of Drug Carriers - Micelles of Poly(Oxyethylene)-Poly(Oxypropylene) Block Copolymers as

Microcontainers for Drug Targeting from Blood in Brain. *J Control Release* **22**, 141-157 (1992).

151 Kabanov, A. V. *et al.* Micelle Formation and Solubilization of Fluorescent-Probes in Poly(Oxyethylene-B-Oxypropylene-B-Oxyethylene) Solutions. *Macromolecules* **28**, 2303-2314 (1995).

152 Chu, B., Zhou, Z. K. & Wu, G. W. Structure and Dynamics of Polymeric Micelles in Solution. *J Non-Cryst Solids* **172**, 1094-1102 (1994).

153 Oh, K. T., Bronich, T. K. & Kabanov, A. V. Micellar formulations for drug delivery based on mixtures of hydrophobic and hydrophilic Pluronic((R)) block copolymers. *J Control Release* **94**, 411-422, doi:DOI 10.1016/j.jcornel.2003.10.018 (2004).

154 Trong, L. C. P., Djabourov, M. & Ponton, A. Mechanisms of micellization and rheology of PEO-PPO-PEO triblock copolymers with various architectures. *J Colloid Interf Sci* **328**, 278-287, doi:DOI 10.1016/j.jcis.2008.09.029 (2008).

155 Barichello, J. M., Morishita, M., Takayama, K. & Nagai, T. Absorption of insulin from pluronic F-127 gels following subcutaneous administration in rats. *Int J Pharm* **184**, 189-198, doi:S0378517399001192 [pii] (1999).

156 Cohn, D. & Sosnik, A. Novel reverse thermoresponsive injectable poly(ether carbonate)s. *J Mater Sci Mater Med* **14**, 175-180, doi:5118710 [pii] (2003).

157 Cohn, D., Sosnik, A. & Garty, S. Smart hydrogels for in situ generated implants. *Biomacromolecules* **6**, 1168-1175, doi:10.1021/bm0495250 (2005).

158 Nguyen, K. T. & West, J. L. Photopolymerizable hydrogels for tissue engineering applications. *Biomaterials* **23**, 4307-4314, doi:Pii S0142-9612(02)00175-8 (2002).

159 Sosnik, A., Cohn, D., San Roman, J. & Abraham, G. A. Crosslinkable PEO-PPO-PEO-based reverse thermo-responsive gels as potentially injectable materials. *J Biomater Sci Polym Ed* **14**, 227-239 (2003).

160 Sosnik, A., Cohn, D., San Roman, J. S. & Abraham, G. A. Crosslinkable PEO-PPO-PEO-based reverse thermo-responsive gels as potentially injectable materials. *J Biomat Sci-Polym E* **14**, 227-239 (2003).

161 Bryant, S. J., Nuttelman, C. R. & Anseth, K. S. Cytocompatibility of UV and visible light photoinitiating systems on cultured NIH/3T3 fibroblasts in vitro. *J Biomater Sci Polym Ed* **11**, 439-457 (2000).

162 Quick, D. J. & Anseth, K. S. DNA delivery from photocrosslinked PEG hydrogels: encapsulation efficiency, release profiles, and DNA quality. *J Control Release* **96**, 341-351, doi:10.1016/j.jconrel.2004.01.021S0168365904000586 [pii] (2004).

163 Tiwari, A., Grailer, J. J., Pilla, S., Steeber, D. A. & Gong, S. Biodegradable hydrogels based on novel photopolymerizable guar gum-methacrylate macromonomers for in situ fabrication of tissue engineering scaffolds. *Acta Biomater* **5**, 3441-3452, doi:DOI 10.1016/j.actbio.2009.06.001 (2009).

164 Cruise, G. M. *et al.* In vitro and in vivo performance of porcine islets encapsulated in interfacially photopolymerized poly(ethylene glycol) diacrylate membranes. *Cell Transplant* **8**, 293-306 (1999).

165 Kim, M. R. & Park, T. G. Temperature-responsive and degradable hyaluronic acid/Pluronic composite hydrogels for controlled release of human growth hormone. *J Control Release* **80**, 69-77, doi:Pii S0168-3659(01)00557-0 (2002).

166 Lee, J. B., Chun, K. W., Yoon, J. J. & Park, T. G. Controlling degradation of acid-hydrolyzable pluronic irilydrogels by physical entrapment of poly(lactic acid-co-glycolic acid) microspheres. *Macromol Biosci* **4**, 957-962, doi:DOI 10.1002/mabi.200400073 (2004).

167 Habas, J. P., Pavie, E., Lapp, A. & Peyrelasse, J. Understanding the complex rheological behavior of PEO-PPO-PEO copolymers in aqueous solution. *J Rheol* **48**, 1-21, doi:Doi 10.1122/1.1634988 (2004).

168 Newby, G. E., Hamley, I. W., King, S. M., Martin, C. M. & Terrill, N. J. Structure, rheology and shear alignment of Pluronic block copolymer mixtures. *J Colloid Interf Sci* **329**, 54-61, doi:DOI 10.1016/j.jcis.2008.09.054 (2009).

169 Dhariwala, B., Hunt, E. & Boland, T. Rapid prototyping of tissue-engineering constructs, using photopolymerizable hydrogels and stereolithography. *Tissue Eng* **10**, 1316-1322 (2004).

170 Quick, D. J. & Anseth, K. S. Gene delivery in tissue engineering: a photopolymer platform to coencapsulate cells and plasmid DNA. *Pharm Res* **20**, 1730-1737 (2003).

171 Atsumi, T., Ishihara, M., Kadoma, Y., Tonosaki, K. & Fujisawa, S. Comparative radical production and cytotoxicity induced by camphorquinone and 9-fluorenone against human pulp fibroblasts. *J Oral Rehabil* **31**, 1155-1164 (2004).

172 Atsumi, T., Iwakura, I., Fujisawa, S. & Ueha, T. Reactive oxygen species (ROS) production by irradiated camphorquinone and cytotoxicity. *J Dent Res* **80**, 1337-1337 (2001).

173 Williams, C. G., Malik, A. N., Kim, T. K., Manson, P. N. & Elisseeff, J. H. Variable cytocompatibility of six cell lines with photoinitiators used for polymerizing hydrogels and cell encapsulation. *Biomaterials* **26**, 1211-1218, doi:DOI 10.1016/j.biomaterials.2004.04.024 (2005).

174 Cohn, D., Sosnik, A. & Levy, A. Improved reverse thermo-responsive polymeric systems. *Biomaterials* **24**, 3707-3714, doi:S014296120300245X [pii] (2003).

175 Jiang, J. *et al.* Rheology of thermoreversible hydrogels from multiblock associating copolymers. *Macromolecules* **41**, 3646-3652, doi:Doi 10.1021/Ma800192m (2008).

176 Parnaud, G., Tache, S., Peiffer, G. & Corpet, D. E. Pluronic F68 block polymer, a very potent suppressor of carcinogenesis in the colon of rats and mice. *Brit J Cancer* **84**, 90-93, doi:DOI 10.1054/bjoc.2000.1540 (2001).

177 Roy, H. K. *et al.* Polyethylene glycol induces apoptosis in HT-29 cells: potential mechanism for chemoprevention of colon cancer. *Febs Lett* **496**, 143-146 (2001).

178 Karlsson, P. C., Hughes, R., Rafter, J. J. & Bruce, W. R. Polyethylene glycol reduces inflammation and aberrant crypt foci in carcinogen-initiated. *Cancer Lett* **223**, 203-209, doi:DOI 10.1016/j.canlet.2004.10.029 (2005).

179 Wali, R. K., Kunte, D. P., Koetsier, J. L., Bissonnette, M. & Roy, H. K. Polyethylene glycol-mediated colorectal cancer chemoprevention: roles of epidermal growth factor receptor and Snail. *Mol Cancer Ther* **7**, 3103-3111, doi:Doi 10.1158/1535-7163.Mct-08-0434 (2008).

180 Parnaud, G., Tache, S., Peiffer, G. & Corpet, D. E. Polyethylene-glycol suppresses colon cancer and causes dose-dependent regression of azoxymethane-induced aberrant crypt foci in rats. *Cancer Res* **59**, 5143-5147 (1999).

181 Corpet, D. E. & Parnaud, G. Polyethylene-glycol, a potent suppressor of azoxymethane-induced colonic aberrant crypt foci in rats. *Carcinogenesis* **20**, 915-918 (1999).

182 Mortensen, K. PEO-related block copolymer surfactants. *Colloid Surface A* **183**, 277-292 (2001).

183 Feng, S. S. New-concept chemotherapy by nanoparticles of biodegradable polymers: where are we now? *Nanomedicine-Uk* **1**, 297-309, doi:Doi 10.2217/17435889.1.3.297 (2006).

184 Brigger, I., Dubernet, C. & Couvreur, P. Nanoparticles in cancer therapy and diagnosis. *Adv Drug Deliver Rev* **54**, 631-651, doi:Pii S0169-409x(02)00044-3 (2002).

185 Feng, S. S., Mu, L., Win, K. Y. & Huang, G. F. Nanoparticles of biodegradable polymers for clinical administration of paclitaxel. *Curr Med Chem* **11**, 413-424 (2004).

186 Govender, T., Stolnik, S., Garnett, M. C., Illum, L. & Davis, S. S. PLGA nanoparticles prepared by nanoprecipitation: drug loading and release studies of a water soluble drug. *J Control Release* **57**, 171-185 (1999).

187 Dong, Y. C. & Feng, S. S. Poly(D,L-lactide-co-glycolide)/montmorillonite nanoparticles for oral delivery of anticancer drugs. *Biomaterials* **26**, 6068-6076, doi:DOI 10.1016/j.biomaterials.2005.03.021 (2005).

188 Panyam, J. & Labhasetwar, V. Biodegradable nanoparticles for drug and gene delivery to cells and tissue. *Adv Drug Deliver Rev* **55**, 329-347, doi:Doi 10.1016/S0169-409x(02)00228-4 (2003).

189 Jain, R. A. The manufacturing techniques of various drug loaded biodegradable poly(lactide-co-glycolide) (PLGA) devices. *Biomaterials* **21**, 2475-2490 (2000).

190 Ouyang, N. *et al.* Nitric oxide-donating aspirin prevents pancreatic cancer in a hamster tumor model. *Cancer Res* **66**, 4503-4511 (2006).

191 Kashfi, K. & Rigas, B. Molecular targets of nitric-oxide-donating aspirin in cancer. *Biochem Soc Trans* **33**, 701-704 (2005).

192 Leonetti, C. *et al.* Efficacy of a nitric oxide-releasing nonsteroidal anti-inflammatory drug and cytotoxic drugs in human colon cancer cell lines in vitro and xenografts. *Mol Cancer Ther* **5**, 919-926 (2006).

193 Eggers, P. E. Unitized Thermoelectric Module Concept. *Mech Eng* **94**, 62-& (1972).

194 Liang, L., Feng, X. D., Martin, P. F. C. & Peurrung, L. M. Temperature-sensitive switch from composite poly(N-isopropylacrylamide) sponge gels. *J Appl Polym Sci* **75**, 1735-1739 (2000).

195 Eggers, P. E. Unitized Thermoelectric Module Concept. *Combustion* **43**, 19-& (1972).

196 Kraftmakher, Y. Simple experiments with a thermoelectric module. *Eur J Phys* **26**, 959-967, doi:Doi 10.1088/0143-0807/26/6/003 (2005).

197 Wu, K. H. & Hung, C. I. Thickness Scaling Characterization of Thermoelectric Module for Small-scale Electronic Cooling. *J Chin Soc Mech Eng* **30**, 475-481 (2009).

198 Hamon, L., Grohens, Y., Soldera, A. & Holl, Y. Miscibility in blends of stereoregular poly(methyl methacrylate)/poly(ethylene oxide) based oligomers. *Polymer* **42**, 9697-9703 (2001).

199 Silvestre, C., Cimmino, S., Martuscelli, E., Karasz, F. E. & Macknight, W. J. Poly(Ethylene Oxide) Poly(Methyl Methacrylate) Blends - Influence of Tacticity of Poly(Methyl Methacrylate) on Blend Structure and Miscibility. *Polymer* **28**, 1190-1199 (1987).

200 Straka, J., Schmidt, P., Dybal, J., Schneider, B. & Spevacek, J. Blends of Poly(Ethylene Oxide) Poly(Methyl Methacrylate) - an Ir and Nmr-Study. *Polymer* **36**, 1147-1155 (1995).

201 Soppimath, K. S., Aminabhavi, T. M., Kulkarni, A. R. & Rudzinski, W. E. Biodegradable polymeric nanoparticles as drug delivery devices. *J Control Release* **70**, 1-20 (2001).

202 Suh, H., Jeong, B. M., Liu, F. & Kim, S. W. Cellular uptake study of biodegradable nanoparticles in vascular smooth muscle cells. *Pharmaceut Res* **15**, 1495-1498 (1998).

203 Sun, B., Ranganathan, B. & Feng, S. S. Multifunctional poly(D,L-lactide-co-glycolide)/montmorillonite (PLGA/MMT) nanoparticles decorated by Trastuzumab for targeted chemotherapy of breast cancer. *Biomaterials* **29**, 475-486, doi:DOI 10.1016/j.biomaterials.2007.09.038 (2008).

204 Dong, Y. & Feng, S. S. Poly(D,L-lactide-co-glycolide) (PLGA) nanoparticles prepared by high pressure homogenization for paclitaxel chemotherapy. *Int J Pharm* **342**, 208-214, doi:DOI 10.1016/j.ijpharm.2007.04.031 (2007).

205 Acharya, S., Dilnawaz, F. & Sahoo, S. K. Targeted epidermal growth factor receptor nanoparticle bioconjugates for breast cancer therapy. *Biomaterials* **30**, 5737-5750, doi:DOI 10.1016/j.biomaterials.2009.07.008 (2009).

206 Desai, M. P., Labhasetwar, V., Walter, E., Levy, R. J. & Amidon, G. L. The mechanism of uptake of biodegradable microparticles in Caco-2 cells is size dependent. *Pharmaceut Res* **14**, 1568-1573 (1997).

207 Zhang, Z. P. & Feng, S. S. The drug encapsulation efficiency, in vitro drug release, cellular uptake and cytotoxicity of paclitaxel-loaded poly(lactide)-tocopheryl polyethylene glycol succinate nanoparticles. *Biomaterials* **27**, 4025-4033, doi:DOI 10.1016/j.biomaterials.2006.03.006 (2006).

208 Fonseca, C., Simoes, S. & Gaspar, R. Paclitaxel-loaded PLGA nanoparticles: preparation, physicochemical characterization and in vitro anti-tumoral activity. *J Control Release* **83**, 273-286, doi:Pii S0168-3659(02)00212-2 (2002).

209 Jeong, B., Bae, Y. H. & Kim, S. W. Drug release from biodegradable injectable thermosensitive hydrogel of PEG-PLGA-PEG triblock copolymers. *J Control Release* **63**, 155-163 (2000).